Technische Universität München

TUM School of Engineering and Design

THE CAD-INTEGRATED DESIGN CYCLE FOR STRUCTURAL MEMBRANES

Ann-Kathrin Goldbach

Vollständiger Abdruck der von der TUM School of Engineering and Design der Technischen Universität München zur Erlangung des akademischen Grades einer

Doktorin der Ingenieurwissenschaften

genehmigten Dissertation.

Vorsitzender:

Prof. Dr.-Ing. habil. Fabian Duddeck

Prüfer der Dissertation:

1. Prof. Dr.-Ing. Kai-Uwe Bletzinger
2. Prof. Dr. ir. Marijke Mollaert
3. Prof. Dr.-Ing. Rainer Barthel

Die Dissertation wurde am 17.05.2021 bei der Technischen Universität München eingereicht und durch die TUM School of Engineering and Design am 09.11.2021 angenommen.

Schriftenreihe des Lehrstuhls für Statik TU München

Band 50

Ann-Kathrin Goldbach

THE CAD-INTEGRATED DESIGN CYCLE FOR STRUCTURAL MEMBRANES

München 2021

Abstract

Membrane structures are wide-span lightweight structures that can withstand external loads by means of pure tensile forces, leading to an optimal material utilization and thus highly efficient structures. In contrast to more conventional buildings, the design and analysis of membrane structures requires an iterative process with the aim of aligning the tasks of formfinding, structural analysis and cutting pattern generation alongside functional and aesthetic requirements.

The CAD-integrated design cycle presented in this thesis takes the interactions of the different analysis stages of the iterative design process into account in a beneficial way. Isogeometric B-Rep Analysis (IBRA) is the basis of the CAD-integrated design cycle and was developed, to consistently use the NURBS-based model for analysis. Design and analysis models thus become one and a unified design process emerges - facilitating the interaction and communication of architects and engineers. For the iterative design process that often requires geometrical changes, this constitutes a significant advantage, as geometrical changes can be implemented at any stage of the model by standard CAD operations.

Apart from explaining the concepts of Isogeometric B-Rep Analysis and the mechanical solution strategies for formfinding and structural analysis, the development and implementation of cutting pattern generation with IBRA is established as a milestone of this research.

The advantages of CAD integration and the emerging unified workflow for the design cycle of membrane structures along with the possibility of parametrisation for geometrical and mechanical properties are demonstrated with a variety of application examples. The development of the parametric CAD-integrated design cycle facilitated the investigation of uncertainty quantification of membrane structures, especially with respect to their non-linear load-bearing behaviour. In the light of the development of a harmonized verification standard on a European level, this aspect is investigated as a final topic in this thesis.

Zusammenfassung

Membrantragwerke sind weit gespannte Flächentragwerke, die äußere Lasten über reine Zugkräfte abtragen können und somit eine optimale Materialausnutzung aufweisen. Hierfür muss in Entwurf und Analyse in einem iterativen Prozess der Einklang zwischen Formfindung, Strukturanalyse und Zuschnittsanalyse unter Berücksichtigung von funktionellen und aesthetischen Anforderungen gefunden werden.

Im CAD-integrierten Entwurfskreislauf werden die Abhängigkeiten der unterschiedlichen Analyseschritte berücksichtigt. Isogeometrische B-Rep-Analyse ist die Grundlage des CAD-integrierten Entwurfskreislaufs und wurde entwickelt, um NURBS-basierte Modelle direkt für die Analyse zu verwenden. Entwurfs- und Analysemodelle werden so zu einem einheitlichen Entwurfsprozess zusammengeführt, der die Interaktion und Kommunikation von Architekten und Ingenieuren wesentlich erleichtert. Für den Entwurfskreislauf von Membrantragwerken entsteht so ein bedeutender Vorteil, da oftmals erforderliche geometrische Anpassungen jederzeit durch einfache CAD Operationen implementierbar sind.

Neben der grundlegenden Erläuterung der Isogeometrischen B-Rep-Analyse und der mechanischen Lösungsstrategien für Formfindung und Strukturanalyse wird in dieser Arbeit die Entwicklung des Zuschnitts mit IBRA als Meilenstein meiner Forschung vorgestellt. Die Vorteile der CAD Integration und der so entstehende einheitliche Arbeitsablauf für den Entwurfskreislauf von Membrantragwerken mit der Möglichkeit der Parametrisierung für geometrische und mechanische Eigenschaften wird hervorgehoben und an einer Vielzahl von Anwendungsbeispielen veranschaulicht. Die Entwicklung des parametrischen CAD-integrierten Entwurfskreislaufs erleichtert Untersuchungen zur Quantifizierung der Unsicherheit von Membranstrukturen, insbesondere hinsichtlich ihres nichtlinearen Tragverhaltens. In Bezug auf die Entwicklung eines harmonisierten Nachweisformats auf europäischer Ebene wird dies als abschließendes Thema in dieser Arbeit untersucht.

Acknowledgments

This thesis was written from 2015 to 2021 during my time as a research and teaching associate at the Chair of Structural Analysis at the Technical University of Munich.

First of all, I would like to express my gratitude towards Prof. Dr.-Ing. Kai-Uwe Bletzinger for providing the possibility to work in the field of lightweight design and membrane structures. His interest and passion for these structures lead to a great working environment.

I also want to thank Prof. Marijke Mollaert Ph.D. and Prof. Dr.-Ing. Rainer Barthel for completing my board of examiners, as well as Prof. Dr.-Ing. Fabian Duddeck for the organization. Their interest in my work is gratefully acknowledged.

Another thank you is directed at all my colleagues at the Chair of Structural Analysis for the cooperation and pleasant times. Thank you Armin Widhammer and Michael Breitenberger, for accelerating my start in this research area by numerous discussions. Thank you Benedikt Philipp and Anna Bauer for the close cooperation over the years. Thank you Benedikt, Anna and Martin Fußeder for proofreading my thesis. I also want to mention Armin Geiser and thank him for the companionship during the final phase of this project and Roland Wüchner for a door that was always open for discussions on- and off-topic.

Finally, I want to thank my family for their unconditional support. Thanks to my husband Christian for being my rock and for understanding the challenges of this demanding but rewarding period in our life and for building as many Lego vehicles as it took to create a relaxed space to finish this thesis.

Ann-Kathrin Goldbach
München
May 2021

Contents

CHAPTER 1

INTRODUCTION AND MOTIVATION

Membrane structures are fascinating wide-span lightweight structures that can withstand external loads by means of pure tensile forces. The presence of pure tension leads to an optimal material utilization and thus highly efficient structures. Due to their double-curved form and because of mechanically or pneumatically applied prestress, membranes achieve the necessary rigidity to meet the requirements of the built environment. Using a rope as an example, it is easy to illustrate how prestressing and geometry are mutually dependent for these form-active structures. Under its own weight, the cable takes on the shape of a catenary, but its shape can be changed by applying tension. Different tensioning conditions lead to different geometries under given boundary conditions, each geometry representing an equilibrium figure - or surface for membranes. Such equilibrium surfaces are determined in the formfinding process. In the early days of membrane construction, this included physical experiments with stocking models and soap skins. Nowadays numerical methods are mostly used for shape finding. Already in the preliminary design stage, only a formfound surface can represent the shape of the prestressed geometry.

In contrast to more conventional buildings, the design and analysis of membrane structures is an iterative process with the aim of aligning the tasks of formfinding, structural analysis and cutting pattern generation, in order to reach a feasible design. The formfound model builds the basis for these mentioned analyses. In structural analysis, the behaviour of the membrane under external loads is examined. The results are directly related to formfinding. If, for example, the prestress is not sufficiently high to avoid compressive stresses (and thus failure) in the membrane, it may be necessary to increase it and thus to carry out a new formfinding yielding a changed shape and prestress state. Verification of stability and serviceability can be carried out at this point, possibly introducing further requirements that might call for calibration of some input parameters. Finally, the cutting pattern is determined in the cutting pattern generation, which leads to the desired shape and prestress after the assembly of initially flat textile pieces. Due to the double curvature of the membrane surfaces, it is not possible to determine the pattern geometry by unfolding the surface without distortion. Instead, optimisation procedures are necessary to determine a suitable compromise solution, which shows additional stress states due to the distortion during installation. In addition to the material properties, the boundary conditions of the production, such as the width of the textile web, must also be taken into account. In a mounting analysis, the assembly of the pattern geometry can be simulated. Again, the resulting shape and stress state can reignite the whole design cycle. Knippers et al. [67] summarises the design cycle as a complex and iterative process, that lasts until the end of the planning phase and requires an extensive insight and expertise, due to the close interaction of material, shape and load bearing behaviour, as well as the consequences of manufacturing.

The dependencies between the analyses of the mentioned subtasks (formfinding, cutting pattern generation, simulation of the loaded state) must be mapped by suitable numerical solution methods, which typically only succeeds iteratively. In the CAD-integrated analysis, the interactions of the different analysis stages and the iterative design process are optimally taken into account by preserving the B-Rep model, as shown in Philipp [91] and Goldbach et al. [46] with the help of some examples. In addition to creating the necessary links between analysis steps, geometrical changes can be implemented at any stage of the model by standard CAD operations. For the iterative design process that often requires geometrical changes,

this constitutes a significant advantage. The basis for CAD integration is the Isogeometric Analysis (IGA), which has been continuously developed further according to the initial idea of Hughes et al. [61]. The Isogeometric B-Rep Analysis (IBRA) according to Breitenberger et al. [25] is an extension of IGA, which enables the complete integration of the calculation model into the CAD environment (see also Breitenberger [24], Bauer et al. [12]). The CAD model also serves as an analysis model and is available in pre- and postprocessing with its complete geometric description as a B-Rep model (B-Rep: ''Boundary Representation'', i.e. a model hierarchically described by its edges, geometry and topology). This means that further calculations can be performed directly on the deformed initial geometry. A further advantage of CAD-integrated analysis is the inherent parametrisation. Changes in geometry and mechanical properties can be made quickly and easily and their effects investigated without affecting the discretisation or existing dependencies between individual analyses. Discretisation using smooth NURBS curves and surfaces instead of straight-line polygon meshes leads to a more accurate description of the geometry and curvature of the numerical models due to the higher polynomial degree of the basis functions. Design and analysis models become one and a unified design process emerges - facilitating the interaction and communication of architects and engineers. Finally, the data management for the manufacturing process is also worth mentioning. The cutting pattern geometries are directly available as CAD data within the CAD-integrated design chain and are therefore ideal for further processing with Computer-aided Manufacturing (CAM).

In the process of this dissertation project, the main goal was the creation of a fully CAD-integrated design cycle for structural membranes in a parametric environment. As a first step, the cutting pattern generation with IBRA elements was implemented and the previously existing gap in the CAD-integrated design cycle was thus closed. The introduction of the design cycle disciplines into a parametric environment with Kiwi!3d [66] allowed for extensive testing and exploration of the links between the steps, finally giving rise to the unified workflow. In addition to the models and tests that were created in the research process, teaching a course on membrane design gave the possibility to delve into the provided framework with a diverse group of students and thus gain different perspectives (see Appendix B).

The European efforts towards a harmonised standard for structural membrane design and verification lead to the recently published prCEN/TS, 19102:2021 [95] on the *design of tensioned membrane structures*. During the discussions and developments of the document, further questions emerged regarding the uncertainty quantification of membrane structures, especially with respect to non-linear load-bearing behaviour and the qualitative assessment of simplified model assumptions. The development of the parametric CAD-integrated design cycle facilitated the investigations performed in this area of research and will continue to do so in the future.

Outline

Chapter 2 begins with an overview of the particularities of structural membranes and highlights the necessity of a powerful numerical toolchain in order to reliably model their structural behaviour. For this, the fundamentals of differential geometry and continuum mechanics, that are the basis of the methods presented in this thesis, are given. In addition, the concept of Isogeometric B-Rep Analysis (IBRA) is introduced and the necessary terms of Computer Aided Design (CAD) and Finite Element Method (FEM) are explained.

In Chapter 3, a detailed description of the design cycle of structural membranes is conveyed. Formfinding, structural analysis, cutting pattern generation and mounting analysis are described as the highly interactive steps that build the design cycle. For each discipline, an overview of relevant solution methods in research and engineering practice is provided. The mechanical aspects for the CAD-integrated analyses presented in this thesis are introduced. In addition, the recently developed European design requirements are summarised.

Based on these explanations of the individual analyses in the design cycle, Chapter 4 focuses on the CAD integration of the design and analysis of membrane structures. The unified workflow within the CAD environment, allowing architects and engineers to work on one model, is illustrated. As parametric design significantly enlarges the design space, its benefits are emphasized with the help of a simple membrane model. Furthermore, the specific advantages of CAD-integrated analysis for cutting pattern generation are highlighted. Several models that were inspired by built large-scale membrane structures highlight various aspects of the CAD-

integrated design cycle. The power of a parametric design environment is established for both geometrical and mechanical properties of structural membranes. Furthermore, the benefits of a CAD-integrated design model and the corresponding unified workflow are shown in detail for these selected examples.

Chapter 5 concentrates on verification and sensitivity analysis for membrane structures. After a brief description of the code framework and the challenges of uncertain input parameters as well as non-linear load-response curves, the application to membrane structures is laid out. A review of solution strategies is laid out, along with an extensive investigation of the uncertainties for a hypar. In addition, four distinctive classical membrane shapes are evaluated with respect to non-linearities in the structural behaviour under representative load conditions. Parametric studies indicate the influences of curvature and load intensity on these structures.

A conclusion is provided in Chapter 6 alongside an outlook on future research possibilities in the field of structural membrane design and analysis.

Remark

All numerical simulations displayed in this thesis were conducted with the research code Carat++ [28] of the Chair of Structural Analysis, TUM. The CAD integration is realised with the plugin Kiwi!3d [66] for the software Rhinoceros [101]. Kiwi!3d was developed in a cooperation between the Chair of Structural Analysis and str.ucture GmbH.

CHAPTER 2

FUNDAMENTALS FOR THE DESIGN AND ANALYSIS OF STRUCTURAL MEMBRANES

In this chapter, the particularities of membrane structures and their design challenges are introduced. The properties of membrane structures which are essential for the applicable numerical modelling of their mechanical behaviour are identified. Starting with a short overview of the applied differential geometry, the explanations proceed to continuum mechanical basics. Additionally, material modelling for coated woven textiles and foils is discussed and appropriate constitutive laws are presented. Furthermore, the application of the Finite Element Method for the analysis of structural membranes is summarised — more specifically the highly beneficial usage of Isogeometric B-Rep Analysis for the design and analysis.

2.1 Characteristics of Structural Membranes

Membrane structures can be found in a number of facilities, enriching the built environment with the playfulness and lightness of their shapes. Combining the functions of skin and structure, their typically double-curved, large surfaces build a strong juxtaposition to conventional rectangular buildings. The most common application fields for large structural membranes are sports stadia, buildings of infrastructure and leisure facilities. Smaller structures can often be found as shading elements and pavilions, or architectural sculptures. Structural membranes build landmarks wherever they appear, affecting the observer with their unique language of shapes.

Figure 2.1 shows three membrane structures that were built in Munich, giving an impression of typical shapes and applications: the ETFE roof over the jungle tent in Hellabrunn Zoo, photovoltaic ETFE cushions as a cover at the municipal waste management department and the roof of Fröttmaning subway station.

With a thickness of about 1 mm, structural membranes commonly span large distances and are hence characterised by an extreme slenderness and very low self-weight. Coated woven textiles and foils are the most common membrane materials. Since they carry external forces through tension and avoid compression by wrinkling, tension in the membrane needs to be kept in all load cases. In order to ensure this, membranes are prestressed either mechanically or pneumatically, i.e. by pulling deliberately small parts to the support positions or inflating them. Being lightweight structures, the structural behaviour of membranes is governed by the interaction of form and force. Therefore, the shape (the curvature in particular) in combination with the existing stress state constitutes the load bearing behaviour. As it is usually necessary to resist both uplift and downward forces in tension, membranes are built from a variation of double curved shapes.

These shapes need to be in equilibrium for given prestress and boundary conditions and hence necessitate a formfinding analysis, as they cannot simply be designed. If the design is to be performed numerically, the applied software needs to be able to solve this mechanically inverse problem, as will be explained in Chapter 3. For the assessment of a membrane structure's safety through structural analysis and for the cutting pattern generation needed for the manufacturing, the geometrically non-linear

behaviour, as well as material non-linearities need to be considered. The basis for these non-linear analyses, namely differential geometry and continuum mechanics, will be given in the next section.

Figure 2.1: Membrane roofs in Munich. Top: Photovoltaic ETFE cushions at the municipal waste management department (©MdCAlmeida Villafuerte). Middle: Hellabrunn Zoo: ETFE roof over jungle tent. Bottom: Fröttmaning subway station (©Florian Schütz).

2.2 Differential Geometry

Conventions
The formulae presented in this thesis are subject to the following conventions, if not indicated otherwise:

- Greek letters (α, β) are in the range of $\{1,2\}$.
- Latin letters (i, j) are in the range of $\{1,2,3\}$.
- Capital letters refer to the reference configuration $\mathbf{X}$.
- Lower case letters refer to the current configuration $\mathbf{x}$.
- Einstein summation convention is used, i.e. $a_i b^i = a_1 b^1 + a_2 b^2 + a_3 b^3$.

In order to mathematically describe surfaces in space, they are usually reduced to their mid-surface. For membranes this is permissible, as their thickness is very small compared to the curvature radii, leading to constant strains in the membrane fibres and the so-called membrane stress state. The membrane stress state hence implies a constant stress distribution in thickness direction. A pre-integration over the thickness is performed in many cases.
Differential geometry is used to represent surfaces in space and has been treated in detail in numerous publications(e.g. Başar et al. [10], Holzapfel [59], Bischoff et al. [18] and Pottmann [94]). The following section provides a brief summary of the aspects of differential geometry that are fundamental for the analysis of structural membranes.

Surface description in space

In a Cartesian coordinate system, any point $\mathbf{P}$ can be described by its position vector $\mathbf{r}$. The base vectors $\mathbf{e}_i$ build the Euclidean space in a global Cartesian coordinate system. The formulation of the position vector in terms of its coefficients x^i along the base vectors $\mathbf{e}_i$ reads

$$\mathbf{r} = x^i \mathbf{e}_i. \tag{2.1}$$

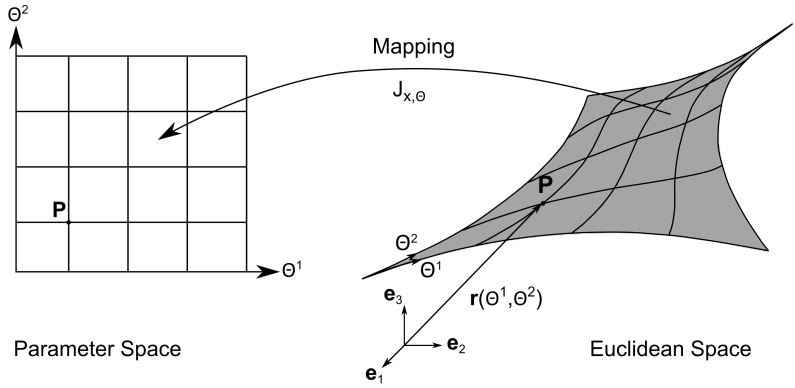

Figure 2.2: Parametric surface representation with local parameters θ^1 and θ^2 in the Parameter and Euclidean space.

Parametric surface representation

The parametric surface description makes use of a set of local parameters θ^1 and θ^2 that are orthogonal in the parameter space and (mostly) curvilinear on the surface, see Figure 2.2. The position vector $\mathbf{r}$ of a point $\mathbf{P}$ can now be described in terms of these curvilinear coordinates:

$$\mathbf{r}(\theta^1,\theta^2) = x^i(\theta^1,\theta^2)\,\mathbf{e}_i = \left[x(\theta^1,\theta^2)\;\; y(\theta^1,\theta^2)\;\; z(\theta^1,\theta^2)\right]^T. \tag{2.2}$$

Mapping between the parameter space and euclidean space is computed with

$$J_{x,\theta} = \left\| \frac{\partial \mathbf{X}}{\partial \theta^1} \times \frac{\partial \mathbf{X}}{\partial \theta^2} \right\|_2. \tag{2.3}$$

The derivation of the position vector $\mathbf{r}(\theta^1,\theta^2)$ with respect to the surface parameters leads to the covariant base vectors $\mathbf{g}_1$ and $\mathbf{g}_2$ (Equation 2.4, 2.5), which are tangential to the surface at any point and aligned with the surface parameters θ^1 and θ^2, see Figure 2.3.

$$\mathbf{g}_1 = \frac{\partial \mathbf{r}(\theta^1,\theta^2)}{\partial \theta^1} \tag{2.4}$$

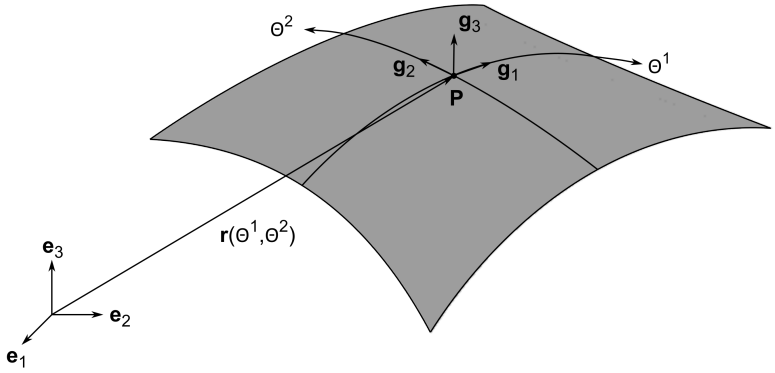

Figure 2.3: Covariant base vectors at point **P** of a surface.

$$\mathbf{g}_2 = \frac{\partial \mathbf{r}\,(\theta^1, \theta^2)}{\partial\, \theta^2} \tag{2.5}$$

The third base vector $\mathbf{g}_3$ can be deduced in normal direction $\mathbf{n}$ to the surface and is commonly normalised to unit length:

$$\mathbf{g}_3 = \frac{\mathbf{g}_1 \times \mathbf{g}_2}{||\mathbf{g}_1 \times \mathbf{g}_2||} = \mathbf{n}. \tag{2.6}$$

A second set of base vectors, the contravariant base vectors $\mathbf{g}^1$ and $\mathbf{g}^2$, can be formulated such that the scalar product satisfies the condition of the Kronecker delta δ^α_β :

$$\mathbf{g}^\alpha \cdot \mathbf{g}_\beta = \delta^\alpha_\beta = \begin{cases} 1, & \alpha = \beta \\ 0, & \alpha \neq \beta \end{cases}. \tag{2.7}$$

The third co- and contravariant base vectors $\mathbf{g}_3$ and $\mathbf{g}^3$ are aligned, i.e. $\mathbf{g}_3 = \mathbf{g}^3$.

First fundamental form: metric tensor

The co- and contravariant base vectors can be used to deduce local properties of a surface. The first fundamental form of a surface gives information

on the metric properties. These entail the lengths of base vectors, as well as the angle between them and can be used to calculate the area of a differential area element da. The metric tensor $\mathbf{I}$ can be calculated as follows:

$$\mathbf{I} = g_{\alpha\beta}\ \mathbf{g}^{\alpha} \otimes \mathbf{g}^{\beta} = g^{\alpha\beta}\ \mathbf{g}_{\alpha} \otimes \mathbf{g}_{\beta} \tag{2.8}$$

with

$$g_{\alpha\beta} = \mathbf{g}_{\alpha} \cdot \mathbf{g}_{\beta} \tag{2.9}$$

$$g^{\alpha\beta} = \mathbf{g}^{\alpha} \cdot \mathbf{g}^{\beta} \tag{2.10}$$

The evaluation of the surface area content of a differential area element da (also called Lagrange identity) reads:

$$da = ||\mathbf{g}_1 \times \mathbf{g}_2||\ d\theta^1 d\theta^2 = \sqrt{(\mathbf{g}_1 \times \mathbf{g}_2)(\mathbf{g}_1 \times \mathbf{g}_2)}\ d\theta^1 d\theta^2 \tag{2.11}$$

Second fundamental form: curvature tensor

The second fundamental form of the surface describes the curvature and takes the normal vector $\mathbf{n}$ or $\mathbf{g}_3$ into account. The curvature tensor $\mathbf{K}$ measures the change of the normal vector along the surface parameters θ^1 and θ^2, see Equation 2.12

$$\mathbf{K} = b_{\alpha\beta}\ \mathbf{g}^{\alpha} \otimes \mathbf{g}^{\beta} \tag{2.12}$$

with

$$b_{\alpha\beta} = -\,\mathbf{g}_{\alpha}\ \frac{\partial \mathbf{n}}{\partial \theta^{\beta}} = \frac{\partial \mathbf{g}_{\alpha}}{\partial \theta^{\beta}} \mathbf{n} \tag{2.13}$$

The Gaussian curvature K separates curved surfaces into synclastic, anticlastic and developable surfaces, see Table 2.1 and Figure 2.4.

$$K = \frac{\det\left[b_{\alpha\beta}\right]}{\det\left[g_{\alpha\beta}\right]} \tag{2.14}$$

It can also be expressed by principal curvatures κ_1 and κ_2 and principal radii R_1 and R_2, see Equation 2.15. The principal curvatures are defined as the eigenvalues of the curvature tensor $\mathbf{K}$ with maximum curvature values.

Table 2.1: Types of curved surfaces and Gaussian curvature K.

synclastic	anticlastic	developable
$K > 0$	$K < 0$	$K = 0$

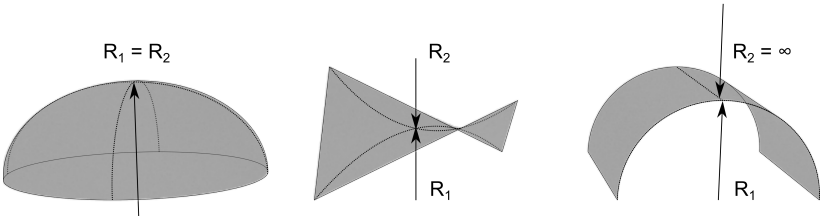

Figure 2.4: Types of curved surfaces and principal radii R_α.

The inverted principal curvatures are called principal radii of a point on a surface.

$$K = \kappa_1 \cdot \kappa_2 = \frac{1}{R_1} \cdot \frac{1}{R_2} \tag{2.15}$$

The mean curvature H represents the arithmetic mean of the principal curvatures κ_1 and κ_2 and can be expressed as:

$$2H = \kappa_1 + \kappa_2 = \frac{1}{R_1} + \frac{1}{R_2} \tag{2.16}$$

$H = 0$ holds for minimal surfaces, which are of particular interest for the formfinding of membrane structures, see Section 3.1.2.

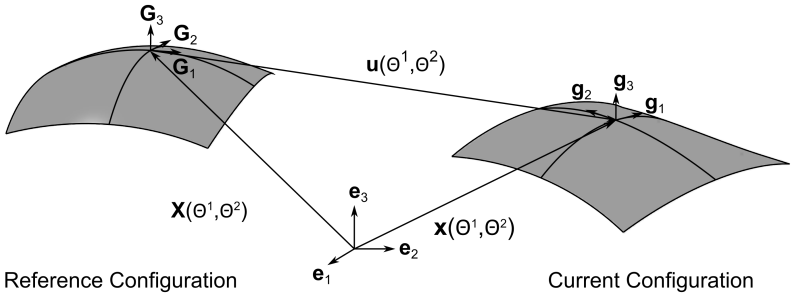

Figure 2.5: Reference and current configuration **x** and **X**.

2.3 Continuum Mechanics

In order to capture the structural behaviour of membrane structures, the accurate description of large deformations is crucial. Continuum mechanics provide the necessary tools to correctly describe these deformations. The fundamentals for kinematics, as well as strain- and stress-relations will be summarised in the following section.

Configurations

In continuum mechanics, there is a distinction between the reference configuration **X** and current configuration **x** as depicted in Figure 2.5. The reference configuration relates to the undeformed or initial geometry and the current configuration entails a deformation due to external loads. In the Lagrangian description, all deformations are observed from a fixed point in space. In contrast to this, the Eulerian description contains a deformation of the viewpoint. This will not be used for the methods shown in this thesis. The deformation from the reference to the current configuration **u** can thus be stated as:

$$\mathbf{u}(\theta^1,\theta^2) = \mathbf{x}(\theta^1,\theta^2) - \mathbf{X}(\theta^1,\theta^2) \tag{2.17}$$

Kinematics

The deformation gradient $\mathbf{F}$ describes the change of a differential element from the reference to the current configuration, i.e. the kinematics:

$$d\mathbf{x} = \mathbf{F} \cdot d\mathbf{X}$$
$$\mathbf{F} = \frac{d\mathbf{x}}{d\mathbf{X}} \tag{2.18}$$

The relation of the base vectors of each configuration can also be expressed with the deformation gradient $\mathbf{F}$:

$$\mathbf{g}_i = \frac{\partial \mathbf{x}}{\partial \theta^i} = \frac{\partial \mathbf{x}}{\partial \mathbf{X}} \frac{\partial \mathbf{X}}{\partial \theta^i} = \mathbf{F} \cdot \mathbf{G}_i \tag{2.19}$$

Based on this, the definitions of the deformation gradient can be derived as denoted in Equations 2.20 to 2.23.

$$\mathbf{F} = \mathbf{g}_i \otimes \mathbf{G}^i \tag{2.20}$$
$$\mathbf{F}^{-T} = \mathbf{g}^i \otimes \mathbf{G}_i \tag{2.21}$$
$$\mathbf{F}^{-1} = \mathbf{G}_i \otimes \mathbf{g}^i \tag{2.22}$$
$$\mathbf{F}^T = \mathbf{G}^i \otimes \mathbf{g}_i \tag{2.23}$$

The deformation gradient $\mathbf{F}$ can be useful for a number of calculations. One of them is the relation of a differential element of area da in the current to dA in the reference configuration.

$$\mathbf{n}\, da = \det\mathbf{F}\ \mathbf{F}^{-T}\ \mathbf{N}\, dA \tag{2.24}$$

Or written in terms of the determinant of the deformation gradient $\det\mathbf{F}$:

$$\det\mathbf{F} = \frac{da}{dA} = \frac{(\mathbf{g}_1 \times \mathbf{g}_2)\, \mathbf{g}_3}{(\mathbf{G}_1 \times \mathbf{G}_2)\, \mathbf{G}_3} \tag{2.25}$$

Hence, in order to calculate the area of a deformed differential element, the deformation gradient can be used as shown in Equation 2.26.

$$da = \det\mathbf{F}\ dA \tag{2.26}$$

Strain measures

The deformation of a body can be divided into a rigid body motion and the change in size and shape. This change in size and shape is the so-called strain. It can be mathematically described from different perspectives, resulting in different strain measures. Only two of them will be represented here, as they are relevant for the mechanical aspects of the following chapters.

The Euler-Almansi strain $\mathbf{e}$ is defined in the current configuration (Equation 2.27). It can be used to describe large deformations and is thus suitable for the analysis of structural membranes.

$$\mathbf{e} = \frac{1}{2}\left(g_{\alpha\beta} - G_{\alpha\beta}\right)\mathbf{g}^{\alpha} \otimes \mathbf{g}^{\beta} = \frac{1}{2}\left(\mathbf{I} - \mathbf{F}^{-T}\,\mathbf{F}^{-1}\right) \tag{2.27}$$

As can be seen in Equation 2.28, the Green-Lagrange strain $\mathbf{E}$ is defined in the reference configuration and is also applicable for large deformations.

$$\mathbf{E} = \frac{1}{2}\left(g_{\alpha\beta} - G_{\alpha\beta}\right)\mathbf{G}^{\alpha} \otimes \mathbf{G}^{\beta} = \frac{1}{2}\left(\mathbf{F}^{T}\,\mathbf{F} - \mathbf{I}\right) \tag{2.28}$$

Having the same coefficients, the difference between Euler-Almansi and Green-Lagrange strains is the perspective only. They can thus be transformed into each other by the so-called Push-Forward- and Pull-Back-Operations (χ_* and χ_*^{-1}), see Equations 2.29 and 2.30.

$$\mathbf{e} = \chi_*(\mathbf{E}) = \mathbf{F}^{-T}\,\mathbf{E}\,\mathbf{F}^{-1} \tag{2.29}$$

$$\mathbf{E} = \chi_*^{-1}(\mathbf{e}) = \mathbf{F}^{T}\,\mathbf{e}\,\mathbf{F} \tag{2.30}$$

Stress measures

In general, strain in a body also leads to stress, with the magnitude depending on the material properties. Again, stress can be defined in different configurations and thus be related to different strain measures to build conjugate pairs.

Cauchy stress $\boldsymbol{\sigma}$ is defined in the current configuration only and is therefore interpreted as the physical stress. The conjugate strain measure is Euler-Almansi strain $\mathbf{e}$.

The 2^{nd} Piola Kirchoff stress $\mathbf{S}$ is defined in the reference configuration only. Green-Lagrange strains $\mathbf{E}$ and 2^{nd} Piola Kirchoff stresses $\mathbf{S}$ build

a conjugate pair. It does not have a physical meaning but is very useful for the definition of governing equations for the solution of mechanical problems.

As with the strain measures, the deformation gradient can be applied to transform the stress measures into one another. The following relation holds:

$$\mathbf{S} = \det\mathbf{F}\ \mathbf{F}^{-1}\ \boldsymbol{\sigma}\ \mathbf{F}^{-T} \tag{2.31}$$

Furthermore, the 1^{st} Piola Kirchoff stress $\mathbf{P}$ is a stress measure, defined in both reference and current configuration, that can be computed from $\mathbf{S}$ or $\boldsymbol{\sigma}$, see Equation 2.32.

$$\mathbf{P} = \det\mathbf{F}\ \boldsymbol{\sigma}\ \mathbf{F}^{-T} = \mathbf{F}\ \mathbf{S} \tag{2.32}$$

Constitutive laws

Constitutive laws provide the link between strains and stresses and depict the material properties. This can be formulated with the help of the Elasticity Tensor $\mathbb{C}$. In the most simple case of linear elasticity, Equation 2.33 holds for $\mathbb{C}$ in terms of 2^{nd} Piola Kirchoff stresses $\mathbf{S}$ and Green-Lagrange strains $\mathbf{E}$.

$$\mathbb{C} = \frac{\mathbf{S}}{\mathbf{E}} \tag{2.33}$$

If the material behaviour is non-linear, this relation is only true on an incremental level:

$$\mathbb{C} = \frac{\partial\,\mathbf{S}}{\partial\,\mathbf{E}}. \tag{2.34}$$

Hyperelastic material models are well-suited for the representation of non-linear material behaviour and are explained to a larger extent in Holzapfel [59], Belytschko et al. [16] and Ogden [88]. The strain-energy function $\Psi = \Psi(\mathbf{F})$ is used to compute the stresses arising in a deformed state (see Equation 2.35). The scalar strain-energy function can incorporate a variety of material properties, including anisotropic behaviour, and is often expressed in terms of principal stretches or invariants of the right Cauchy-Green tensor $\mathbf{C}$ (Equation 2.33). The combination of these invariants basically determines the model's material behaviour. In order to ensure the

solvability while using hyperelastic material models, they need to be polyconvex (see Holzapfel [59], Schröder et al. [104] and Balzani [8]).

$$\boldsymbol{\sigma} = J^{-1}\ \mathbf{F}\left(\frac{\partial \Psi(\mathbf{F})}{\partial\, \mathbf{F}}\right)^{T} = 2J^{-1}\ \mathbf{F}\left(\frac{\partial \Psi(\mathbf{C})}{\partial\, \mathbf{C}}\right)\ \mathbf{F}^{T} \tag{2.35}$$

or

$$\mathbf{S} = 2\left(\frac{\partial \Psi(\mathbf{C})}{\partial\, \mathbf{C}}\right) \tag{2.36}$$

For the formulation of the Elasticity Tensor $\mathbb{C}$ in terms of the strain-energy function Ψ, Equations 2.34 and 2.36 lead to:

$$\mathbb{C} = 4\frac{\partial^2 \Psi(\mathbf{C})}{\partial\, \mathbf{C} \partial\, \mathbf{C}} \tag{2.37}$$

2.4 Membrane Materials

This section aims at an overview of the most common materials used for the building of membrane structures, as well as the comprehension of their mechanical properties. Available material models for numerical analysis are introduced and categorised with respect to their ability to represent these properties.

The materials that are commonly used to build structural membranes can be divided into two main categories: foils or films and coated woven fabrics. Foil structures are mostly built from ethylene tetrafluoroethylene (ETFE), whereas the most frequently used fabric materials are polyvinyl chloride (PVC)-coated polyester and polyfluoroethylene (PTFE)-coated glassfibre. The most important properties from a mechanical point of view are the material's tensile strength and its elastic properties. However, other factors like durability, insulation properties, fire protection, light transmission, foldability and cost also play a significant role in membrane design.

The interested reader is referred to Wagner [115], Knippers et al. [67] and Berger et al. [17] for detailed information on membrane materials; Al-

tenbach et al. [4], Colasante [32], Bridgens et al. [26] for material mechanics and modelling of textiles and foils; and Galliot et al. [45], Beccarelli [15] and Uhlemann [112] on testing procedures needed in order to generate mechanical constants for a predictive analysis.

Mechanical properties

While foils can be regarded as isotropic materials (i.e. the same elastic properties in all directions), coated woven fabrics are characterised by an orthotropic behaviour, governed by the interlacing warp and fill (or weft) yarns and the weaving techniques. Other techniques for interlacing yarns such as knitting, braiding and stitching can also be used for technical textiles but their application in membrane structures is very rare up to now (see e.g. Tamke et al. [108] and Popescu [93] for applications of knitted fabrics in the built environment). The plain weave and panama weave, shown in Figure 2.6, are usually found in woven membrane fabrics (compare e.g. Colasante [32]), placing the warp and fill yarns at a 90 °angle and interlacing every or every second yarn, respectively.

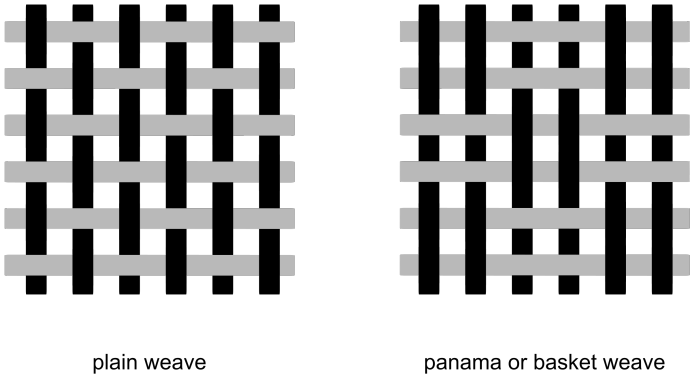

Figure 2.6: Warp and fill yarn orientation in plain weave and panama (or basket) weave.

The mechanical properties of membrane materials lie in a broad range. Starting from the category (foil or fabric), a number of factors can help to limit this range so that distinct values can be implemented into the available material models for analysis. It is current practice to use biaxial testing in order to determine these values on a project level. Uhlemann [112] and Mollaert et al. [79] summarise the requirements for adequate testing and explain the procedure. Being subjected to cyclic loading, membrane materials show hysteretic stress-strain curves. This means that the material properties are depending on the load-history, which is considered by the test protocols that were developed by material testing institutions as can be seen in Mollaert et al. [79]. Both foils and coated woven fabrics undergo creep, as described in Wagner [115]. This is usually considered in the magnitude of the initially applied prestress. Creep is a current research topic in the field of membrane design and future discoveries will be implemented in a harmonised code on compensation values for manufacturing.

Foils

Foils require complex numerical modelling due to the highly non-linear relationship between stresses and strains, as depicted in Figure 2.8 on the left. As mentioned above, they can be modelled as isotropic materials, i.e. by a Young's modulus E_{iso} and Poisson's ratio ν. For small strains, a linear-elastic part can be detected on the stress-strain path (see Figure 2.8), allowing for a simplification of the foil's material behaviour and the utilisation of the typically available St. Venant-Kirchoff material law (reduced to in-plane stresses and strains, see 2.7):

$$\begin{bmatrix} \epsilon_{11} \\ \epsilon_{22} \\ \gamma_{12} \end{bmatrix} = \begin{bmatrix} 1/E_{\text{iso}} & -\nu/E_{\text{iso}} & 0 \\ -\nu/E_{\text{iso}} & 1/E_{\text{iso}} & 0 \\ 0 & 0 & 1/G \end{bmatrix} \begin{bmatrix} \sigma_{11} \\ \sigma_{22} \\ \tau_{12} \end{bmatrix} \tag{2.38}$$

with the shear modulus G defined as:

$$G = \frac{E_{\text{iso}}}{2\,(1+\nu)} \tag{2.39}$$

In terms of hyperelasticity, with Lamé parameters λ and μ:

$$\Psi_{\text{StVenKir}} = \frac{1}{2}\,\lambda\,(\text{tr}(\mathbf{E}))^2 + \mu\,\text{tr}(\mathbf{E}^2) \tag{2.40}$$

$$\mu = \frac{E_{\text{iso}}}{2\,(1+\nu)} \tag{2.41}$$

$$\lambda = \frac{\nu\, E_{\text{iso}}}{(1+\nu)(1-2\,\nu)} \tag{2.42}$$

As the assumption of linear-elastic material behaviour is only valid for a very small range of strains, more complex constitutive models are needed. An overview of these is presented in the following section.

Coated woven fabrics

Coated woven fabrics consist of the weave and at least one layer of coating. While the yarns provide the necessary tensile strength and stiffness, coating is necessary in order to achieve sufficient weatherability and hence durability and additionally influences the shear stiffness. The material behaviour of these composites hence depends on the mechanical characteristics of the single components, as well as their interaction. Since the manufacturing of these fabrics has a major influence on the mechanical properties, it is briefly explained. Polyester and glassfibre yarns are used in the majority of membrane materials nowadays, but fabrics made from aramid, nylon, liquid crystal polymer (LCP), cotton and PTFE yarns also exist, see Colasante [32] for the specific properties and fields of application. Warp yarns typically run along the length of a roll and are kept fairly straight during production, or even prestressed, while fill yarns are woven between them in orthogonal direction, resulting in a high crimp (see Figure 2.6). Apart from the individual strength of the warp and fill yarns, this crimp influences the overall material behaviour. Being subjected to tension, the fill yarns will initially straighten (this is called constructional stretch) before they transfer forces and fully interact with the warp yarns in the so-called crimp-interchange. For a material built in this way, the Poisson's ratio can be beyond 0.5 (see e.g. Wagner [115] and Gade et al. [43]). This results in a highly non-linear, orthotropic material behaviour depending on the weave, applied stress ratio and loading history. Apart from the protection against water and stains, the coating provides shear stiffness. Polyester yarns are mostly coated by polyvinyl chloride (PVC) and glassfibre yarns by polyfluoroethylene (PTFE). Among other factors, the stress-strain behaviour of the coating is influenced by the strain state of the yarns.

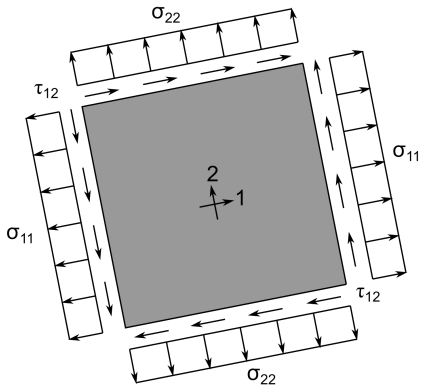

Figure 2.7: Plane stress components.

The overall stress-strain relations of coated woven fabrics can be subdivided into three regions: inter-fibre-friction, constructional stretch or decrimping and material strain of yarns, see Figure 2.8. Hence different Young's moduli and Poisson's ratios are needed for the fundamental construction stages of prestressing and initial subjection to loading, as well as for the compensation values. In Wagner [115], the kinematics of the yarns is illustrated in relation to this.

As for foils, a simplified approach to the material modelling can be chosen for limited strain ranges of coated woven fabrics. However, St. Venant Kirchoff material law has to be extended to account for the different Young's moduli in warp and fill direction, E_1 and E_2. This was done by Münsch et al. [84], leading to the following expression:

$$\begin{bmatrix} \epsilon_{11} \\ \epsilon_{22} \\ \gamma_{12} \end{bmatrix} = \begin{bmatrix} 1/E_1 & -\nu_{12}/E_1 & 0 \\ -\nu_{21}/E_2 & 1/E_2 & 0 \\ 0 & 0 & 1/G \end{bmatrix} \begin{bmatrix} \sigma_{11} \\ \sigma_{22} \\ \tau_{12} \end{bmatrix} \tag{2.43}$$

with

$$\frac{\nu_{12}}{E_1} = \frac{\nu_{21}}{E_2} \tag{2.44}$$

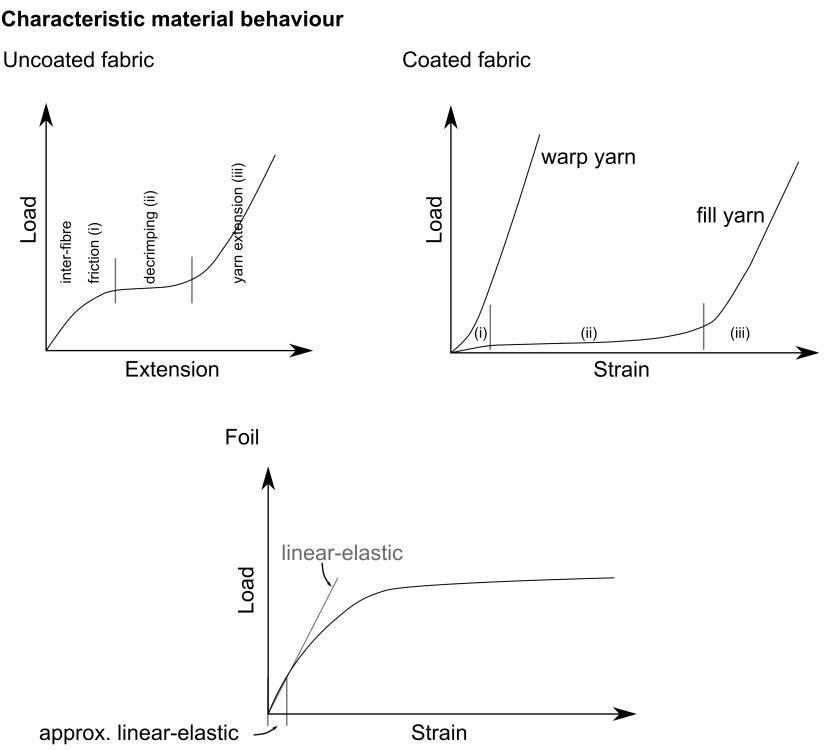

Figure 2.8: Top: characteristic load-extension graphs of fabric and foil. Bottom: characteristic material behaviour of foils and fabric under cyclic loading, according to Blum et al. [20] and Reinhardt [100]

Constitutive models

Membrane materials hence typically show a highly non-linear, hysteretic and in the case of woven fabrics anisotropic behaviour that needs to be represented by material models in numerical analysis. In order to do this, the main characteristics need to be captured by a number of parameters that finally build up the elasticity tensor $\mathbb{C}$ (see Equations 2.33 and 2.37).

The simplest approaches by using the St. Venant Kirchoff material law and its extension to orthogonal material was briefly shown in the previous section. However, since the already mentioned limitations are not satisfactory, material modelling remains a current research topic. This section will provide an overview of the prevailing methods and their applicability for the analysis of structural membranes made from textiles and foils. A summary of selected models along with the publications are given in Table 2.3 at the end of this section.

In general, material behaviour can be described by micro-, meso- and macro-level models. The main characteristics that distinguish these models are listed in Table 2.2.

Table 2.2: Material modelling on different levels.

micro-model	meso-model	macro-model
molecular interactions are modelled	single elements for characteristic properties (unit-cell method)	material as a continuum (incl. directional properties)

Micro-models consider molecular interactions and are far too detailed and computationally costly for the purpose of structural analysis for membranes, see e.g. Ballhause [7].

Meso-models

The unit-cell method on a meso-level is particularly suitable to model woven fabrics, as the single yarns and their interactions can be represented appropriately, see e.g. Colasante [32] and Wagner [115] for an overview. In this method, fabric is classified as a composition of repetitive entities, the so-called unit-cells. Within these, every yarn is represented by a truss element and the crimp interchange as well as shear is considered through

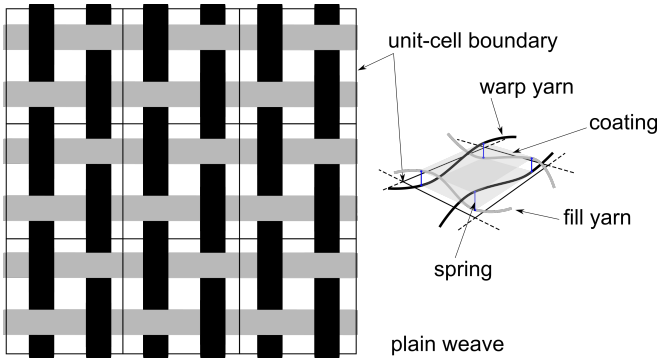

Figure 2.9: Unit-cell model for woven fabric: basic sketch.

springs inbetween, as indicated by the schematic sketch in Figure 2.9. The unit-cell is linked to each finite element of the analysis model and adds a computational step and interface in every analysis step, as shown in Figure 2.10. This leads to numerically costly analyses and possibly to limitations of the FE mesh, see Kaiser [64]. However, as shown in Gade et al. [43], the detail in the characteristics of coated woven fabrics can be extended to the desired level in an intuitive way, by e.g. allocating springs. For further reading and the detailed explanation of some meso-models fitted for coated woven fabrics, Menges, G. and Meffert, B. [75], Bridgens et al. [27] and Bögner-Balz et al. [22] are suggested. A profound knowledge of the processing of biaxial test data to the respective elements of the unit-cell is substantial for their successful usage in predictive analysis.

Macro-models

The phenomenological approach regards the material as a continuum. So-called macro-models are defined with the aim of representing the material properties on this continuous level.

In principle, this can be dealt with in two ways for membranes: one either guarantees the stresses and strains of a membrane to stay in a certain range and limits the material model to this range or considers an extension to multi-linear elastics models, see Dieringer [37] and Uhlemann et al. [113] or one tries to apply a more sophisticated material model that can represent

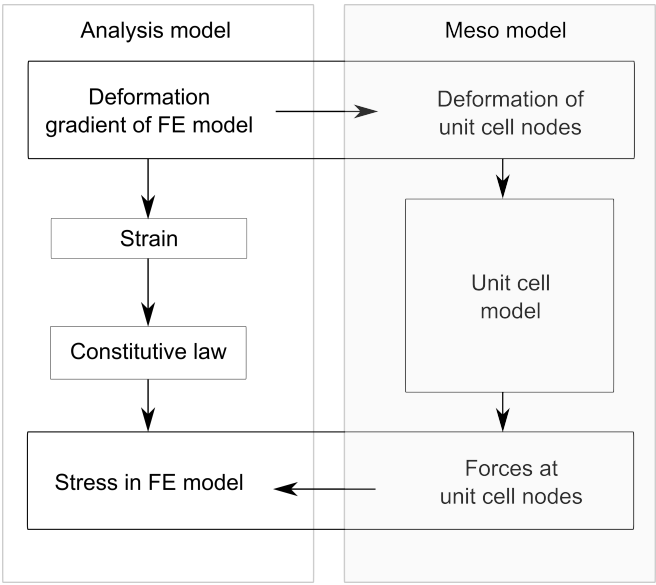

Figure 2.10: Unit-cell model for woven fabric: process in FE program.

the textile's behaviour over a large range of stresses and strains.

In many cases, linear elastic material models are applied for the analysis of membranes. As an extension of Hooke's law to two dimensions, the St. Venant-Kirchoff material model is the simplest macro-model that can be used for large deformations and small strains, assuming isotropic properties, see Equation 2.38. It was extended to orthotropic linear elasticity by Münsch et al. [84] so that warp and fill can be represented with individual Young's moduli, see Equation 2.43. Multi-linear models have also been investigated in order to account for the non-linear behaviour by introducing several stages, see Dieringer [37].

Furthermore, a large number of hyperelastic material models have been developed to deal with non-linear material behaviour and anisotropy. Colasante [32] provides a detailed overview of a large number of hyperelastic models for coated woven fabrics and introduces a new approach. Based

on this, further developments are presented in Motevalli et al. [83], considering the key prerequisite of polyconvexity to ensure the solvability (see e.g. Schröder [103], Balzani [8]). Recent publications show, that hyperelastic material models are able to represent the behaviour of coated woven fabrics to an acceptable extent, see Table 2.3.

However, these models require complex testing procedures and data processing to be performed in order to determine the necessary input parameters. Therefore, the development of suitable material models for membrane structures is presently pursued as a relevant research topic at a number of institutes.

Table 2.3: Material models and applicability for textiles and foils.

model	non-linearity	anisotropy	further reading
unit-cell	yes	yes	Gade et al. [43], Kaiser [64]
St. Venant Kirchoff	no	no	Holzapfel [59]
Münsch-Reinhardt	no	yes	Münsch et al. [84]
Neo-Hooke	yes	no	Holzapfel [59]
Bonet-Burton	yes	yes	Bonet et al. [23]
Aimene	yes	yes	Aimene et al. [1]
Colasante	yes	yes	Colasante [32]
response surfaces	yes	yes	Widhammer [116], Coelho et al. [29]
polyconvex hyperelastic	yes	yes	Motevalli et al. [83]

2.5 Discretisation and Finite Element Method

The well-known Finite Element Method (FEM) uses spatial discretisation in order to approximate the description of geometry and solution fields (e.g. displacements, stresses), limiting the infinite number of unknowns to a finite one and thus ensuring the solvability of mechanical problems. Any mechanical analysis is solved at the discrete nodes of the Finite Elements and approximated by basis functions within the elements. The discretised model of a continuum is generated by the meshing process. Detailed explanations of this can be found in a vast variety of literature, for example Bathe [11], Belytschko et al. [16], Zienkiewicz [119] and Topping [110].

A continuous surface $\mathbf{S}$ is approximated by n_{ele} elements, see Equation 2.45. The approximated entity is usually indexed by h. With the exception of this section, the index h is implied but not explicitly given in this thesis.

$$\mathbf{S} \approx \mathbf{S}_h = \bigcup_{e=1}^{n_{\text{ele}}} \Omega_e \tag{2.45}$$

The basis functions $N_i(\xi, \eta)$ can be linear or of higher order and provide the approximation of solution fields within the elements with local coordinates (ξ, η), e.g. the displacements $\mathbf{u}_h$ calculated from the discrete displacements $\hat{u}_i$ as shown in Equation 2.46.

$$\mathbf{u}_h = \sum_{i=1}^{n_{\text{nodes}}} N_i(\xi, \eta)\hat{u}_i \tag{2.46}$$

Solution approach: weak form

Mechanical analyses looking for an equilibrium of internal and external forces can be solved in two general ways: solving the equilibrium directly, i.e. the strong form, or solving the weak form of an equation. The weak form of a static equilibrium can be expressed by the principle of virtual work and split up into internal and external work contributions (Equations 2.48 and 2.49). The latter can be defined in the reference configuration denoted by Ω_0 with density ρ_0, body forces $\mathbf{B}$, and Γ_0 for the boundaries subjected to forces $\mathbf{T}$. In the current configuration Ω, body forces $\mathbf{b}$ and

forces $\mathbf{t}$ on the boundaries Γ are considered.

$$\delta W = \delta W_{\text{int}} + \delta W_{\text{ext}} = 0 \tag{2.47}$$

$$-\delta W_{\text{int}} = \int_{\Omega_0} \mathbf{S} : \delta \mathbf{E} \; d\Omega_0 = \int_{\Omega} \boldsymbol{\sigma} : \delta \mathbf{e} \; d\Omega \tag{2.48}$$

$$\begin{aligned} \delta W_{\text{ext}} &= \int_{\Gamma_0} \mathbf{T} \cdot \delta \mathbf{u} \; d\Gamma_0 + \int_{\Omega_0} \rho_0 \mathbf{B} \cdot \delta \mathbf{u} \; d\Omega_0 \\ &= \int_{\Gamma} \mathbf{t} \cdot \delta \mathbf{u} \; d\Gamma + \int_{\Omega} \rho \mathbf{b} \cdot \delta \mathbf{u} \; d\Omega \end{aligned} \tag{2.49}$$

As the virtual strains $\delta \mathbf{E}$ and $\delta \mathbf{e}$ arise from the virtual displacements $\delta \mathbf{u}$, Equation 2.47 can be written in terms of $\delta \mathbf{u}$ as follows:

$$\delta W = \frac{\partial W}{\partial \mathbf{u}} \delta \mathbf{u} = 0 \tag{2.50}$$

The non-trivial solution of Equation 2.47 requires $\delta \mathbf{u}$ to be unequal zero. In a discretised field, it can be written that

$$\delta W = \frac{\partial W}{\partial \mathbf{u}_h} \delta \mathbf{u}_h = -\mathbf{R} \; \delta \mathbf{u}_h = 0, \tag{2.51}$$

with $\mathbf{R}$ denoting the vector of unbalanced forces that needs to vanish. The Newton-Raphson algorithm can be used to solve Equation 2.51:

$$LIN(\mathbf{R}) = \mathbf{R} + \frac{\partial \mathbf{R}}{\partial \mathbf{u}_h} \Delta \mathbf{u}_h = \mathbf{R} + \mathbf{K} \Delta \mathbf{u}_h \tag{2.52}$$

Equation 2.52 already implies the interpretation of $\partial \mathbf{R} / \partial \mathbf{u}_h$ as the stiffness matrix $\mathbf{K}$. Written in components, the vector of unbalanced forces R_r and the stiffness matrix K_{rs} can be expressed with $r, s = 1, ..., n_{\text{DOF}}$:

$$R_r = -\frac{\partial W}{\partial u_r} = -\frac{\partial W_{\text{int}}}{\partial u_r} - \frac{\partial W_{\text{ext}}}{\partial u_r} = R_r^{\text{int}} + R_r^{\text{ext}} \tag{2.53}$$

$$K_{rs} = \frac{\partial R_r}{\partial u_s} = -\frac{\partial^2 W}{\partial u_r \partial u_s} = -\frac{\partial^2 W_{\text{int}}}{\partial u_r \partial u_s} - \frac{\partial^2 W_{\text{ext}}}{\partial u_r \partial u_s} = K_{rs}^{\text{int}} + K_{rs}^{\text{ext}} \tag{2.54}$$

2.6 Isogeometric B-Rep Analysis

The aim of Isogeometric Analysis (IGA) and Isogeometric B-Rep Analysis (IBRA) as its extension, is to use the design model from Computer Aided Design (CAD) for analysis and hence to contain all data of the geometry. It thus overcomes the problems related to the conversion of CAD models to classical meshed FEM models (e.g. data loss, time and computational effort spent) and unifies CAD and Computer Aided Engineering (CAE). IGA was first introduced by Hughes et al. [61] with the basic idea of applying the isoparametric concept of FEM to NURBS and the CAD model. A large number of developments in various engineering disciplines followed, as well as the introduction of IGA to the industry.
Throughout this thesis, the concept of IBRA and analysis in computer aided design (AiCAD) by Breitenberger et al. [25] is applied. Details on the method can be found in Breitenberger [24] and Bauer [14]. IBRA uses the full B-Rep model from CAD for analysis, i.e. the geometry and topology. The B-Rep entities are consistently enhanced with mechanical properties. The possibility of analysing trimmed multipatch models within a possibly parametric CAD environment holds a number of advantages for the design of lightweight structures and membranes in particular, as will be shown in detail in Chapter 4. This section will briefly describe the fundamentals of IBRA as the basis of the CAD-integrated design cycle of structural membranes.

NURBS

The concept of Non-Uniform Rational B-Splines, or NURBS, is the foundation of surface and curve description in most modern CAD programs. The NURBS curve $\mathbf{C}(\xi)$ is described by the sum of its n control points $\mathbf{P}_i$ and the related weighted (w_i) B-Spline functions ($N_{i,p}(\xi)$), summarised as $R_{i,p}(\xi)$, see Equations 2.55 and 2.56.

$$\mathbf{C}(\xi) = \sum_{i=1}^{n} R_{i,p}(\xi) \cdot \mathbf{P}_i \tag{2.55}$$

$$R_{i,p}(\xi) = \frac{N_{i,p}(\xi) \cdot w_i}{\sum_{j=1}^{n} N_{j,p}(\xi) \cdot w_j} \tag{2.56}$$

B-Splines are defined by their knot-vector Ξ and the polynomial degree p, see Equation 2.57. They are C^∞-continuous inside a knot span, while the continuity across knots depends on the multiplicity k of the knot, C^{p-k}. More details on NURBS and B-Splines can be found in Cohen et al. [31], Cottrell et al. [35] and Piegl et al. [92].

$$N_{i,p}(\xi) = \frac{\xi - \xi_i}{\xi_{i+p} - \xi_i} N_{i,p-1}(\xi) + \frac{\xi_{i+p+1} - \xi}{\xi_{i+p+1} - \xi_{i+1}} N_{i+1,p-1}(\xi) \tag{2.57}$$

The following holds for the B-Spline basis functions:

- partition of unity: $\sum_{i=1}^{n} N_{i,p}(\xi) = 1$
- non-negativity: $N_{i,p}(\xi) \geq 0$
- linear independence: $\sum_{i=1}^{n} \alpha_i N_{i,p}(\xi) = 0$ only if $\alpha_i = 0$

Figure 2.11 shows a NURBS curve (polynomial degree $p = 3$) with knot vector $\Xi = [0,0,0,0,0.25,0.5,0.75,1,1,1,1]$, control points $\mathbf{P}_i$ and corresponding basis functions.
NURBS surfaces $\mathbf{S}$ are defined with the parametric dimensions ξ, η within the control point net $m \times n$. The respective polynomial degrees of the basis functions $N_{i,p}(\xi)$ and $M_{j,q}(\eta)$ are p and q.

$$\begin{aligned} \mathbf{S}(\xi,\eta) &= \sum_{i=1}^{n}\sum_{j=1}^{m} \frac{N_{i,p}(\xi) M_{j,q}(\eta) w_{ij}}{\sum_{k=1}^{n}\sum_{l=1}^{m} N_{k,p}(\xi) M_{l,q}(\eta) w_{kl}} \mathbf{P}_{ij} \\ &= \sum_{i=1}^{n}\sum_{j=1}^{m} R_{ij,pq}(\xi,\eta) \mathbf{P}_{ij} \end{aligned} \tag{2.58}$$

NURBS are used for the geometry representation as well as the basis functions for the mechanical analysis in IBRA. Consequently, the displacements are also described by the same basis functions. Note that the discrete degrees of freedom, here displacements $\hat{u}_i$, are also attributed to the control points of the NURBS geometry, as shown in Figure 2.12.

$$u(\xi) = \sum_{i=1}^{n} R_{i,p}(\xi) \cdot \hat{u}_i \tag{2.59}$$

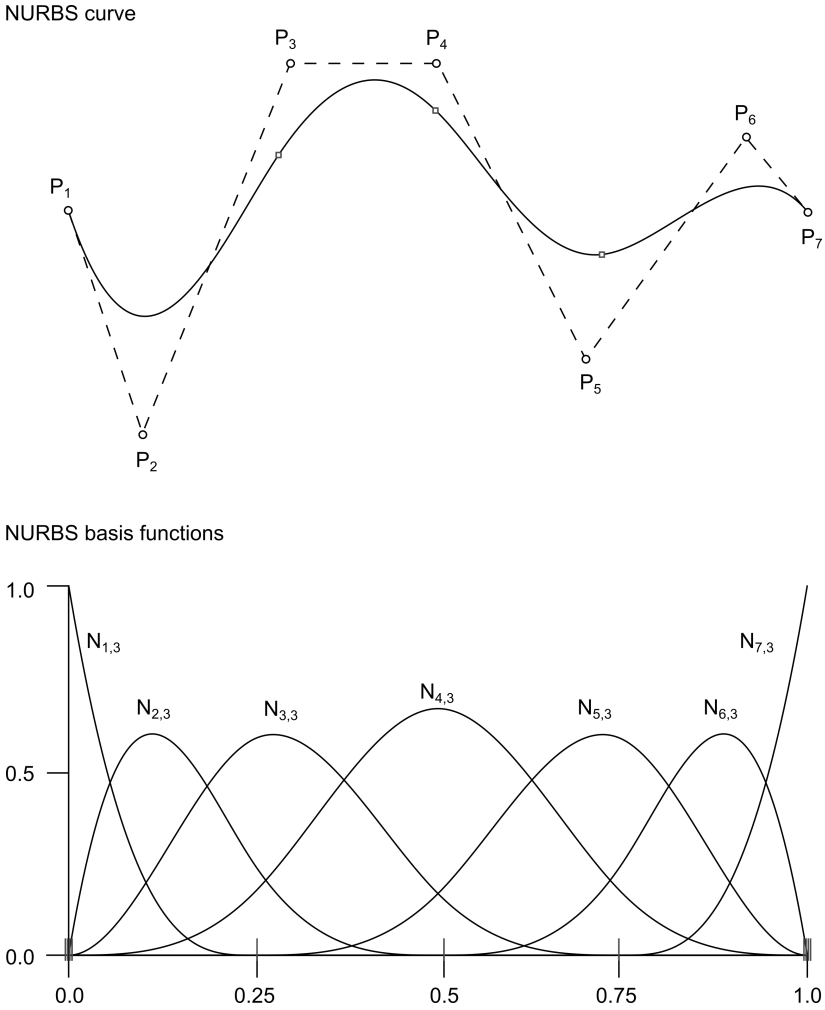

Figure 2.11: NURBS curve (polynomial degree $p = 3$) with knot vector $\Xi = [0,0,0,0,0.25,0.5,0.75,1,1,1,1]$, control points $\mathbf{P}_i$ and corresponding basis functions.

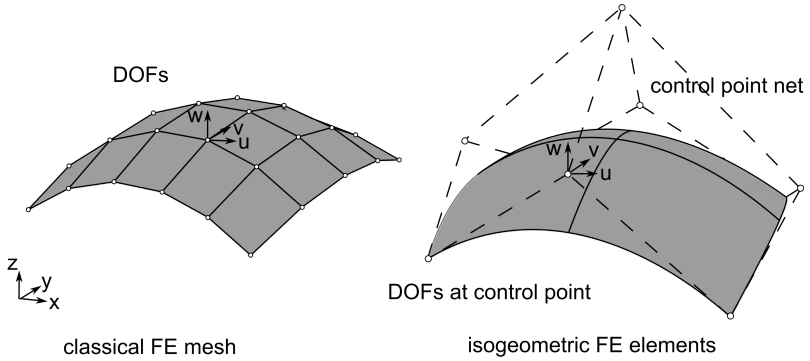

Figure 2.12: Left: classical FE mesh with DOFs on the approximated surface. Right: isogeometric FE elements with DOFs at the control points of the control point net.

B-Rep models

The description of a geometry as a B-Rep (Boundary-Representation) model is very common in CAD software. As suggested by the name, it entails the description of the geometrical entities and their connections with the boundaries, i.e. edges as face boundaries or vertices as edge boundaries. Table 2.4 lists the topological entities of B-Rep models along with the corresponding geometrical ones. Figure 2.13 illustrates the principle for a volumetric body built from several faces. See e.g. Mäntylä [70] and Mortenson [81] for in-depth information.

Table 2.4: B-Rep models: topology and geometry.

topological entity	geometrical entity
face (F)	surface (S)
edge (E)	curve (C)
vertice (V)	point (P)

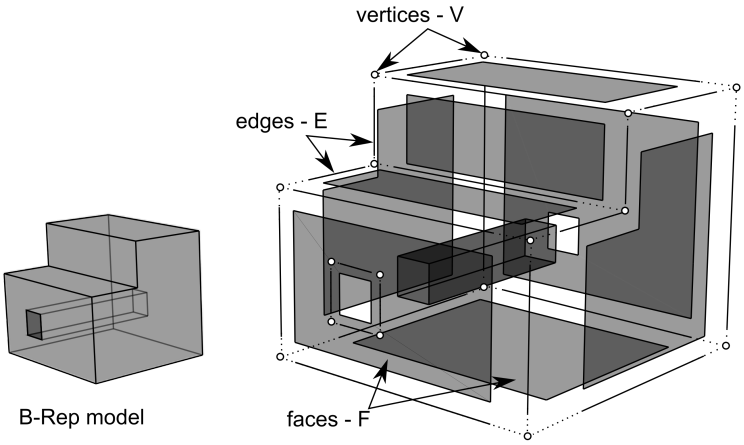

Figure 2.13: Trimmed B-Rep model with topological assembly of faces, edges and vertices.

Trimming

Trimming is a powerful tool in CAD that enlarges the design space significantly. It divides geometries into visible and hidden domains by creating intersections on NURBS surfaces. The geometrical information of a trimmed NURBS surface hence still entails the complete surface description, but trimming curves $\overline{C}(\overline{\xi})$ build its edges, see Figure 2.14. So-called trimming loops are defined in the parameter space by these trimming curves, separating a surface into visible parts (that will later be considered for the analysis) and outside parts.

Refinement

For a sufficient number of design handles and appropriate mechanical approximation of NURBS-based B-Rep models, refinement can be necessary even if the starting geometry is represented accurately. An extreme example for this is shown in Figure 2.15 for the formfinding of a hypar. Due to the intentionally bad discretization created by a polynomial degree

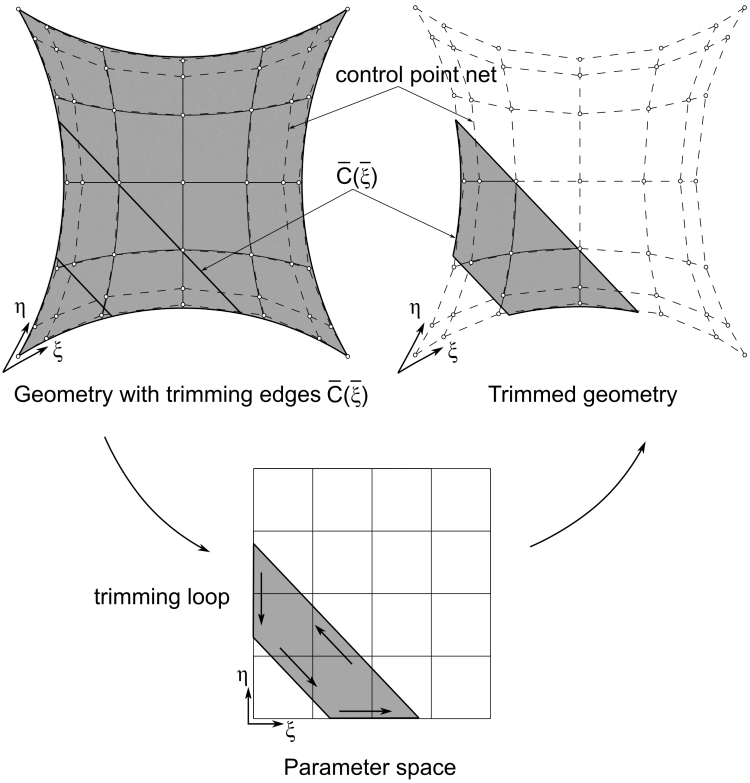

Figure 2.14: Left side: trimming curves $\overline{C}(\overline{\xi})$ on a hypar surface with control point net. Right side: trimmed pattern patch with control point net. Bottom: parameter space with trimming loops.

of $p = q = 1$ for the NURBS basis functions and only 2 elements in both directions, the only control points and thus degrees of freedom lie at the intersections of the depicted parameter lines. On the right side, successful formfinding is depicted for $p = q = 3$ and $u = v = 4$, i.e. a sufficient number of DOFs. More examples and detailed explanations can be found in Bauer [14]. Refinement can be realised by *knot insertion* and *order elevation* or a combination of both, always leading to an increased number of control

points. One of the advantages of CAD-integrated design and analysis is the fact, that the geometry remains intact and does not change with refinement. Further information on refinement and the different techniques can be found in Boehm [21], Cohen et al. [30], Piegl et al. [92] and Rogers [102].

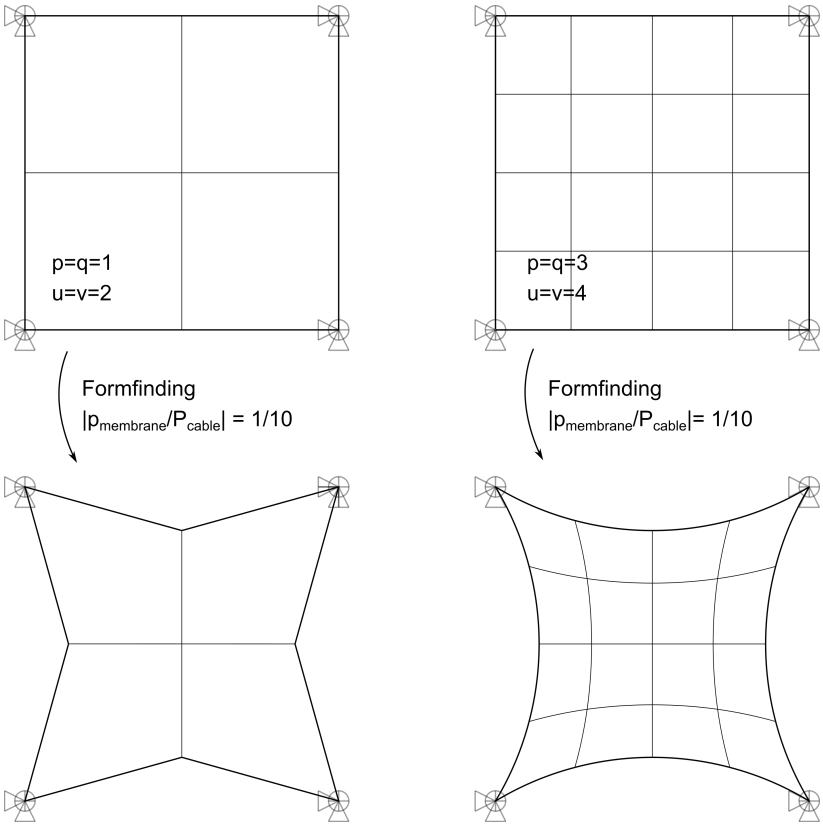

Figure 2.15: Different discretisations of a hypar. Left side: polynomial degree $p = q = 1$ and $u = v = 2$ elements in both directions. Right side: polynomial degree $p = q = 3$ and $u = v = 4$ elements in both directions.

Coupling and embedded elements

The coupling of NURBS-patches is a large field of research within the IGA community. Several branches of coupling methods are currently pursued, but will not be presented here as they were not part of the scope of this thesis. For further reading Apostolatos et al. [6], Bauer [14], Breitenberger [24] and Marussig et al. [71] are suggested. Explicit coupling methods enforce additional conditions by e.g. introducing penalties to deformations of the coupling domain in the weak formulation of equilibrium. A very powerful method for the implicit coupling of different geometric entities is the concept of embedded elements by Bauer et al. [12] and Philipp et al. [90]. In this concept, mechanical properties like support and coupling conditions are defined inside the parameter space of a master patch, redefining the geometry description of a slave patch. A number of embedded elements has been developed, including trusses, beams, cables, membranes, plates and shells.

Summary

This chapter reviews the characteristics of membranes and links them to the challenges arising in the Computer-Aided Design and Engineering of these especially light structures. Furthermore, it summarises the essential parts of differential geometry and continuum mechanics needed for the analysis of structural membranes under consideration of the interaction of form and force. The most common materials for membranes and their properties are introduced and the challenges of material modelling are pointed out along with available constitutive models. Finally, Finite Element Method (FEM) and Isogeometric B-Rep Analysis (IBRA) are explained as the basic techniques for solving the analyses of the parametric CAD-integrated design cycle of structural membranes as constituted in Chapter 3.

CHAPTER 3

THE DESIGN CYCLE OF STRUCTURAL MEMBRANES

Membrane structure design and analysis entails the highly non-linear and interactive steps of formfinding, structural analysis and cutting pattern generation, as shown in Figure 3.1. All three steps must be completed in accordance with each other, in order to successfully design a structure that meets both aesthetic and structural requirements. This leads to the so-called design cycle of structural membranes, which explicitly considers the interactivity of the design steps.

Membranes exclusively withstand external loads through tensile forces. Hence, membrane structures function through the stiffness generated by the combination of geometry (curvature) and prestress, in contrast to more conventional structures that have a considerable bending stiffness. This chapter presents the challenges of performing formfinding, structural analysis and cutting pattern generation and additionally shows the benefits of mounting analysis for the designer. Apart from the general problem definition for every design step, successful numerical solution strategies

are demonstrated. The described analyses for the design steps are available for CAD-integrated design within the research code Carat++ [28] and can be accessed by the plug-in Kiwi!3d [66], as is highlighted in Chapter 4 along with the interactivity of the design steps.

Parts of this chapter were originally published in Goldbach et al. [49] and have been translated from German.

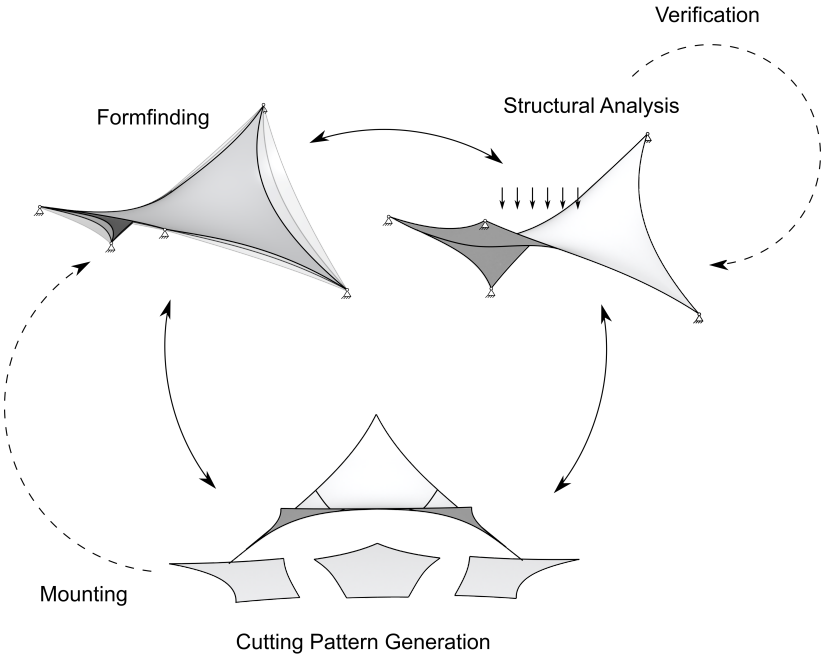

Figure 3.1: Design cycle of structural membranes.

3.1 Formfinding

In the formfinding of membranes, an equilibrium surface is determined which fulfils the specified conditions of prestress in both the membrane and the cables for defined boundary conditions. It is not possible to draw these mostly double-curved geometries without formfinding "just so" that the forces from prestress are in equilibrium in the unloaded state. Consequently, one needs to predefine fixed boundaries for a design idea, such as anchorage points or supported edges, as well as flexible boundaries such as edge cables. The membrane surface can then span the distances between these boundaries with a predefined stress (so-called prestress). Since the geometry of a membrane structure is found for the named conditions, numerical formfinding is classified as an inverse problem. Altering the relation of prestress in the membrane and edge cables in the design phase of formfinding leads to different surface geometries (and support forces). It is the designer's task to find the optimal ratio of prestress in the structure for the original design idea.
The Boiler formula depicts the equilibrium between an edge cable and the attached membrane and the correlation of curvature, as portrayed in Figure 3.2, and can help to define a prestress ratio for first design iterations. From physical models to numerical methods, there is a wide variety

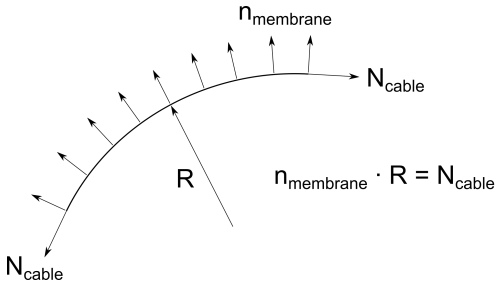

Figure 3.2: Boiler formula

of methods for formfinding (see Veenendaal et al. [114] for an overview), which will be summarised in the following.

3.1.1 Physical formfinding strategies

Especially in the beginnings of building membrane structures, designers like Frei Otto used soap films, cable net models and tight models to investigate different shapes and the structural behaviour of their design ideas. With the help of tight models, the designer quickly gets a feeling for various shapes and the effect of different boundary conditions by pulling tights or other flexible textiles into them. They are still used today to generate and test initial design ideas. Figure 3.3 shows a variety of early-stage tight models built in a students' workshop at TUM. Soap film models provide a good insight into possible minimal surface geometries, as the condition of isotropic stress is naturally fulfilled in a soap film or soap bubble. At the Institute for Lightweight Structures (IL) in Stuttgart, a soap film machine was built within a pressurized chamber in order to stabilize soap film models for photography - making it possible to study their geometries in detail (Otto et al. [89]). With the help of cable net models that were equipped with small weights and devices tracking the cable forces, insight into the structural behaviour was generated. Several membrane and cable-net structures were successfully built based on physical models, see Meissner et al. [74]. While these physical models are easily built on a rather simple level in order to generate a large variety of shapes in a small scale, the mechanical interpretation requires sophisticated models. In times of readily available simulation tools, the expertise of crafting these models has become uncommon.

3.1.2 Numerical formfinding strategies

With computational tools and power being commonly available, numerical formfinding has become the standard approach to generate equilibrium surfaces for structural membrane design. The mathematical and mechanical approach are presented in the following.

Mathematical approach

For the condition of isotropic prestress, formfound surfaces coincide with minimal surfaces, i.e. the surface with the minimum area content between the given boundaries. Minimal surfaces have been investigated by mathematicians for a very long time. In general, they can be found by solving

Figure 3.3: Students' experimental tight models from a workshop at TUM.

the optimisation problem stated in Equations 3.1 and 3.2.

$$a = \int da \rightarrow \min \tag{3.1}$$

or

$$\delta a = \int_A \det \mathbf{F}\, \mathbf{F}^{-T} : \delta \mathbf{F}\, dA = 0 \tag{3.2}$$

Minimal surfaces are characterized by zero mean curvature at any point of the surface (as introduced in Equation 2.16), i.e. the radii of curvature at any point have the same size but opposite directions.

Mechanical approach

The mechanical approach to formfinding allows the designer to find equilibrium surfaces for arbitrary anisotropic stress fields. Since a large number of membrane structures are built from woven textiles with different properties in warp- and weft-direction, and construction conditions might require anisotropic prestressing, this is beneficial for the design. The input parameters for numerical formfinding with a mechanical approach are the prestress in membrane (for woven fabrics p_{warp} and p_{weft})and cables (P_{cables}), as well as the geometry and topology of the boundaries. For hybrid

structures consisting of tensile and compressive elements, the bending stiffness of compressive elements can be included in the formfinding. This is explained in detail in e.g. Bauer [14]. For pneumatic structures the internal pressure needs to be considered as a permanent load. Other permanent loads can also be considered for formfinding, of course. The aim of finding an equilibrium surface can be reached by various strategies. This section gives an overview of the most prominent ones.

The force density method was the first numerical method for formfinding and was developed by Linkwitz et al. [69] for cable-net structures during the planning and construction of the roofs at the Olympic Park in Munich. Due to the size and complexity of the cable-net roofs, the limits of physical models were reached. The introduction of the *force density* led to a feasible problem formulation that is still in use in modern programs for the formfinding of cable-nets and membranes today.

The Updated Reference Strategy (URS) by Bletzinger et al. [19] is based on the force density method and extends it to surfaces. As this method is used for the formfinding in the presented CAD-integrated design cycle, it will be explained in more detail.

A different approach to formfinding that is widely used, is the method of dynamic relaxation, that was initially developed by Barnes [9]. Dynamic relaxation finds an equilibrium surface by letting it oscillate until the equilibrium state is reached.

Updated Reference Strategy

The Updated Reference Strategy (URS) by Bletzinger et al. [19] is a generalisation of the force density method for membrane surfaces. In the URS, the equilibrium is searched for with the help of the virtual work δW_{URS}, where the so-called homotopy factor λ determines the respective influence of the virtual work δW_{cur} of the current geometry in the course of the iterative process and of the virtual work δW_{ref} of an initially freely selectable reference geometry, see Equation 3.3. In the formfound state, the reference and the current state correspond to each other and the working expression δW_{URS} vanishes. Both states are evaluated in a completely geometrically non-linear way. Thus the actual virtual work δW_{cur}, Equation 3.4, is formed from Cauchy stresses $\boldsymbol{\sigma}_0$, virtual Euler-Almansi strains $\delta\mathbf{e}$, external loads $\mathbf{p}$ and virtual deformations $\delta\mathbf{u}$, while Piola-Kirchhoff 2^{nd} order stresses $\mathbf{S}_0$

and virtual Green-Lagrange strains $\delta \mathbf{E}$ are included in the stabilisation term - the virtual work of the reference state δW_{ref}, Equation 3.5. Further details are described in Bletzinger et al. [19]. Figure 3.4 shows the formfinding process with URS for a simple membrane structure. The homotopy factor λ was set to 1 for this example.

$$\delta W_{\text{URS}} = \lambda \cdot \delta W_{\text{cur}} + (1-\lambda) \cdot \delta W_{\text{ref}} = 0 \tag{3.3}$$

$$\delta W_{\text{cur}} = \delta W_{\text{int}} + \delta W_{\text{ext}} = -\int_{\Omega} (\boldsymbol{\sigma}_0 : \delta \mathbf{e}) d\Omega + \int_{\Omega} (\mathbf{p} : \delta \mathbf{u}) d\Omega = 0 \tag{3.4}$$

$$\delta W_{\text{ref}} = \delta W_{\text{ref,int}} + \delta W_{\text{ref,ext}} = -\int_{\Omega_0} (\mathbf{S}_0 : \delta \mathbf{E}) d\Omega_0 + \int_{\Omega_0} (\mathbf{p} : \delta \mathbf{u}) d\Omega_0 = 0 \tag{3.5}$$

In order to solve the governing equations of URS, the Newton-Raphson algorithm can be applied as mentioned in Section 2.5.

As the equations of the URS show, external loads can also be included in the formfinding process. This is especially important for the formfinding of pneumatic membranes, also considering the changes of direction of the compressive loads during formfinding, which leads to further nonlinear relationships between shape and load and consequently to further contributions to the geometric stiffness of the structure.

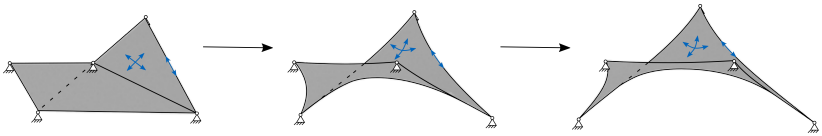

Figure 3.4: Formfinding process of a simple membrane structure with URS: from left to right: initially defined geometry and boundary conditions, geometry after one analysis step, geometry converged to an equilibrium surface.

3.2 Structural Analysis and Verification

The structure resulting from the formfinding process is examined in the structural analysis in order to predict its deformation and stress state under external loads. The main design requirements can be summarised in the following four points:

- stress limits (based on material strength and stress factors)
- deflection limits (based on serviceability and contact to supporting structures)
- avoidance of ponding (positive drainage)
- avoidance of slackness and wrinkling (to ensure durability and aesthetics)

The validity of structural analysis of membranes under external loading is a current research topic aiming at reliable verification procedures, e.g. investigated in Gosling et al. [53], Pyl et al. [97, 98], Smedt et al. [106, 107] and Zhang et al. [118].

Typical loads on membrane structures emerge from snow and dead loads (with a constant load direction along gravity) and wind (in normal direction to the surface, hence changing with deformation). Figure 3.5 shows the deformation of a highly curved membrane under snow and wind load, highlighting the respective tension areas that mainly transfer the load to the supports.

Particular attention needs to be paid to wind loads, especially for large structures. On the one hand, the double-curved shapes of membrane structures rarely allow a normative determination of wind pressures and hence surface loads. On the other hand, the often very large deformations result in changes of shapes and thus volatile surfaces of attack. Wind-tunnel testing can only give limited information, because of scaling challenges arising due to the membranes' extremely low section height and the lack of flexibility of the mostly rigid models. By means of fluid-structure interaction (FSI), membranes can be investigated in the numerical wind tunnel. This is the subject of other, current research projects, see e.g. Zorrilla Martinez [120], Colliers et al. [33], Michalski et al. [77, 78] and Apostolatos et al. [5]. These FSI simulations can also be used to account for the added mass effect,

which deals with the behaviour of a wind-induced oscillating membrane and the damping due to the surrounding air's mass. The added mass effect appears for very light structures and has been researched in-depth in the work of AlSofi et al. [3].

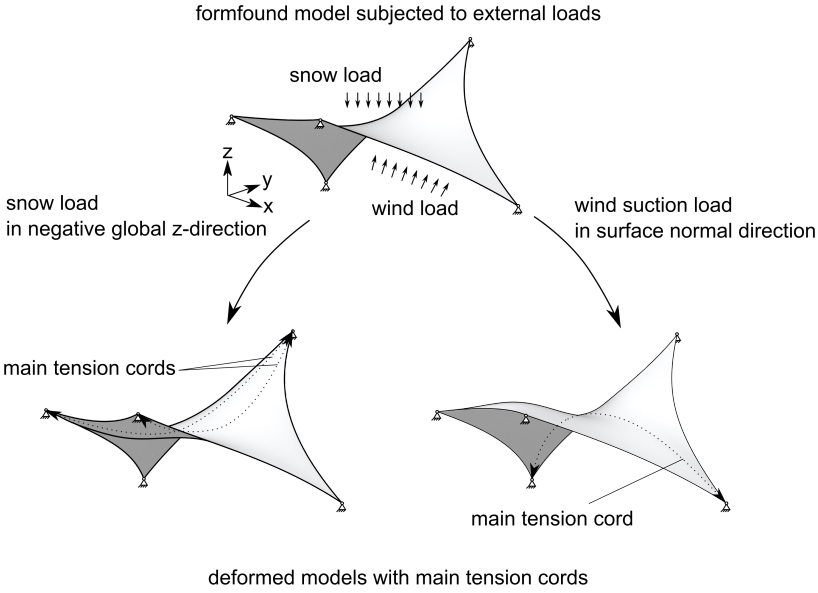

Figure 3.5: Membrane structure deforming under exemplary loads with resulting main tension cords.

A load scenario that is unique for membrane structures, is the so-called ponding. Ponding implies the accumulation of water at a point where the surface is nearly horizontal, with low curvature and no gradient, that can lead to drastic deformations and failure of the textiles (i.e. tearing) or even the whole structure. The simulation of ponding is a challenging task, as it entails very large deformations that lead to changing system parameters, see e.g. Narayanan et al. [85] for recent investigations. One remedy is to ensure a sufficiently large gradient of the surface for positive drainage, see e.g. Wagner [115].

Wrinkling of membrane structures appears if the tension is lost in one direction: since membranes cannot carry compressive forces, a local buckling or loss of stability occurs in the shape of wrinkles, see Figure 3.6. All external forces have to be beared in orthogonal direction to those wrinkles, leading to significantly higher tensile stresses. Even in a short time-span, the appearance of wrinkles can be harmful and lead to tears, depending on the material (e.g. glass-fibre getting brittle). In order to avoid wrinkling, the prestress and curvature need to be carefully calibrated. The simulation of wrinkling with numerical models is a challenging task. If it is performed with membrane elements, a very fine mesh needs to be used in order to approximately account for the effect. Even though the wrinkle shapes are arbitrary, a fine mesh can help to reach reliable conclusions on the wrinkling areas. Shell elements with a very low bending stiffness are also suitable to model wrinkling behaviour, see e.g. Oesterle et al. [87]. Wrinkling models can also be implemented for membrane elements in order to ensure failure under the loss of tension, i.e. elements going slack in one direction instead of falsely transferring compressive forces. A detailed description of the effects and solution strategies can be found in Wüchner [117] and Jrusjrungkiat [63]. Jrusjrungkiat [63] differentiates between distinct membrane states in preparation of applying wrinkling models: undeformed, taut, wrinkled and slack, see Figure 3.6 and Table 3.1. The presence of prestress also needs to be kept at all times in order to avoid the membrane going completely slack.

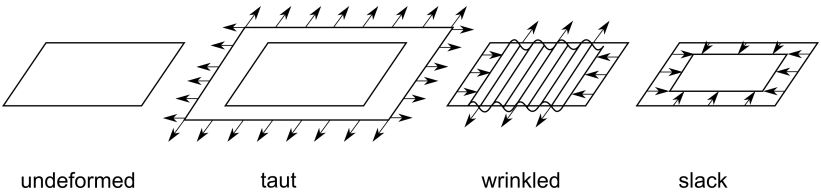

Figure 3.6: Membrane states: undeformed, taut, wrinkled and slack, adapted from Jrusjrungkiat [63].

Since the membrane derives its stiffness from prestress and curvature, a deformation under load leads to a changed system behaviour. In order to take this dependence between shape and force into account, a geometrically non-linear analysis is carried out. For the representation of the material

Table 3.1: Membrane states deduced from principal stress and strain state, adapted from Jrusjrungkiat [63].

State	Principal stress criterion	Principal strain criterion	Mixed criterion
Taut	$S_{\min} > 0$	$E_{\min} > 0$	$S_{\min} > 0$
Wrinkled	$S_{\min} \leq 0 \wedge S_{\max} > 0$	$E_{\min} \leq 0 \wedge E_{\max} > 0$	$S_{\min} \leq 0 \wedge E_{\max} > 0$
Slack	$S_{\min} \leq 0 \wedge S_{\max} \leq 0$	$E_{\min} \leq 0 \wedge E_{\max} \leq 0$	$E_{\max} \leq 0$

behaviour, it may also be necessary to consider material non-linearity, as introduced in Section 2.3. With the virtual work, the weak form of the equilibrium in the current state Ω between internal and external forces is established for a steady state analysis (with Cauchy stresses $\boldsymbol{\sigma}$, virtual Euler-Almansi strains $\delta\mathbf{e}$, external loads $\mathbf{p}$ and virtual deformations $\delta\mathbf{u}$) and solved with numerical methods, see Equation 3.6 and Section 2.5.

$$\delta W = -\delta W_{\text{int}} + \delta W_{\text{ext}} = -\int_{\Omega} (\boldsymbol{\sigma} : \delta\mathbf{e}) d\Omega + \int_{\Omega} (\mathbf{p} : \delta\mathbf{u}) d\Omega = 0 \tag{3.6}$$

Note that the Cauchy stresses $\boldsymbol{\sigma}$ entail the elastic stresses $\boldsymbol{\sigma}_{\text{el}}$ as well as the prestress $\boldsymbol{\sigma}_0$, see Equation 3.7. The usage of the Cauchy stress implies that the prestress can either be prescribed on the formfound equilibrium surface or arise from a mounting analysis, i.e. from defining the pattern as the reference configuration (see Section 3.4).

$$\boldsymbol{\sigma} = \boldsymbol{\sigma}_{\text{el}} + \boldsymbol{\sigma}_0 \tag{3.7}$$

The non-linearity of the system behaviour does not allow a superposition of stresses resulting from individual loads into a result combination (as is usually done for conventional building design under the assumption of linear structural behaviour). Therefore, the design engineer determines and investigates decisive load combinations (see e.g. Corne et al. [34], Gosling et al. [53], Uhlemann et al. [113] for the safety concept for membrane structures, as briefly described in the next section).

Verification of a sufficient safety level

On a European level, the verification of a sufficient safety level for structural membranes is not defined by means of a standardised procedure in a code (like the Eurocodes that exist for conventional structures) yet. However, by initiative of a European working group, the development of a standard for the design and analysis of membrane structures is currently in progress. As a first step in this procedure, a design guide was published by the TensiNet Association in 2004, Mollaert et al. [79]. This design guide gives an overview of current practice and quality requirements with respect to the materials and the built structures. The assembly of the working group WG5 within the European Commission followed and a Science and Policy Report was published in 2016 as a "Support to the implementation, harmonisation and further development of the Eurocodes", Corne et al. [34]. In a next step, the Technical Specification for the "design of tensioned membrane structures", prCEN/TS, 19102:2021 [95], was devised and has recently been published for a test phase in engineering practice. As the working groups consist of representatives of research facilities, testing institutes, engineering offices as well as manufacturing companies, the code combines the different perspectives and incorporates the experiences made in over 50 years of building membrane structures. As a member of the Chair of Structural Analysis at TUM, it was a privilege to join the discussions and the progress of the working groups both on a national and a European level.

The verification strategy that is presented on the following pages is currently implemented in the Technical Specification, prCEN/TS, 19102:2021 [95]. It was devised in accordance with the semiprobabilistic safety concept of the Eurocodes for the built environment. The verification approaches differ slightly for fabrics and foils, in order to take the specific material characteristics into account. Starting from a basis of design, that introduces the general resistance variables needed for fabrics and foils, expressions are provided for the verification of ultimate limit states (ULS - i.e. maximum utilisation of the material strength) and serviceability limit states (SLS - i.e. reaching predefined deformation limits). The concept and relevant expressions are laid out, replicating the definitions of variables and factors. In Appendix A, the verification strategy of prCEN/TS, 19102:2021 [95] is applied to an exemplary membrane structure.

Basis of design and basic variables for structural analysis

The basis of design introduces basic variables that need to be considered in order to calculate the design actions and design resistance for a membrane structure. The magnitude of actions for the design of membrane structures is determined according to the regulations defined in DIN EN 1991 [38]. Furthermore, the combination of actions for the ULS and SLS, as well as the partial factors of actions are applied as defined in prEN 1990:2020-09 [96]. Additionally, the recommended values for the lower and upper partial safety factor for prestress are $\gamma_{\mathrm{Pinf}} = 0.9$ and $\gamma_{\mathrm{Psup}} = 1.25$, respectively.

The design values R_{d} of a resistance for textile and foil structures is determined with the following expression,

fabrics	$R_{\mathrm{d}} = \frac{1}{\gamma_{\mathrm{M}}} R_k \left(k_{\mathrm{age}}; k_{\mathrm{biax}}; k_{\mathrm{dur}*}; k_{\mathrm{temp}*}; k_{\mathrm{size}}; k_x\right)$
foils	$R_{\mathrm{d}} = \frac{1}{\gamma_{\mathrm{M}}} R_k \left(k_{\mathrm{age}}; k_{\mathrm{biax}}; k_{\mathrm{dur}*}; k_{\mathrm{temp}*}; k_{\mathrm{single}}; k_x\right)$

with:

R_{k}	is the characteristic value of the particular resistance determined with characteristic or nominal values for the material properties and dimensions;
γ_{M}	for simplicity, the partial factors γ_{m} and γ_{Rd} given in Formula (8.18) of prEN 1990:2020 may be combined into a single partial material factor ($\gamma_{\mathrm{M}} = \gamma_{\mathrm{m}} \cdot \gamma_{\mathrm{Rd}}$);
k_{age}	is the modification factor for environmental (aging, deterioration) effects;
k_{biax}	is the modification factor for biaxial effects;
$k_{\mathrm{dur},*}$	is the modification factor for various load durations (permanent: more than 10 years - $k_{\mathrm{dur,P}}$, long-term: 6 months to 10 years - $k_{\mathrm{dur,L}}$, medium-term: 1 to 6 months - $k_{\mathrm{dur,M}}$, short-term: less than 1 month - $k_{\mathrm{dur,S}}$ and instantaneous);
$k_{\mathrm{temp}*}$	is the modification factor for various temperature effects (elevated temperature for fabrics: 70°C, foils: 0° C, 40° C and 50° C);
k_{size}	is the modification factor linked to the panel size;
k_{single}	is the modification factor for single layer ETFE structures, only applied in SLS;
k_{x}	is a variable for a modification factor for not yet specified effects;

The modification factors can be taken from a table with preliminary empirical values or determined in an experimental manner, which is defined in the Annexes of prCEN/TS, 19102:2021 [95].

Apart from the definitions of design actions and resistance expressions, prCEN/TS, 19102:2021 [95] also provides guidance for the generation and handling of material parameters. The testing procedures are specified in consideration of the respective codes. Furthermore, recommendations are given based on empirical values for the shear modulus (1/30 or 1/20 of the warp tensile stiffness), the consideration of creep and the determination of compensation values.

A summary of the expressions for the verification of membrane structures in ULS and SLS is given in the following, divided in fabrics and foils. Since the aim of this summary is to give a brief insight into the verification concept of prCEN/TS, 19102:2021 [95], the verification for connection details is neglected at this point.

Ultimate Limit States

The design resistance f_{Rd} has to be higher than the design action effect or combination of effects at any location of the structure.

For fabric, this can be confirmed by applying the following formulae:

$$f_{\mathrm{Ed}} \leq f_{\mathrm{Rd}} \tag{3.8}$$

where

f_{Ed} is the design membrane stress in the considered direction

f_{Rd} is the design tensile strength of the membrane or the connection related to the specific design situation;

Under consideration of the different material properties in warp and weft direction, the material strength is generally defined as

$$f_{\mathrm{Rd}} = \frac{f_{\mathrm{k,23}}}{\gamma_{\mathrm{M}} \cdot \left(k_{\mathrm{age}} \cdot k_{\mathrm{biax}} \cdot k_{\mathrm{dur,*}} \cdot k_{\mathrm{temp}} \cdot k_{\mathrm{size}} \cdot k_{x}\right)}, \tag{3.9}$$

with $k_i \geq 1.0$ and the recommended value of $\gamma_{\mathrm{M}} = 1.4$ for fabric structures made from PES-PVC or glass-PTFE. The characteristic resistance $f_{\mathrm{k,23}}$ is determined from uniaxial testing at a temperature of 23° C.
Instead of applying the individual modification factors k_{age} , k_{biax} , $k_{\mathrm{dur,*}}$, k_{temp}, some or all may be combined to a modification factor k_{comb}. This

factor should be obtained from experimental tests which should consider the different influencing parameters that are part of the combination, leading to the following equation for the calculation of the design resistance:

$$f_{\mathrm{Rd}} = \frac{f_{\mathrm{k,23}}}{\gamma_{\mathrm{M}} \cdot \left(k_{\mathrm{comb}} \cdot k_{\mathrm{size}}\right)} \tag{3.10}$$

prCEN/TS, 19102:2021 [95] provides typical design situations for the verification of the ULS for fabrics (see Table 3.2).

Table 3.2: Design situations for fabric structures.

design situation	k_{biax}	k_{age}	$k_{\mathrm{dur,*}}$	k_{temp}	k_{size}
prestress	x	x	P	x	x
prestress temp. increased	x	x	L	x	x
snow > 1000 m altitude	x	x	L		x
snow ≤ 1000 m altitude	x	x	M		x
wind	x	x			x
wind at elev. temperature	x	x		x	x

The verification of foil structures can be performed with the following formulae:

$$f_{\mathrm{Ed}} \leq f_{\mathrm{Rd,mod}} \tag{3.11}$$

f_{Ed} is the design membrane stress in the considered direction;

$f_{\mathrm{Rd,mod}}$ is the design tensile strength of the foil related to the specific design situation;

As a recommended value, $\gamma_{\mathrm{M0}} = 1.1$ is given for the determination of the resistance of ETFE foil material and γ_{M1} ranges from 1.15 to 1.45 for the resistance of connections.

The design tensile strength is calculated by a general term for foil material:

$$f_{\mathrm{Rd,mod}} = \frac{f_{\mathrm{Rd}}}{\left(k_{\mathrm{biax}} \cdot k_{\mathrm{age}} \cdot k_{\mathrm{dur},*} \cdot k_{\mathrm{temp},*} \cdot k_x\right)} \tag{3.12}$$

with $k_i \geq 1.0$ and f_{Rd} as the minimum design resistance deduced from the value determined by testing of the foil (f_{u23}) and connections (f_{uw23}) at 23°C:

$$f_{\mathrm{Rd}} = \min\left\{ f_{1\mathrm{Rd}} = \frac{f_{\mathrm{u23}}}{\gamma_{\mathrm{M0}}} \text{ and } f_{2\mathrm{Rd}} = \frac{f_{\mathrm{uw23}}}{\gamma_{\mathrm{M1}}} \right\} \tag{3.13}$$

If the product of all modification factors is used, the expression is simplified to:

$$f_{\mathrm{Rd,mod}} = \frac{f_{\mathrm{Rd}}}{k_{\mathrm{total}}} \tag{3.14}$$

As for fabrics, typical design situations are given as shown in Table 3.3.

Table 3.3: Design situations for foil structures.

design condition	k_{biax}	k_{age}	$k_{\mathrm{dur},*}$	$k_{\mathrm{temp},*}$
prestress mechanical	x	x		50
prestress pneumatic	x	x	P	50
prestress incr. pressure	x	x	L	
snow > 1000 m altitude	x	x	L	0
snow ≤ 1000 m altitude	x	x	M	0
wind	x	x		
wind at elev. temp. 40°C	x	x		40
wind at elev. temp. 50°C	x	x		50
water ponding	x	x	S	

Serviceability Limit States

For the SLS, prCEN/TS, 19102:2021 [95] states, that the requirements as well as the corresponding models are defined on a project basis and characteristic values can be used as a design resistance as $\gamma_{M,ser} = 1.0$ if not specified differently in a National Annex. Further requirements for the primary load bearing components are made, as these need to be stable even if the membrane or parts of it are removed or collapse. In addition to these basic requisitions, a number of design conditions is introduced, see Table 3.4. Additionally, specific requirements are described for the particularities of foil structures.

Table 3.4: Design conditions of the SLS of membrane structures and necessary requirements or actions.

design condition	requirement
maximum deflection	defined in accordance with prEN 1990:2020-09 [96] and in agreement with the project specifications
ponding	observation of the shape - ensure sufficient gradient or perform predictive analysis if ponding cannot be omitted
wrinkling	avoidance of significantly high principal stress ratios (and loss of prestress)
post tensioning	avoided by appropriate compensation and sufficient pressure in pneumatic structures or enabled by the planning
tear control	regular observation of the structure, repairs and replacement actions where necessary
distance to other parts	enabled by the planning

3.3 Cutting Pattern Generation

Membrane structures are usually characterised by a double curvature to achieve sufficient geometric stiffness. These double-curved surfaces need to be joined from several parts (usually stripes), since the materials are only produced in limited width. However, the double curvature does not allow unfolding, as only surfaces with zero Gaussian curvature are developable (see Figure 3.7). An approximation or optimisation is necessary to determine the plane cutting geometry even for the stripes. The method of finding the planar pattern with the least deviations from the wanted

geometry and stress state is called cutting pattern generation. Various methods have been developed for this purpose.

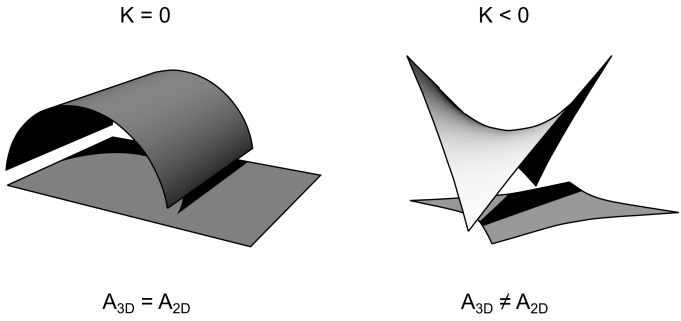

Figure 3.7: Developable surface with zero Gaussian curvature K: cylinder. Non-developable doubly curved surface with negative Gaussian curvature K: hypar.

Before performing cutting pattern analysis, the pattern layout has to be defined for the spatial surface. Depending on the membrane material and joining technique, this layout can have a major effect on the appearance of the overall structure. Apart from the architectural considerations, the width of the textile rolls also needs to be considered when designing the pattern layout, as the stripes obviously need to fit in size. By considerate pattern design, the material waste can also be minimised, e.g. through the usage of geodesic lines as pattern edges (compare Linhard [68]). Note that prCEN/TS, 19102:2021 [95] states that "geodesic lines should be used to define the seam lines" (7.3.1(2)). This will be discussed in more detail in Chapter 4. In many cases, the pattern layout also indicates the orientation of the material directions. It thus influences the structural behaviour, as most woven materials are characterised by different properties in warp- and weft-direction.

In general, most approaches divide the cutting pattern generation, or patterning, into two steps:

1) Projection and Relaxation
2) Compensation.

In the first step, a stress-free planar surface is generated from the three-dimensional one, aiming at approximately the same surface area. Afterwards, compensation is applied to the patterns in order to account for the prestress, i.e. the planar surface is reduced in size. The compensation values are determined by material tests for the respective material directions. The most basic approach to patterning is triangulation (see Moncrieff et al. [80]), which approximates a spatial structure by triangles and then projects these triangles into the plane for an optimisation, e.g. by angle-based flattening (Sheffer et al. [105]) or optimal element edge length (Gründig et al. [55]). Other methods that exclusively consider the geometry for patterning are summarised in Topping et al. [111] as kinematic methods. Maurin et al. [72] developed the stress composition method in order to overcome the shortcomings of purely kinematic methods by including the material behaviour. Kim et al. [65] further developed the stress composition method. Haug et al. [56] approached the cutting pattern generation by solving a standard problem in structural mechanics, called the metric retrieval method. McCartney et al. [73] developed a patterning algorithm for orthotropic materials. A more detailed summary of the different approaches can be found in Widhammer [116]. An approach for already considering the cutting pattern during the formfinding analysis was presented by Gade et al. [44].

Linhard [68], Dieringer [37] and Widhammer [116] developed inverse solution approaches for the cutting pattern generation. This implies that the plane pattern is regarded as the reference geometry for the three-dimensional membrane structure. Therefore, the optimal reference for a known geometry and stress field needs to be found by an optimisation, as depicted in Figure 3.8. Two approaches to solving this inverse mechanical problem are presented in the following, namely the minimisation of stress deviation and the Variation of Reference Strategy. The main difference resulting from the different governing equations lies in the variation which is done in the current configuration or reference configuration.

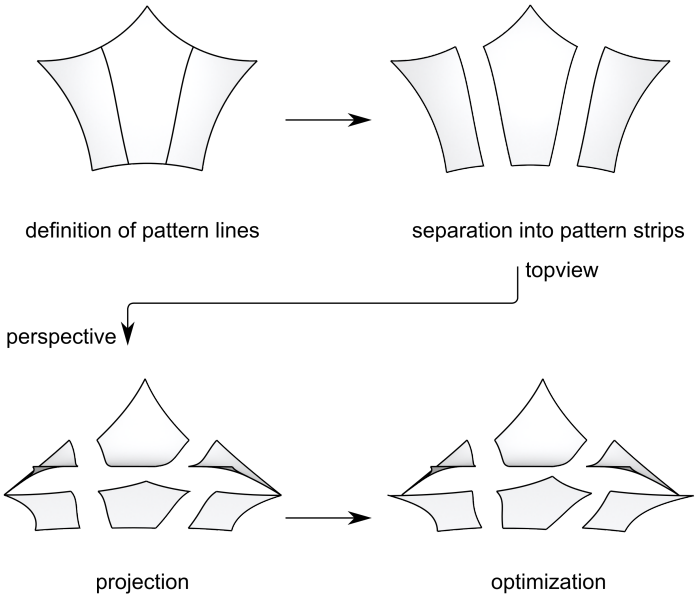

Figure 3.8: Process of a cutting pattern generation with the inverse approach: definition of pattern lines and separation into pattern stripes (on formfound model), projection into plane and optimisation of the plane pattern geometry.

3.3.1 Minimisation of stress deviation

Based on the idea of the stress composition method by Maurin et al. [72], the objective function (Equation 3.15) for the minimisation of stress deviation considers the stresses arising from the deformation $\mathbf{u}_{\text{el},2D\to3D}$ and prestress and aims at minimizing their difference. In other words, the optimal cutting pattern geometry would arrive at the predefined stress distribution through resulting stresses from the erection process and the corresponding deformations.

$$\min_{\mathbf{X}_{2D}} \rightarrow f(\mathbf{X}_{2D}) = \boldsymbol{\sigma}_{\text{el},2D\to3D} - \boldsymbol{\sigma}_{\text{pre}} \tag{3.15}$$

Minimisation of work of stress differences

One approach for solving the minimisation of stress deviation is to apply the principle of weighted residuals, Zienkiewicz [119]. Using a weighting function for multiplication with the objective function leads to the governing equation for the optimisation. Choosing the virtual Euler-Almansi strains $\delta\mathbf{e}$ as a weighting function for the objective of stress deviation (see Equation 3.15) leads to the governing equation in this case. Due to the similarity of this governing equation and the internal virtual work, the name Minimisation of Work of Stress Differences was chosen for this method.

$$\delta W = \int_{\Omega} (\boldsymbol{\sigma}_{\mathrm{el},2D\to 3D} - \boldsymbol{\sigma}_{\mathrm{pre}}) : \delta\mathbf{e}_{\mathrm{el},2D\to 3D}\, d\Omega = 0 \tag{3.16}$$

The solution is found if the first variation is equal to zero, i.e. a linearisation needs to be done w.r.t. the unknown parameters. Dieringer [37] applied this linearisation with these parameters in the unknown geometry $\mathbf{X}_{2D}$ and provides a detailed explanation of the solution with the Newton-Raphson method, as well as the arising challenges, that will not be repeated at this point.

Least square approach

Another solution strategy that can be derived from Equation 3.15 is the Least Square Approach, which integrates the product of the stress deviation over the spatial surface Ω. The governing equation reads as follows:

$$\min_{\mathbf{X}_{2D}} \rightarrow f(\mathbf{X}_{2D}) = \frac{1}{2} \int_{\Omega} (\boldsymbol{\sigma}_{\mathrm{el},2D\to 3D} - \boldsymbol{\sigma}_{\mathrm{pre}}) : (\boldsymbol{\sigma}_{\mathrm{el},2D\to 3D} - \boldsymbol{\sigma}_{\mathrm{pre}}) d\Omega \tag{3.17}$$

In Dieringer [37], the solution possibilities for this approach are described and the solution with the Newton-Raphson method is laid out. Since this approach uses a standard optimisation procedure in order to formulate the governing equation, numerous solution strategies from optimisation can be applied and the inclusion of additional constraints (e.g. equal seam length of neighbouring pattern stripes) is possible.

3.3.2 Variation of Reference Strategy

In order to be able to perform the whole design cycle of membrane structures in a CAD-integrated way (see Chapter 4.1), the development of the

respective process and elements within the framework of IBRA was the first goal. As the Variation of Reference Strategy is the state-of-the art method for cutting pattern generation, it was chosen for this task and is described to some detail in this thesis. The inverse approaches presented before (Minimisation of work of stress differences) were also implemented with IBRA at a later point.

The Variation of Reference Strategy (VaReS), Widhammer [116], treats the cutting pattern analysis as an inverse problem from a mechanical point of view. In contrast to an ordinary static calculation, this means that the deformed, three-dimensional geometry Ω is known from formfinding analysis and the undeformed geometry Ω_0 of the reference must be determined. The criterion for the optimisation is the potential that describes the deformation from the reference geometry to the current geometry, as depicted in Figure 3.9. The methodical challenge is that the undeformed geometry is unknown, but it must nevertheless be used as a reference for determining the deformation. The mechanical formulation by means of VaReS is based on a correct description of the deformation based on consistent mechanics of surface structures. It is consequently demanding, but reliable to apply, with the highest demands on the quality of the result and a minimum of additional engineering approximation assumptions in the modelling. The decisive criterion is the named potential Π_{total}, which is minimal in the optimal state and can be set up as follows:

$$\Pi_{\text{total}}(\mathbf{X}) = \Pi_{\chi}(\mathbf{X}) - \Pi_{\text{pre}}(\mathbf{X}) = \int_{\Omega_0} \Psi(\mathbf{E}(\mathbf{X}))d\Omega_0 - \int_{\Omega_0} \Psi(\mathbf{E}_{\text{pre}})d\Omega_0 \quad (3.18)$$

The strain energy can be divided into deformation components $\Psi(\mathbf{E}(\mathbf{X}))$ and the prestressing components $\Psi(\mathbf{E}_{\text{pre}})$ and is determined using Green-Lagrange strains $\mathbf{E}$ and Piola-Kirchhoff 2$^{\text{nd}}$ order stresses $\mathbf{S}$ in the undeformed state Ω_0. To find the minimum, the vanishing point of the variation $\delta\Pi_{\text{total}}$ is determined in the optimisation, see Equation 3.19. The degrees of freedom of the system are the nodal positions of the reference geometry $\mathbf{X}$. In other words, the deformation $\chi(\mathbf{X}, t)$ should not lead to a residual stress field, apart from the desired prestress field.

$$\min_{\mathbf{X}\in\Omega_0} \rightarrow \Pi_{\text{total}}(\mathbf{X}) \quad (3.19)$$

The potential energy $\Pi_{\chi}(\mathbf{X})$ generated by the deformation $\chi(\mathbf{X}, t)$ is exclusively depending on its material position $\mathbf{X}$ in Ω_0. However, the potential

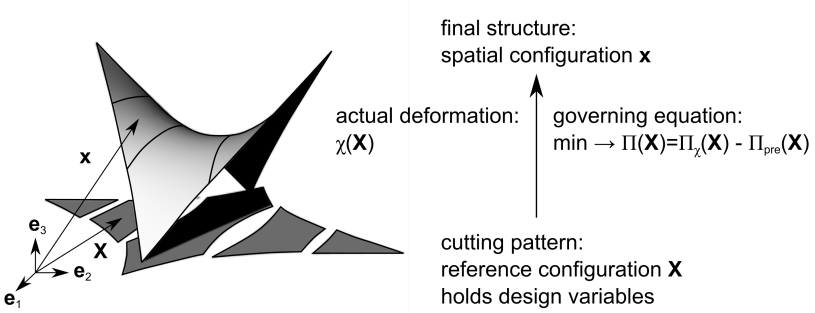

Figure 3.9: The inverse approach of the Variation of Reference Strategy, adapted from Goldbach et al. [51].

energy Π_{pre} depends on the material behaviour. In order to compute the strain energy produced by prestress, one needs to know the exact stress-strain relations. One way to determine the strain energy for a certain prestress is the usage of response surfaces generated by biaxial tests, as described in Widhammer [116]. More general hyper-elastic material laws can also be used (e.g. Neo-Hooke material law) but might lead to limitations w.r.t. the solvability of the problem, because only a polyconvex function provides a stable solution space. This is explained in detail in Widhammer [116]. Recent developments in constitutive laws show very promising results for polyconvex hyperelastic material models to approximate the stress-strain relations of structural textiles Motevalli et al. [82].

In order to find the minimum of the total potential energy, the stationary point of its derivative, i.e. $\delta\Pi_{\text{total}} = 0$ needs to be found with respect to a field of virtual material position vectors $\delta\mathbf{X}$. Applying the chain rule to Equation 3.18, the governing equation of the Variation of Reference Strategy thus reads

$$\begin{aligned}\delta\Pi_{\text{total}}(\mathbf{X}) = &\int_{\Omega_0} \left[\mathbf{S}(\mathbf{E}(\mathbf{X})) - \mathbf{S}(\mathbf{E}_{\text{pre}})\right] : \delta\mathbf{E}(\mathbf{X}) d\Omega_0 \\ &+ \int_{\Omega_0} \left[\Psi(\mathbf{E}(\mathbf{X})) - \Psi(\mathbf{E}_{\text{pre}})\right] \delta d\Omega_0 \qquad \stackrel{!}{=} 0 \end{aligned} \tag{3.20}$$

with

$$\delta\Psi(\mathbf{E}(\mathbf{X})) = \mathbf{S}(\mathbf{E}(\mathbf{X})) : \delta\,\mathbf{E}(\mathbf{X}) \tag{3.21}$$

$$\delta\Psi(\mathbf{E}_{\text{pre}}) = \mathbf{S}(\mathbf{E}_{\text{pre}}) : \delta\,\mathbf{E}(\mathbf{X}) \tag{3.22}$$

To solve for the root, the governing equation (3.20) is linearised as described in Section 2.5 and pre-integrated over the thickness t. It can thus be rewritten for Finite Element Analysis in residual form in the normalised parameter space:

$$0 \stackrel{!}{=} R_r + K_{rs} \cdot \Delta X_s \tag{3.23}$$

with

$$\begin{aligned} R_r = t \int_0^1 \int_0^1 \det J(\mathbf{S}(\mathbf{E}(\mathbf{X})) - \mathbf{S}_{\text{pre}}) : \frac{\partial\,\mathbf{E}(\mathbf{X})}{\partial X_r} d\theta_1 d\theta_2 \\ + t \int_0^1 \frac{\partial \det J}{\partial X_r} (\Psi(\mathbf{E}(\mathbf{X})) - \Psi(\mathbf{E}_{\text{pre}})) d\theta_1 d\theta_2 \end{aligned} \tag{3.24}$$

and

$$\begin{aligned} K_{rs} = t \int_0^1 \int_0^1 \det J(\mathbf{S}(\mathbf{X}) - \mathbf{S}_{\text{pre}}) \frac{\partial^2 \mathbf{E}(\mathbf{X})}{\partial X_r \partial X_s} d\theta_1 d\theta_2 \\ + t \int_0^1 \int_0^1 \det J(\mathbb{D}_\chi - \mathbb{D}_{\text{pre}}) : \frac{\partial\,\mathbf{E}(\mathbf{X})}{\partial X_s} : \frac{\partial\,\mathbf{E}(\mathbf{X})}{\partial X_r} d\theta_1 d\theta_2 \\ + t \int_0^1 \int_0^1 \frac{\partial \det J}{\partial X_s} (\mathbf{S}(\mathbf{E}(\mathbf{X})) - \mathbf{S}_{\text{pre}}) : \frac{\partial\,\mathbf{E}(\mathbf{X})}{\partial X_r} d\theta_1 d\theta_2 \\ + t \int_0^1 \int_0^1 \frac{\partial \det J}{\partial X_r} (\mathbf{S}(\mathbf{E}(\mathbf{X})) - \mathbf{S}_{\text{pre}}) : \frac{\partial\,\mathbf{E}(\mathbf{X})}{\partial X_s} d\theta_1 d\theta_2 \\ + t \int_0^1 \int_0^1 \frac{\partial^2 \det J}{\partial X_s \partial X_r} (\Psi(\mathbf{E}(\mathbf{X})) - \Psi_{\text{pre}}) d\theta_1 d\theta_2 \end{aligned} \tag{3.25}$$

and

$$\mathbb{D} = \frac{\partial\,\mathbf{S}(\mathbf{E})}{\partial\,\mathbf{E}}. \tag{3.26}$$

3.4 Mounting Analysis

Finally, the pattern geometry can be deformed to the three-dimensional boundary conditions in a non-linear structural analysis called mounting. This allows deviations from the desired shape to be shown and stress conditions in the assembled state to be quantified, i.e. compared to the desired prestress. The interaction of the different analyses of the design cycle becomes clear again here: the result of the patterning and consecutive mounting analysis may require a change of the boundary conditions or prestressing. Therefore a new iteration of the design cycle would follow, starting at formfinding to generate new input for structural analysis as well as cutting pattern generation.

The specific mechanical and numerical properties, as well as the challenges of a mounting analysis can be found in Dieringer [37] and Bauer [14] with IBRA. Two different methods are suggested: assembly in the target configuration and assembly in the initial configuration. In the assembly in the target configuration, the known deformation from the pattern to the formfound boundaries is applied as an initial displacement and weak coupling is used in order to link the seam lines of the pattern patches. If assembly in the initial configuration is performed, the seam lines are linked in the two-dimensional pattern geometry and then the boundary points are pulled to the supports of the target. Bauer [14] provides solutions for the inclusion of edge cables for both types of mounting. As a comparison for a membrane structure yielded more evenly distributed stress results for the assembly in the target configuration, this approach is used within this thesis.

The mounting of an exemplary membrane structure, resulting in an acceptable assembled geometry in space is shown in 3.10. For this example, the method of assembly in the target configuration was used, i.e. the initial displacement $\mathbf{u}_0$ was applied to the plane reference geometry.

For hybrid and active bending structures, mounting analysis starting from the ''correct'' reference is crucial to model the structural behaviour of the assembled model. This was investigated in depth in e.g. Philipp [91] and Bauer [14] and is only mentioned as a side note at this point.

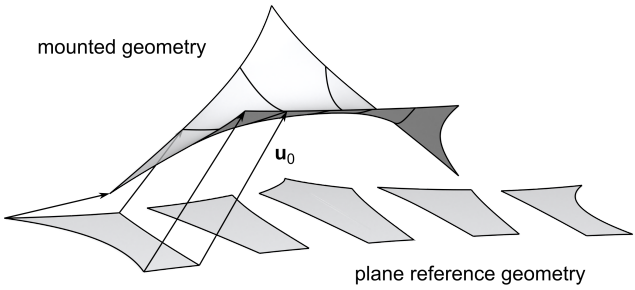

Figure 3.10: Mounting analysis of a membrane structure: assembly of the pattern stripes into the 3d boundaries.

Summary

The design cycle of structural membranes was discussed with its individual steps and the interactions between them. The challenges of the design disciplines of formfinding, structural analysis and cutting pattern generation were presented and the mechanical background for computational analysis with state-of-the-art approaches was provided. Furthermore, an insight into current verification standard development and a brief description of mounting analysis was given. Treating verification as an integral part of the design cycle adds an additional loop to the design cycle, as depicted in Figure 3.1 at the beginning of this chapter. The same holds for a mounting analysis and the arising additional bond between the pattern geometry and the formfound shape.

The knowledge of the particularities of each step in the design cycle, its iterative nature and the links between the analyses is the basis for a successful design of membrane structures. The introduction of the CAD-integrated design cycle is built on this basis and will be described in Chapter 4.

CHAPTER 4

ISOGEOMETRIC B-REP ANALYSIS FOR STRUCTURAL MEMBRANES

Isogeometric B-Rep Analysis allows designers and engineers to perform the design and analysis on one model within the CAD environment. IBRA applied to the highly non-linear analyses of the design cycle (see Chapter 3) can account for the interaction of form and force - which is crucial for the design of membrane structures - by incorporating consecutive non-linear analyses in the CAD environment. The highly beneficial unified workflow resulting from this, including pre-processing, multiple linked analyses and postprocessing, is presented in this chapter. Furthermore, parametrising both geometrical and mechanical entities of the CAD-integrated model significantly enlarges the design space in a very flexible way. The remarkable advantages of CAD-integrated cutting pattern generation are pointed out in addition. A simple exemplary membrane structure highlights the advantages of the parametric CAD-integrated workflow. The applicability of the presented method for large-scale structures is shown with the examples at the end of this chapter.

4.1 The CAD-integrated Design Cycle Workflow

As introduced in Section 2.6, Isogeometric Analysis (IGA) enables the design and analysis of engineering structures with the Finite Element Method to be performed directly on the NURBS-based CAD model. The idea of IGA is taken one step further by Isogeometric B-Rep Analysis (IBRA) (Breitenberger et al. [25]) by assessing a CAD model's topology in addition to the geometrical description by NURBS. CAD models are typically stored as B-Rep models (see Chapter 2). All B-Rep entities (i.e. faces, edges, vertices) can be enhanced by mechanical properties in CAD-integrated analysis with IBRA. In consequence, the vast design space offered by trimmed NURBS curves and surfaces is available for analysis.

Figure 4.1 shows the general process of CAD-integrated design and analysis. Both pre- and postprocessing are being performed within the CAD environment. Preprocessing entails the construction of the B-Rep geometry and its enhancement by mechanical properties to define structural elements, boundary conditions and the analysis type in order to yield an analysis model. The generated analysis model is forwarded as the input for the numerical simulation with the solver. The results are provided at the integration points and at the control points for postprocessing and can be visualised on the now deformed CAD model. This deformed CAD model can again be manipulated by geometrical operations or mechanical properties and be forwarded to the next analysis. The interfaces for a unified workflow for the design cycle of structural membranes thus arise, as will be presented in this chapter.

Designers or architects and engineers can communicate on the basis of a common CAD model, as no conversion between design and analysis model is needed. This can be an opportunity to rule out misunderstandings in interdisciplinary teams and to incorporate constructive details. The prevention of model conversion saves time and computational effort and maintains the geometry description's standard (as highlighted in the next section). In addition to the advantages already mentioned, extended CAD functions (such as daylight analysis) can be applied directly to the model and provide information on further design aspects. The CAD-integrated design cycle for structural membranes and the benefits of the contained links between several analysis models were previously published in e.g. Philipp et al. [90] and Goldbach et al. [46] and Goldbach et al. [49].

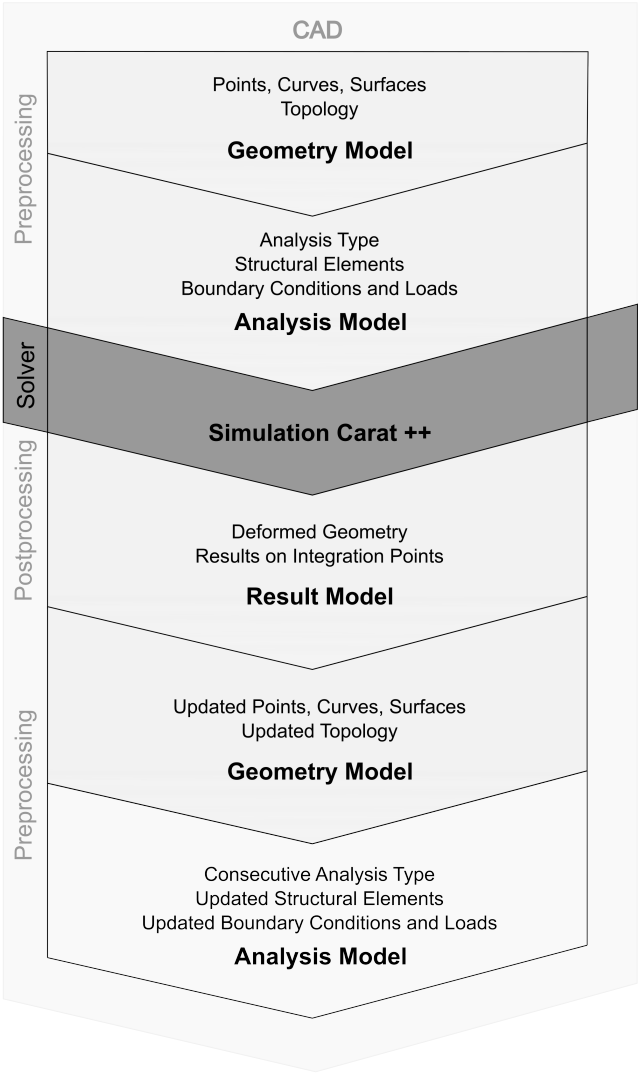

Figure 4.1: CAD-integrated analysis and design: pre- and postprocessing performed within the CAD environment.

Advantages of NURBS geometries for the analysis

NURBS surfaces can be used to construct nearly any free-form geometry (with the exception of e.g. mechanically motivated shapes like the catenary, see Philipp et al. [90]), often with a comparatively low number of control points or design handles. One of the most prominent advantages of using these surfaces for the analysis is the preservation of the smooth shapes for all analysis steps. It entails the preservation of exact curvature properties, which are lost once a classical facetted FE-mesh is generated.

Minimal surfaces are characterised by zero mean curvature at any point of the surface and can be used to emphasise the advantage of keeping curvature properties intact, as well as to assess the numerical formfinding results that were conducted with the Updated Reference Strategy and Isogeometric B-Rep Analysis. Within common CAD programs (e.g. Rhinoceros [101]), the mean curvature can be analysed using the provided tools. Figure 4.2 shows two minimal surfaces that were generated with CAD-integrated formfinding using URS. The initial geometry, modelled from adjacent plane surface patches as the analysis model, an intermediate iteration and the converged geometry are portrayed. The curvature analysis can be used to control the expected zero mean curvature over the surfaces. It can thus be concluded, that the CAD-integrated formfinding procedure was successful, even for a low number of elements (4 by 4 elements per patch and a polynomial degree of 3).

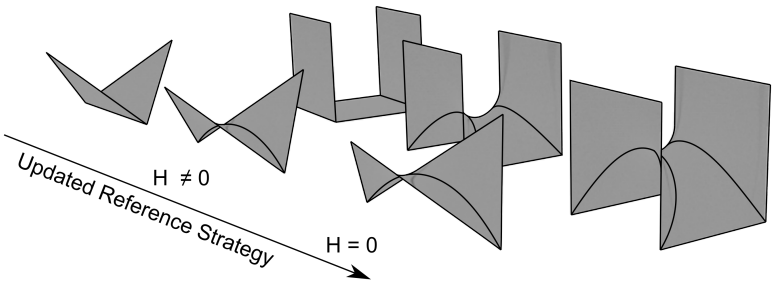

Figure 4.2: Schwarz (left side) and Scherk (right side) minimal surfaces: CAD-integrated formfinding process with URS resulting in surfaces with zero mean curvature H.

Unified workflow

The design cycle for membrane structures is characterised by the dependencies between formfinding, structural analysis and cutting pattern generation, as was pointed out in Chapter 3. In addition, mounting analysis and verification conditions can be appended to the before mentioned analyses. In CAD-integrated design, these dependencies can be easily mapped, since a complete model is available at any time. This model can be adapted via geometric operations and assigned with mechanical properties.

Formfinding is performed within the CAD environment and the result is available again as a complete NURBS-based CAD model, enhanced with information on deformations and stresses. For the next steps of the design cycle, namely structural analysis and cutting pattern generation, the formfound model can now be used as an input that may need to be modified. Again, both geometrical and mechanical properties can be manipulated. All analysis steps can be linked in this manner, i.e. the deformed model resulting from an analysis is forwarded as an input to the next one, as depicted in Figure 4.3. Every change of the parameters is now automatically passed on to the successive analyses and allows for an efficient and multivariant design process. Since the design cycle is often of highly iterative nature, this inherent updating possibility is the key feature of the unified workflow.

The design cycle workflow benefits from working on the unified model significantly. Figure 4.4 shows how the design cycle steps can be linked for a five-point sail using the plugin Kiwi!3d [66] for Grasshopper within Rhinoceros [101]. It was developed at the Chair of Structural Analysis in cooperation with the engineering office str.ucture and was used to generate and investigate all the examples shown in this thesis.

The formfound geometry is forwarded to structural analysis and cutting pattern generation. As the full CAD model of the deformed geometry is available, standard CAD operations can be performed - e.g. the portrayed trimming operations separating the membrane into several parts for cutting pattern generation - before further analyses are connected. In addition, a mounting analysis that simulates the assembly of the pattern stripes into the final shape (see Section 3.4) can help to evaluate the deviation from the formfound geometry and assess the necessity of another iteration in the design cycle. The same holds for a structural analysis with the assembled

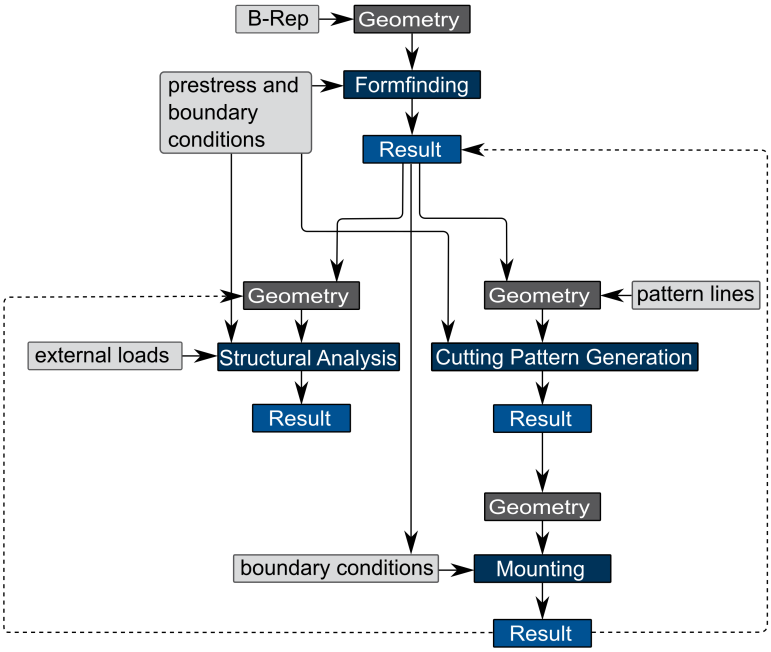

Figure 4.3: Links between design steps.

model as a starting point. Once the design cycle is set up in the unified workflow, the mentioned links between the analyses automatically forward all model updates as depicted by the lines between the component boxes in the Figure.

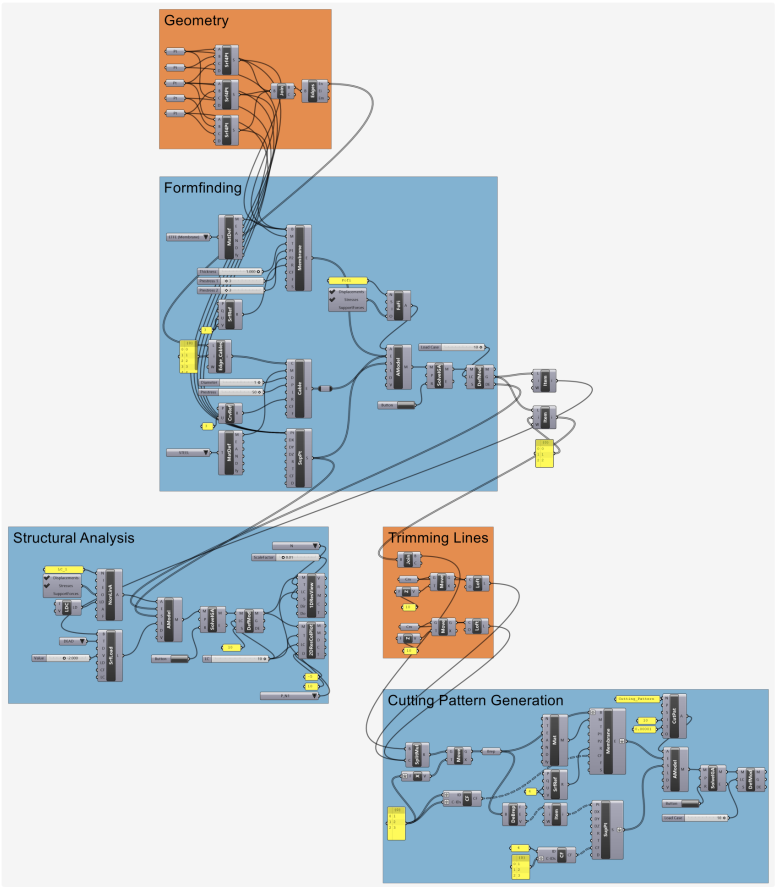

Figure 4.4: CAD-integrated parametric design cycle of a five-point sail in Kiwi!3d [66]. Geometrical operations are highlighted in orange and mechanical ones in blue.

Trimming, refinement and embedded elements

IBRA allows for CAD functions such as trimming to be applied to the model without restricting the analysis model. The variety of available shapes rises significantly, once trimmed multipatch surfaces can be integrated. It also creates the possibility to investigate details of the structure in depth. Trimming and coupling operations as well as the mechanical and numerical effects are explained in detail in e.g. Breitenberger et al. [25] and Apostolatos et al. [5].

If a refinement of the discretisation is necessary for the analysis, the model can either be represented by more knots or higher order polynomials, as was explained briefly in Section 2.6. The geometry does not change because of refinement, while the results for e.g. vertical displacements under external loading converge to one result, see Figure 4.5. The displayed example was modelled as a surface consisting of trimmed and coupled multipatches (the triangular surface on the top is trimmed from a rectangular one and coupled to the rectangular surface on the bottom). In this example, the refinement was applied simultaneously for both patches. However, one could also apply different levels of discretisation to the single patches.

As was introduced in Section 2.6, several so-called embedded elements have been developed for beams, shells, cables and membranes and have successfully been applied to various problem settings, as explained in detail in Bauer et al. [12] and Bauer [14] and Philipp et al. [90]. Embedded elements are not restricted to a mesh, but can be positioned freely and are thus flexible with respect to parametrisation. With weak coupling and embedded elements, it is possible to build analysis models from nonmatching grids and thus freely apply trimming operations across the existing parametrisation. With regard to the modelling of membrane structures, the embedding of cable elements can be a powerful tool to model seam lines, belts and ridge or valley cables, which are often attached to the membrane.

Furthermore, the development of sliding cable elements (see Bauer et al. [13]) provides the possibility to model edge cables without restricting the movement alongside the membrane. Cables are typically free to move within pockets that are fixed to the membrane, instead of being continuously fixed. By explicitly considering these degrees of freedom in the numerical model, more continuous stress results are achieved in the sur-

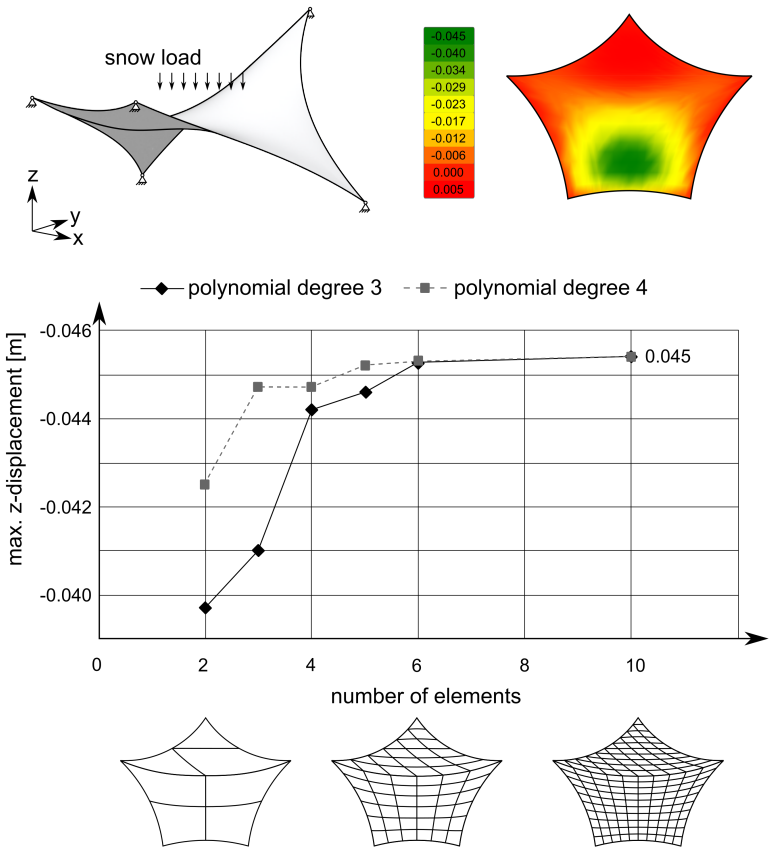

Figure 4.5: CAD-integrated analysis of a formfound five-point sail under snow-load with evolving discretisation and resulting deformation in z-direction.

face. The same holds for rigid edge boundaries, e.g. attachments to walls. If the supporting situation is continuous, it can lead to a high concentration of stresses in one direction and hence wrinkling. If it is more flexible, it should best be modelled as such to correctly account for the resulting stress distribution.

4.2 Parametric Design for Structural Membranes

By parametrising the geometric and mechanical properties of the CAD-integrated analysis model, its advantages for design and analysis are multiplied. Numerous options of the parameters can be combined and examined using one model. As the interaction of form and force in lightweight structures does not allow designers and engineers to predict the structural behaviour resulting from parameter changes, the opportunity to test them in the presented intuitive and effective way provides a significant enlargement of the design space. This section will describe the benefits separated in those for formfinding and shape generation and those for further analyses. Studies of parametric design and analysis with IGA have also been published by Bauer [14], Alic [2], Herrema [57] and Hsu et al. [60].

4.2.1 Parametric formfinding and shape generation

The ratio of the prestress in a membrane and the edge cables determines the curvature of the surface and consequently influences its geometrical stiffness. In order to arrive at an equilibrium shape for a given prestress, formfinding needs to be performed. Different prestress settings often need to be investigated before the design satisfies all preconditions, also with respect to the before mentioned geometric stiffness. A parametric model evidently reforms this iterative process, as different options can be explored with one model.

For the basic example of a five-point sail, a variety of formfound shapes is shown in Figure 4.6. The chosen parameters for formfinding were the cable force P_c for a given isotropic prestress in the membrane p_{iso}. Different prestress ratios were investigated for three fundamentally different shapes, resulting from varying the height h (0 m height leads to the front supports on the ground, 2 m height positions the front supports at half of the maximum height h_{high} and 4 m is the maximum height h_{high}).

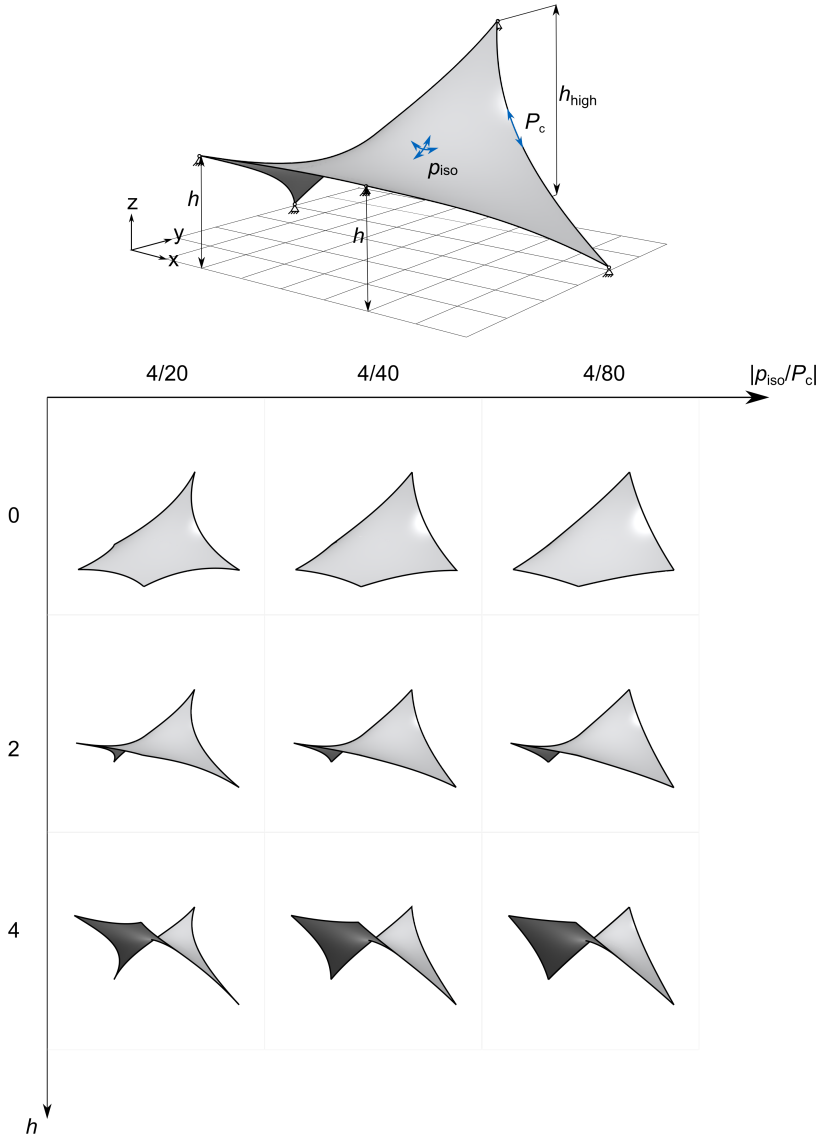

Figure 4.6: Parametric formfinding model: exploring the effects of varying geometrical and mechanical parameters of a five-point sail. Exemplary parameter changes for height h and cable prestress P_c.

In Goldbach et al. [48] and Bauer [14], the shape generation of bending active and hybrid structures is shown in great detail for parametric CAD-integrated models. For these types of lightweight structures, preserving the NURBS geometries for consecutive analysis steps leads to advantages with regard to the available design space.

4.2.2 Advantages of parametric analysis models

The advantages of parametric CAD-integrated models for the analysis of membrane structures lie at hand: being able to investigate the changes of the structural behaviour for both geometrical and mechanical parameter changes in a fast and efficient way is beneficial for the design. This will be highlighted with the application examples of Section 4.4 for the presented CAD-integrated design cycle.

The ability to work with CAD-integrated models enables designers and engineers to work together more closely, as they are able to communicate with one model. With regard to data exchange and possible data loss during the transfer between different programs, this is another key advantage of the CAD-integrated design cycle for structural membranes and a significant step towards the creation of a digital twin.

An automated parameter optimisation by adding optimisation methods aimed at single parameters or a combination of those is also possible, as was suggested in Goldbach et al. [47, 48]. This can be especially useful for the verification of a sufficient safety level, where certain stress and deformation limits are given and the parameter combination has to be found, such that the structural answers lie within these limits.

4.3 Cutting Pattern Generation with IBRA

The possibility of analysing trimmed geometries saves time and computational effort when conducting a cutting pattern generation. The advantages arise from the mesh-independent discretisation and trimming possibilities and will be explained in detail in this section. In addition to this, the significance of geodesic lines is explained and the benefits of CAD-integrated models to this regard are shown.
The advantages of a CAD-integrated cutting pattern generation were first introduced in Goldbach et al. [50–52].

4.3.1 Advantages of CAD-integrated patterning

In a classical FE environment, the separation of a surface into several pieces can be restricted by the element borders and thus depend on the mesh size. If the pattern lines can be placed arbitrarily, the resulting elements may not possess a regular shape and can be regarded as of poor quality. In most cases, the patterning will require a remeshing of the three-dimensional model in order to ensure sufficient mesh quality and numerical stability. In Dieringer [37], two remedies were introduced for this that ensure a good mesh quality after separation for patterning, but still the computational costs remain. Furthermore, once a meshed model has been separated into stripes, the information on how to "go back" is no longer available, unless explicit measures have been taken to track the separation.

The CAD-integrated analysis model is not restricted in these ways, as it can simply be separated into pattern pieces by trimming operations along arbitrary curves. The geometric information is preserved and the trimming curves can be changed in shape and position at any point. Figure 4.7 shows the trimmed multipatch B-Rep model of a five-point sail, that has been separated into several stripes. It can be seen that the complete control-point net is kept in the three-dimensional shape, but only those control-points influencing a strip are projected into the plane and thus considered for the following analysis, as is the principle for analysing trimmed geometries in IBRA. A change in the pattern lines would therefore only change the control-points considered for the analysis.

A parametric environment holds further advantages for the patterning, as the effects of altering position, number and orientation of pattern lines can easily be investigated and optimised with a single model. A mounting analysis can help this optimisation procedure, especially with regard to how many pattern lines need to be considered (influencing appearance, waste of material, joining efforts, etc.). In contrast to this, in a classical FE-model with a polygonal mesh, every change in the pattern lines requires a new model.

Additionally, the effects of the iterative design of membrane structures need to be considered once more. In a unified workflow, an update in e.g. the formfound geometry can directly be forwarded to the consecutive analyses, as was explained in Section 4.1. As the deformed geometry serves as the input for the cutting pattern generation together with the trimming

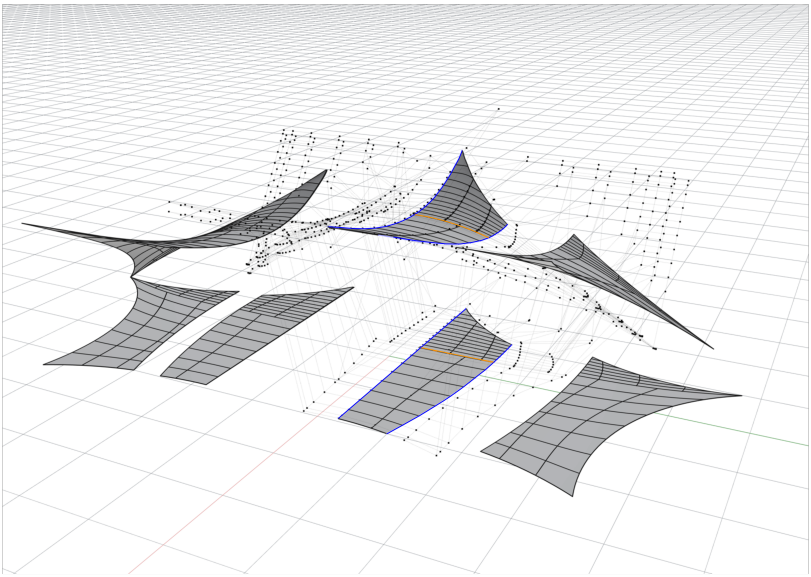

Figure 4.7: Trimmed multipatch five-point sail and its projection into the plane with respective control-point net of the highlighted stripe. Analysis model within the CAD environment, adapted from Goldbach et al. [51].

operations, it can simply rerun, provided that the update of the formfound model did not lead to topological changes.

The final cutting pattern geometry must be forwarded to production and therefore the data needs to be in a suitable format. This is inherent with the CAD-integrated approach, as the geometric information is readily available and no conversion of a mesh into CAD data is necessary.

4.3.2 Geodesic lines

The geodesic line is the shortest path between two points on any surface and therefore, it is a straight line on a plane. It can be found by various mathematical approaches (see e.g. Do Carmo [40]) and represents a local minimum. In order to minimise the curvature of pattern edges after a

Table 4.1: Summary of advantages of CAD-integrated cutting pattern generation.

	IBRA	classical FEM
geometrical information	inherent and complete	facetted mesh
geodesic lines	CAD operation: shortest path	additional analysis
separation into parts	CAD operation: trimming	remeshing or tolerating "bad" mesh
change pattern lines	change trimming curves	restart separation from original mesh
updates from previous analyses	automatic	restart

cutting pattern generation, the usage of geodesic lines is recommended by Mollaert et al. [79] and prCEN/TS, 19102:2021 [95]. On the one hand, fairly straight pattern edges enable effective material utilisation by decreasing the area of offcuts and on the other hand, joining can be handled better if the edge curvature is low. This was also discussed in Linhard [68] and Dieringer [37] in detail. Figure 4.8 shows the effect of geodesic pattern lines as opposed to pattern lines generated by intersecting planes with the formfound surface: in the pattern layout, the geodesic lines are less curved. The only restriction that should be mentioned here, is that the geodesic lines cannot be generated across patch edges per se, i.e. careful modelling of the surfaces is the basis of simply applying the given CAD tools. Remedies for this are offered by the possibility of including additional optimisation loops within the parametric environment, e.g. the mid-point method as suggested in Goldbach et al. [47]. In contrast to the additional analysis performed on the classical FEM model, the CAD-integrated model does not need to be changed irreversibly with respect to the discretization and hence the geometry stays intact.

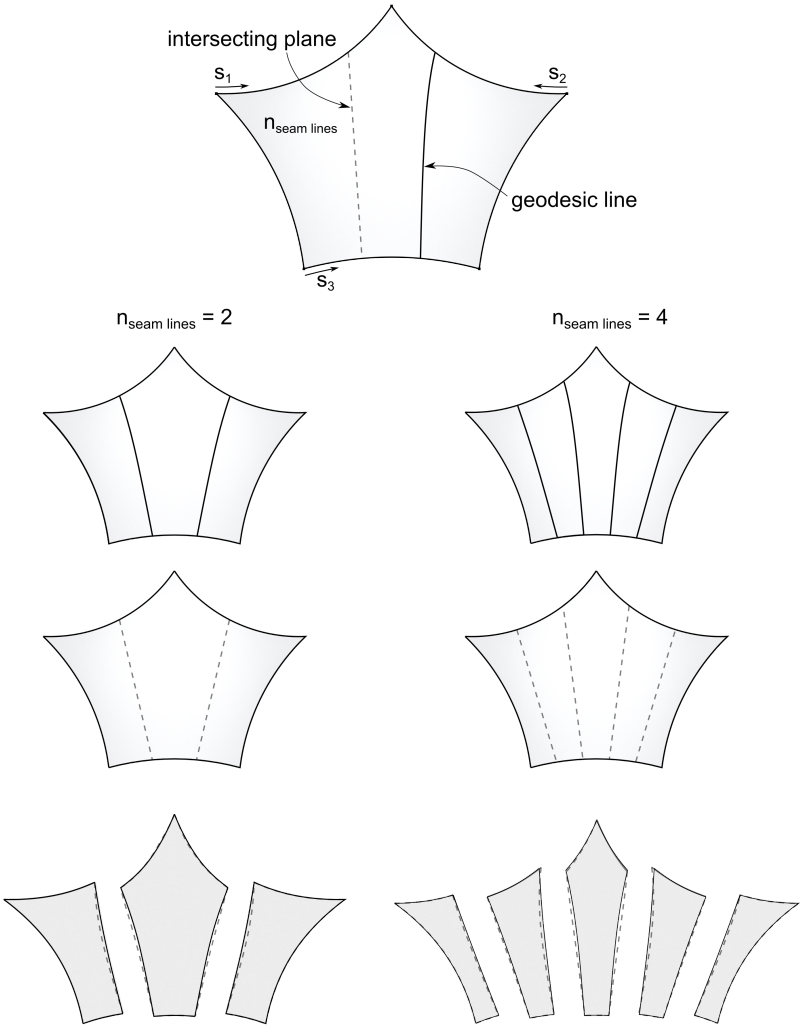

Figure 4.8: Parametric cutting pattern generation: patterning results for dividing the surface along geodesic opposed to straight lines into 5 and 3 parts.

4.4 Application of CAD-integrated Membrane Design

The following application examples exploit the possibilities of parametric design within the CAD framework when using Isogeometric B-Rep Analysis and have been previously published as indicated. Both geometrical and mechanical parameters can be varied simultaneously while working on one model. Due to the preservation of the B-Rep model (see Chapter 3), geometrical and mechanical updates are automatically forwarded to consecutive design steps. This leads to an enlarged design space and provides the freedom to investigate the effects of multiple parameters with regard to the shape and structural behaviour of a membrane structure in a highly efficient way.

4.4.1 Parametric formfinding examples

Skysong

The following section is adapted from Goldbach et al. [46].

The skysong membrane structure, designed by FTL Architects and built by FabriTec Structures, consists of a steel frame supporting eight conical membrane structures with alternating orientation, see Figure 4.9. The model in this example was inspired by the skysong structure and uses parametric design for both geometrical and mechanical properties of the membrane structure. The chosen geometric parameters are the heights of the upward and downward oriented parts $h_{\text{highpoint}}$ and h_{lowpoint}, as well as their orientation $\mathbf{n}_{\text{highpoint}}$ and $\mathbf{n}_{\text{lowpoint}}$, the segmenting angle α and the radii of the inner and outer ring r_i and r_a, as shown in Figure 4.10. The mechanical parameters chosen for the case study are the prestress in the membrane p_{mem} and the edge cables P_{cable}. Figure 4.11 shows the large scale effects of the formfound structure with different segmenting angles. The ratio of prestress in the membrane and cables is varied for a segmenting angle $\alpha = 90$ from 1/10 to 1/5 and 1/20, visibly affecting the edge curvature.

This example shows how CAD-integrated formfinding allows for an efficient investigation of a number of parameters with one model in order to reach a design choice. The formfound model can then be forwarded to consecutive analyses as was pointed out in Section 4.1.

Figure 4.9: The skysong membrane structure in Arizona, USA, adapted in size. ©Cygnusloop99.

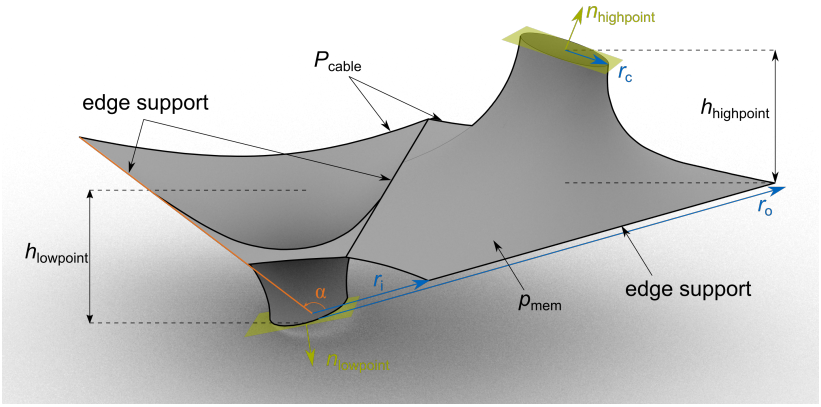

Figure 4.10: Parametric model of large scale membrane structure built with *Rhino3d*, Grasshopper and Kiwi!3d [66], adapted from Goldbach et al. [46].

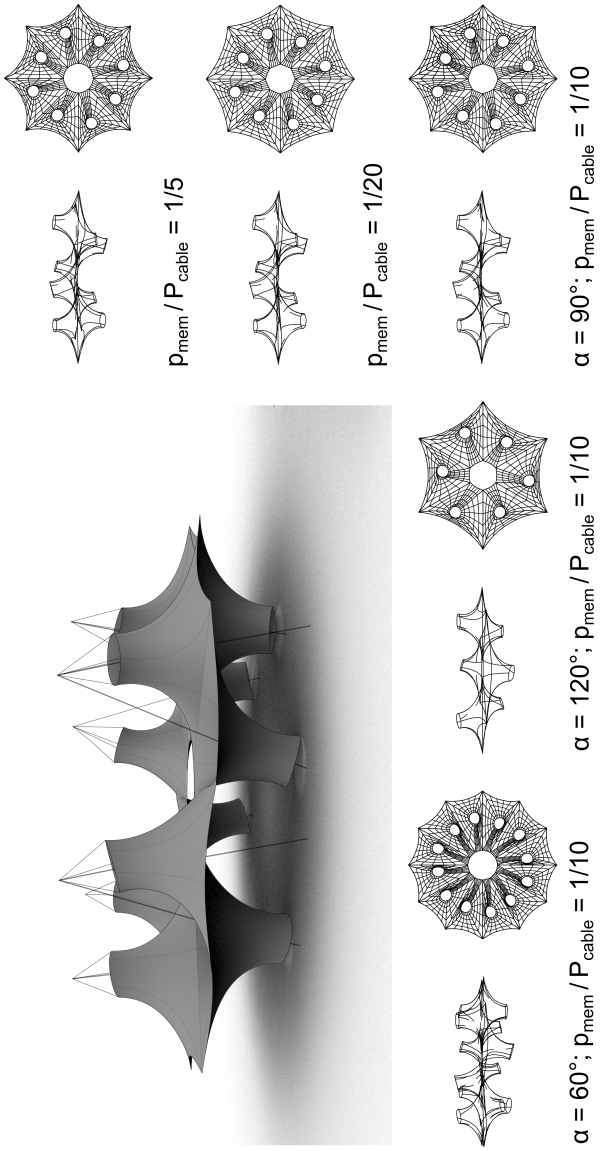

Figure 4.11: Parametric study of a large scale membrane structure with $\alpha = 60°, 90°, 120°$, $h_{\text{highpoint}}/h_{\text{lowpoint}} = 1$ and ratio of prestress in the membrane p_{mem} to cable force $P_{\text{cable}} = 1/5$, 1/10 and 1/20, adapted from Goldbach et al. [46].

King Fahad Library Facade

The following section is adapted from Oberbichler et al. [86].

King Fahad National Library was opened in 2015 with a new membrane facade planned by Gerber Architects. The modular facade offers shading for the library building without blocking the view to the outside, as can be seen in Figure 4.12. Being constructed from repetitive membrane modules, the facade is a prime candidate for parametric modelling both on a small and large scale (see Figure 4.14). The chosen parameters in this example are the module's height h, depth a and width b as well as the ratio of prestress in the membrane (chosen as an isotropic prestress, i.e. $p_1 = p_2 = p_{\text{membrane}}$) and edge cables P_{cable}, see Figure 4.13.

The ratio of the prestress in the membrane and edge cables visibly influences the edge curvature and hence the overall appearance of the modules and the facade. Parametric modelling allows different proportions to be tested conveniently. The established prestressing ratio can then be tested in a structural analysis to ensure that the structural requirements are met. Formfinding is thus used to generate the desired geometry, which also meets the mechanical requirements. Figure 4.14 shows the results of the formfinding with ratios of the isotropic prestress in the membrane p_{membrane} to prestress in the cable P_{cable} from 1:3 to 1:10 and module heights of 4-12 m. Especially with the size of the individual membrane modules, the appearance of the entire facade changes considerably. Again, the parametrised modelling enables the designer to compare the effects of the different options. The impressions of modules with 4-12 m side length show this effect very clearly in Figure 4.14. Since the deformed geometry is preserved as a complete CAD model, further design aspects could also be examined with the tools available in CAD. To name an example, the light and heat transmission of the membrane to the inside of the library which plays an important role for the success of the design, could be investigated.

Figure 4.12: King Fahad library with a modular membrane facade. ©Mrcosch.

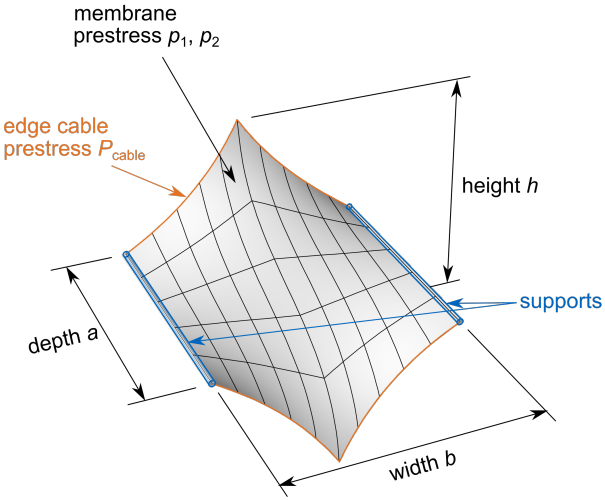

Figure 4.13: Parametric model of King Fahad library facade's membrane module built with *Rhino3d*, Grasshopper and Kiwi!3d [66], adapted from Oberbichler et al. [86].

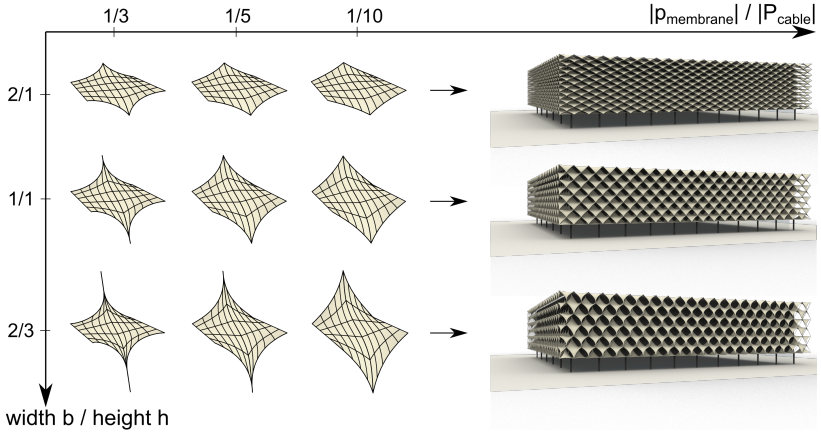

Figure 4.14: Parametric model of King Fahad library facade's membrane structure built with *Rhino3d*, Grasshopper and Kiwi!3d [66], adapted from Oberbichler et al. [86].

4.4.2 Parametric design cycle

In addition to the parametric studies leading to different formfound shapes, the possibility of designing with parametric models also leads to advantages for the design cycle. As the design of membrane structures is an iterative process, it proves to be highly beneficial if the designer can ''go back'' a step and still work on the same model, as the following examples will show.

The following section is adapted from Goldbach et al. [49].

Entrance roof of the Tanzbrunnen in Cologne

In CAD-integrated design, the dependencies between formfinding, structural analysis and cutting pattern generation can be easily mapped, since a complete model is available at any time. The model can be adapted via geometric operations and enhanced by mechanical properties. By parametrising the geometric and mechanical properties, this advantage is multiplied and numerous variants can be combined and investigated on the basis of this model. Figure 4.16 illustrates CAD-integrated design using the entrance roof that was designed by Frei Otto for the Tanzbrunnen area in

Cologne as an example. Figure 4.15 shows the membrane structure that nowadays spans an arch with 40 m width. First, a B-Rep model is created, which uses the parameters B_1, B_2 and W to determine the dimensions of the structure and the arch in the plane, and H to define the height of the structure. For formfinding, the geometric model is enriched with mechanical properties such as the prestress in the membrane (p_1 and p_2) and edge cables (P_{C1} and P_{C2}), as well as support and element properties. At this point, it is also possible to specify whether the geometry of the steel arch is to be determined in the shape determination or fixed as an arch. Formfinding is started from the CAD environment and the result is again available as a complete CAD model, with documented information on deformations and stresses. For the next steps of the design cycle, structural analysis and cutting pattern generation, this model can now be provided with further information and be manipulated. For the seam lines, for example, geodesic lines are a good choice, which are easy to determine with CAD (as explained in Section 4.3.2). Any changes to the parameters are now automatically passed on to the successive analyses, allowing an efficient design process that is rich in variants. In addition to the benefits already mentioned, CAD functions such as daylight analyses can also be applied directly to the model and provide information on other design aspects. Furthermore, the pattern geometry from the CAD can be forwarded to the manufacturer without any loss.

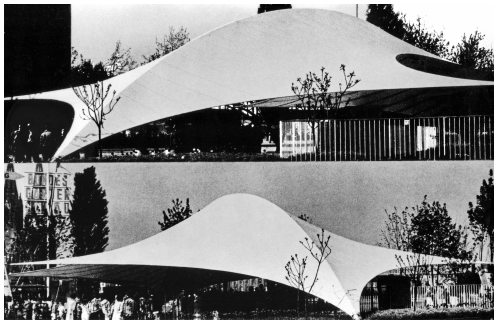

Figure 4.15: Frei Otto's entrance roof at the Tanzbrunnen in Cologne. ©ILEK [62], used with kind permission.

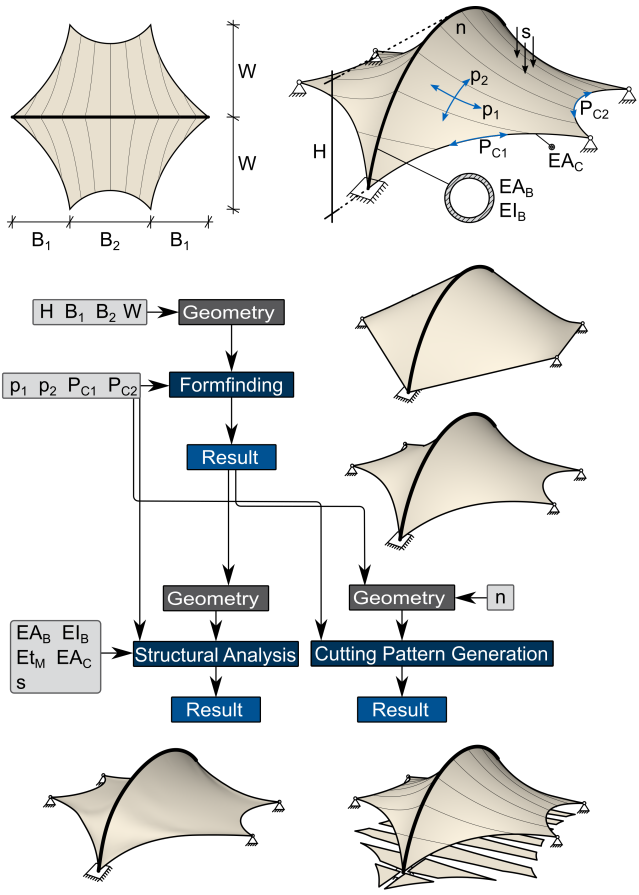

Figure 4.16: Parametric design-cycle with analysis steps and input parameters for Frei Otto's entrance roof at the Tanzbrunnen, adapted from Goldbach et al. [49].

Sternwellenzelt

This is an example of a CAD-integrated design loop on a model of Frei Otto's Sternwellenzelt membrane with an original span of 33 m at the Tanzbrunnen area in Cologne, as depicted in Figure 4.17. A star-shaped structure is created with purely geometric operations and its shape is found by taking into account boundary and prestressing conditions. For this purpose the model is assigned the parameters $p_1 = p_2$ for the isotropic prestressing in the membrane and P_{C1}, P_{C2} and P_{C3} for the prestressing of the cables, see Figure 4.18. First the ratio of the prestressing to $|p_{\text{membrane}}/P_{\text{cables}}| = 1/10$ is chosen as Option 1. Since the geometry found is close to the model of the Sternwellenzelt, the next step is a structural analysis. The formfound model is available as a full B-Rep model and is extended by the mechanical parameters for the structural analysis (snow load s, strain stiffness of the ropes EA_{C}, strain stiffness of the membrane EA_{M} and stiffness of the supports EA_{B} and EI_{B}). Subsequently, the deformation of the inner ring under snow load is evaluated. The resulting deformation is considered too large, therefore a new iteration in the design cycle is started. Formfinding is repeated for adapted prestressing conditions (Option 2 in Figure 4.18), $|p_{\text{membrane}}/P_{\text{cables}}| = 1/20$. Since the analyses in the parametric CAD environment are directly linked to each other, the structural analysis can be carried out directly on the new formfound system and now delivers satisfactory results. Of course, an adjustment of the parameters would also have been possible in this step. In the last step of the design process, the cutting pattern is determined. In this example, the orientation of the seam lines was varied to produce a radial and a tangential pattern. By parametrising the model, these variations can be investigated quickly and easily.

Figure 4.17: Frei Otto's Sternwellenzelt at the Tanzbrunnen in Cologne, adapted in size. ©Raimond Spekking.

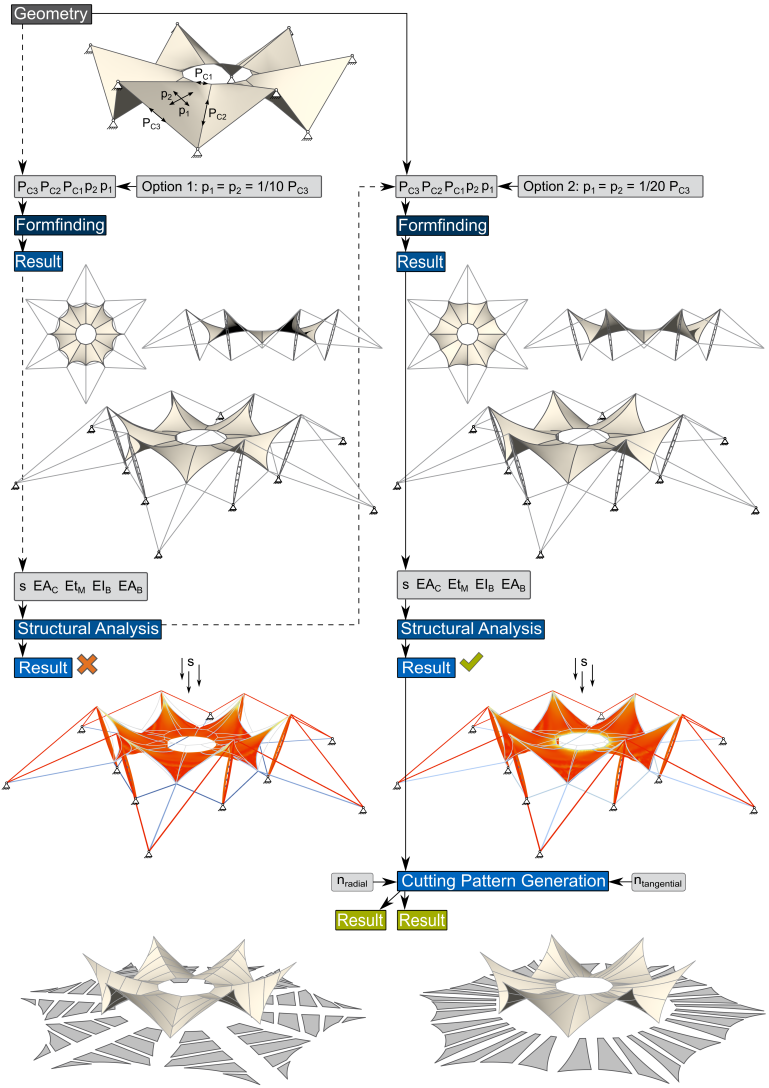

Figure 4.18: Parametric design-cycle with analysis steps and exemplary variation of input parameters for a Sternwellenzelt model, adapted from Goldbach et al. [49].

Summary

The CAD-integrated design cycle workflow was presented in this chapter, highlighting the advantages arising from the possibility of working on a unified model throughout the analysis steps. Being able to perform pre- and postprocessing within the CAD environment with the access to very flexible design tools (like trimming) provides a great freedom for the design of freeform shapes such as membranes. Due to the links between the design cycle steps, changes of both geometrical and mechanical properties can conveniently be forwarded to successive analyses in order to investigate the overall effects on the structure.

Parametric models allow for an effective exploration of design options, as was shown in Section 4.2. The example of a parameter study for the formfinding of a quite simple membrane structure illustrates this.

A special focus was laid on CAD-integrated cutting pattern generation in Section 4.3.1, since the benefits of IBRA are especially significant for this type of analysis. The reasons for this are the flexibility of parametric models and the smooth workflow, based on the ability to analyse trimmed NURBS geometries. Additionally, geodesic lines can be generated without much effort within modern CAD programs.

At the end of this chapter several numerical models are presented, that were inspired by built membrane structures. The applicability of CAD-integrated design and analysis for structural membranes is thus shown. Furthermore, in Appendix B student projects are shown that were developed within the "Membrane Workshop" at TUM. These projects once more showed the applicability of the plugin Kiwi!3d in Rhino for membrane design. Even though many of the students were not used to working within a parametric CAD environment such as Rhino and Grasshopper, they were quickly able to design in a very creative and interdisciplinary way.

CHAPTER 5

RELIABILITY ANALYSIS AND THE VERIFICATION OF STRUCTURAL MEMBRANES

The verification of a sufficient level of safety holds a number of challenges for structural membranes, due to uncertainties in nearly all input parameters. In a series of *Round Robin Exercises* (RR) launched by the TensiNet Association [109], an endeavour towards constraining these uncertainties was made by inviting groups of international experts to investigate certain problem settings. The answers were collated and incorporated in the European efforts towards a standard for the verification of membranes (prCEN/TS, 19102:2021 [95]). In this chapter, the particularities of proofs for non-linear structural behaviour will be laid out and linked to current developments in standardisation. The conceptions of the RR exercises are summarised briefly in this context. Sensitivity analysis is shown as a powerful tool for the investigations of the nature of non-linear structural answers. Furthermore, the findings of the fourth RR (DeSmedt [36]) on reliability analysis are shown and extended by the investigation of selected

prevalent membrane shapes.

5.1 Uncertainties in the Structural Analysis of Membranes

The aim of structural analysis for any type of building is a proof of the structure's safety, expressed with the probability of failure P_f or reliability index β (see Equation 5.1 and Table 5.1 for their relation). Detailed explanations can be found in Ditlevsen et al. [39]. With g being the limit state function, R and E resistance and action variables, μ_g the mean value of g and σ_g the standard deviation of g, the following relations hold:

$$P_\mathrm{f} = \Phi(-\beta) = \mathrm{Prob}(g \leq 0) \tag{5.1}$$

$$g = R - E \tag{5.2}$$

Table 5.1: Relation of P_f and β.

P_f	10^{-1}	10^{-2}	10^{-3}	10^{-4}	10^{-5}	10^{-6}	10^{-7}
β	1.28	2.32	3.09	3.72	4.27	4.75	5.20

Depending on the size and purpose of a building, a classification exists with regard to the acceptable failure probability in prEN 1990:2020-09 [96]. Based on these so-called consequential classes, a building's collapse is ranked according to its effect on, or danger for lives and economy. Reliability classes are deduced from this and linked to requirements for the reliability index β. For most membrane structures, the thus resulting target value of β is 3.8 (specified in Table B.2 of prEN 1990:2020-09 [96]).

The limit state function is considered for the verification of the Ultimate Limit State (ULS) in structural design. In order to ensure a sufficient safety level of a design, the uncertainties of all design parameters can be investigated and incorporated into structural analysis. Sensitivity studies can help to assess the influence of these parameters on the structure and hence their uncertainty. This is especially challenging for non-linear limit-state functions. The results for non-linear structural answers (i.e. strains and stresses) cannot be extrapolated and superposed for changing input parameters, but need to be computed individually.

An excerpt of uncertainties in structural membranes must entail:

- model uncertainty (FEM and design)
  - feasibility of formfound geometry and stress-state
  - deviation of the built shape and stress-state from predictive model
- material uncertainties
  - material properties and processing deficiencies (considered by partial factors in prCEN/TS, 19102:2021 [95])
  - connection properties - execution and resulting stiffness properties of seam lines
- environmental influences
  - uncertainties in load intensity (considered by partial factors in DIN EN 1991 [38])
  - modelling special load cases like wind, ponding (see Section 3.2)

The TensiNet Association launched four *Round Robin Exercises* during the past years, in order to investigate different solution strategies to various problems in the field of structural membrane analysis (and hence narrow down the uncertainties). Figure 5.1 divides the above mentioned uncertainties into categories and links them to the *Round Robin Exercises*.

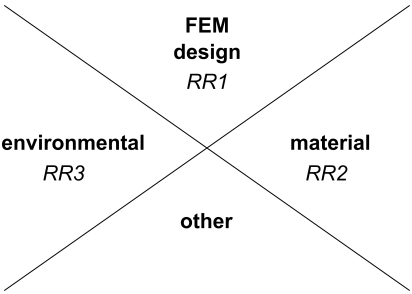

Figure 5.1: Categories of uncertainties for structural membranes, linked to investigations performed in RR1-3.

Round Robin Exercise 1 was launched by the TensiNet Working Group ''Materials and Analysis''. It aimed at a comparative study of analysis methods and results for the formfinding and structural analysis for selected shapes of membrane structures. The results were published in Gosling et al. [54].

Round Robin Exercise 2 was called for by the Working Group ''Materials and Analysis''. The exercise invited engineers and research facilities to share their interpretation of biaxial and shear test data. The findings were aimed at a unified assessment of the stiffness of architectural fabrics, as well as the interpretation of test data for the input into the structural analysis of a membrane. Unfortunately, the results have not been published to this date.

Round Robin Exercise 3 was launched by the TensiNet Working Group ''From Material to Structure and Limit States: Codes and Standardisation''. Wind tunnel and CFD (Computational Fluid Dynamics) data for the basic shapes of structural membranes were collected and evaluated and published in Colliers et al. [33].

Round Robin Exercise 4 treated reliability analysis for defined loading scenarios of a basic membrane shape and thus incorporated the results of the previous investigations, (see DeSmedt [36]). It will be summarised in Section 5.2 along with the presentation of a solution proposal for the task.

5.2 Round Robin Exercise 4

The latest *Round Robin Exercise* (RR4) deals with reliability analysis and aims at an international comparison of methods yielding the reliability index for a simple hyperbolic paraboloid (short: hypar) under defined loading scenarios and parameter distributions, see DeSmedt [36]. It was specified by the TensiNet Working Group ''Specifications and Eurocode'' and the Working Group 5 of the COST Action TU1303 Novel Structural Skins.

This exercise provided an excellent opportunity to advance the design cycle workflow presented in Chapter 3. CAD integration with IBRA allowed for the numerical analyses to be performed in a parametric environment with a very high accuracy. The flexibility with regard to changing mechanical parameters and the discretization facilitated the investigation.

The following paragraphs are adapted from the authors unpublished participation in RR4 in collaboration with A.M. Bauer and M. Fußeder.

Description of the case study

The investigated structure is the hypar shown in Figure 5.2. The membrane and edge cables are fixed at two high- and low-points as indicated by the coordinates in the figure. Formfinding was performed with URS and IBRA elements (see Sections 2.6 and 3.1.2), with the prerequisites of an isotropic prestress in the membrane of 4.0 kN/m and a cable force of 30.0 kN (note that these values differ from DeSmedt [36], as they were adapted internally during the course of the RR4 exercise). Membrane and cable elements were used for the formfinding analysis with a discretisation of 5 elements in u- and v-direction and a polynomial degree of $p = 3$ for the NURBS surface discretisation. The formfound structure was investigated with geometrically non-linear structural analysis and sensitivity studies were conducted for the given distributions of input parameters, as shown in Table 5.2.

For the mean material properties, the elasticity moduli in warp and fill direction, $E_{\text{warp/fill}}$ were given as 600 kN/m (pre-integrated over the thickness t), the shear modulus G was set to 30 kN/m (also pre-integrated over the thickness t) and Poisson's ratio was given as 0.4. The cable's elasticity modulus was given as 205 kN/mm^2. Three load-cases were specified: prestress, prestress combined with a snow load of 0.6 kN/m^2 nominal value and prestress combined with a wind suction load of 1.0 kN/m^2 nominal value. Finally, the material strengths in warp and fill direction were given as 97 kN/m and 87 kN/m. For the structural analyses, the analysis model was refined to 20 by 20 elements in order to achieve sufficient accuracy for the resulting stresses and deformations (polynomial degree of $p = 3$).

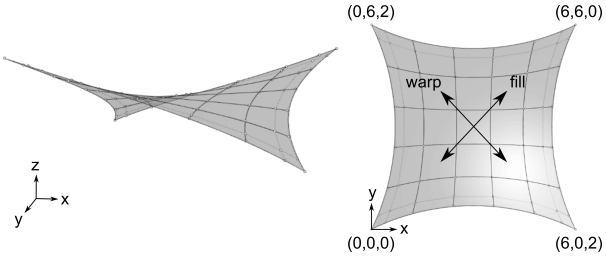

Figure 5.2: Formfound hyperbolic paraboloid from *Round Robin Exercise 4* with dimensions in [m].

Table 5.2: Summary of stochastic characteristics of input parameters from DeSmedt [36].

Variable	distribution	mean value	standard deviation	coefficient of variation
$P_{\text{warp/fill}}$ [kN/m]	normal	4	0.75	0.25
$E_{\text{warp/fill}} \cdot t$ [kN/m]	normal	600	40	0.07
f_{warp} [kN/m]	normal	97	4.3	0.044
f_{fill} [kN/m]	normal	87	3.6	0.041
G [kN/m]	normal	30	3	0.1
Q_{s} [kN/m²]	Gumbel	0.66	0.198	0.3
Q_{w} [kN/m²]	Gumbel	-0.7	-0.245	0.35

Model assumptions and numerical methods

A (force-controlled) geometrically non-linear structural analysis was performed with IBRA for the given load cases and parameter distributions (see Table 5.3). The load was applied in two steps, due to the large variations of the prestress in warp and fill directions:
1) only prestress in the membrane and cables (to find an equilibrium state)
2) full load on the membrane elements.
While the snow-load Q_{s} acted in the negative global z-direction, the implemented wind-load Q_{w} acted in surface normal direction as an uplifting force and was thus updated with the deformation in order to account for

the changes in the geometry and consequently the wind's direction (compare Section 3.2).
The material was modelled with the linear elastic, orthotropic Münsch Reinhardt material law, see Münsch et al. [84], accounting for the different yarn properties (i.e. Young's moduli) in warp and fill direction E_{warp} and E_{fill}, see Section 2.3. The stresses were evaluated in the current deformed state in the material directions. The prestress direction was defined by the global coordinates $p_1 = [1,-1,0]$ (between high points) and $p_2 = [1,1,0]$ (between low points), which corresponds to warp and fill direction in the initial configuration.

Parameters and stochastic characteristics

For a better understanding of the hypar's structural behaviour under the given load scenarios, parameter studies were conducted for the parameters x, given in Table (5.3).

Each parameter x was varied by 50 % and 100 % of its standard deviation σ, i.e. $\gamma = 0.5$ and $\gamma = 1$, according to Equation 5.3. See Table 5.2 for the input and Table 5.3 for the resulting values. The others were set to their mean value μ (and nominal value in case of load intensity), in order to get an estimate on the influence of changing each parameter. Due to this approach, interactions between the parameters could not be detected at this point.

$$x = \mu + \gamma \cdot \sigma \tag{5.3}$$

Table 5.3: Parameter study of the hypar in RR4: input values.

Parameter x	$\gamma = -1.0$	$\gamma = -0.5$	$\gamma = 0$	$\gamma = 0.5$	$\gamma = 1.0$
$P_{\text{warp/fill}}$ [kN/m]	3.25	3.625	**4**	4.375	4.75
$E_{\text{warp/fill}} \cdot t$ [kN/m]	560	580	**600**	620	640
G [kN/m]	27	28.5	**30**	31.5	33
Q_{s} [kN/m^2]	0.402	0.501	**0.6**	0.699	0.798
Q_{w} [kN/m^2]	-0.755	-0.8775	**-1**	-1.1225	-1.245

The parameter studies showed, that a load variation has the biggest impact on the resulting stresses in the membrane. The second largest influence

on the stresses appeared by changing the prestress. Young's moduli and the shear modulus showed a smaller influence than the other parameters. The graphs in Figures 5.3 and 5.4 show the global maximum stresses in the fibre directions for the investigated parameter settings. Evaluation of the mid-point, as well as the principal stresses yielded similar results. For the load case snow, the warp direction whereas for wind loading the fill direction was decisive for the subsequent reliability analysis. Especially for these two cases, the load influence on the stresses was clearly dominating as indicated through the significant larger inclination of the load graphs. In the following section, the reliability analysis will be carried out under exclusive consideration of load and tensile strength as uncertain parameters to investigate this assumption.
Note that no wrinkling occurred for the investigated parameters of this study. Hence, the principal structural behaviour did not change. The validity of the parameter study is tied to this structural behaviour, since the influence of parameters could be different after a load redistribution due to wrinkling.

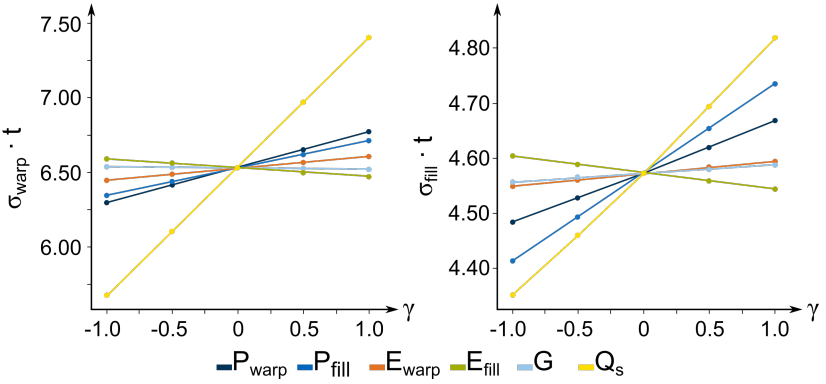

Figure 5.3: Load case snow: maximum stresses in warp and fill direction.

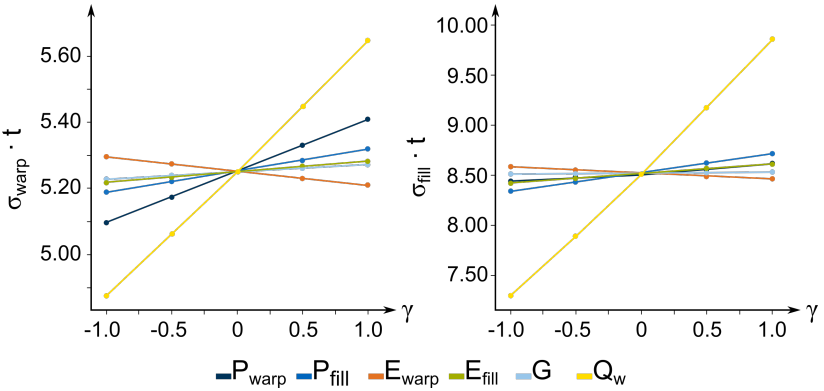

Figure 5.4: Load case wind: maximum stresses in warp and fill direction.

Reliability analysis

For the reliability analysis, the First Order Reliability Method (FORM, see Rackwitz et al. [99]) was used. Within this method, all random variables are transformed into standard normal space. There, the so-called design point is determined, which is the most likely combination of the uncertain variables leading to failure. The design point is the position on the limit state surface that is closest to the origin. Although FORM delivers only an approximation of the probability of failure (the limit state function is linearised in the design point), its usage can be recommended since it solves the reliability problem in a computationally efficient way and it delivers parameter importance measures (α-sensitivities) as a by-product. The absolute values of these sensitivities characterise the influence of the corresponding variable on the failure of the system and thus hold very important information.
Additionally, a Monte-Carlo simulation (Metropolis et al. [76]) was used in order to verify the results of first order reliability analysis. As the results coincided, the approach could be validated and they are not repeated here.

Limit state function
The chosen limit state g was defined as the case when the maximal stress in fill or warp direction $\sigma_{\text{max,fill/warp}}$ in the structure (stress S) exceeds the

corresponding material strength $f_{\text{fill/warp}}$ (resistance R).

$$g = R - S = f_{\text{fill/warp}} - \sigma_{\text{max,fill/warp}} = 0 \tag{5.4}$$

As the resulting stresses in the membrane were much lower than the given material strength, an extremely high reliability index can be assumed, causing numerical problems when applying FORM. In order to avoid this, a slightly modified limit state function g_{mod} was used through multiplying the material strength by a scalar reduction factor θ, with $0 \leq \theta \leq 1$.

$$g_{\text{mod}} = R_{\text{mod}} - S = \theta \cdot f_{\text{fill/warp}} - \sigma_{\text{max,fill/warp}} = 0 \tag{5.5}$$

The scalar factor can also be seen as the inverse of a stress reduction factor (see Gosling et al. [53]) to reduce the ultimate tensile strength, reflecting e.g. the severe reduction of material strength due to a tear. In Gosling et al. [53] the stress reduction factor is assumed to be between 5 and 10, leading to an interval between 0.2 and 0.1 for the factor θ in this study. Note that the appearance of wrinkling in the membrane surface was not defined as a failure criterion for FORM.

Reliability analysis using FORM

When performing FORM-analysis, θ was increased with a step size of 0.05 starting from 0.1 until the reliability index became larger than its target value 3.8. The results are shown in Tables 5.4 and 5.5.

Table 5.4: Reliability indices reached under wind suction load.

strength reduction factor θ	reliability index β	decisive direction
0.1	1.29	fill
0.15	2.68	fill
0.20	3.60	fill
0.25	4.46	fill

Table 5.5: Reliability indices reached under snow load.

strength reduction factor θ	reliability index β	decisive direction
0.1	2.25	warp
0.15	3.65	warp
0.20	4.80	warp

As one can see, the target reliability index of $\beta = 3.8$ can be reached for a utilisation of 20 % resp. 25 % of the material strength. Considering a low percentage of the material strength, one can assume that the uncertainty in the stress state can be covered by the remaining strength reserves.

FORM importance factors

FORM delivers importance factors, called α-sensitivities, along with the reliability index, see Hohenbichler et al. [58]. These importance factors of the considered limit states can be found in Figure 5.5. For all traced limit states, one can observe that the load and the tensile strength are the most important parameters whereas the prestress and the stiffness properties have importance factors smaller than 0.10 and thus only minor influence on the reliability of the system. When comparing the FORM importance factors for $\theta = 0.1$ with the results of the parameter study (see Figures 5.3 and 5.4), one can observe an equivalent parameter ranking and also corresponding signs. For some parameters (prestress and stiffness), the signs of the sensitivities are changing when increasing θ. This can be linked to the wrinkle development in those cases and the resulting change in structural behaviour leading to a different impact of some parameters.

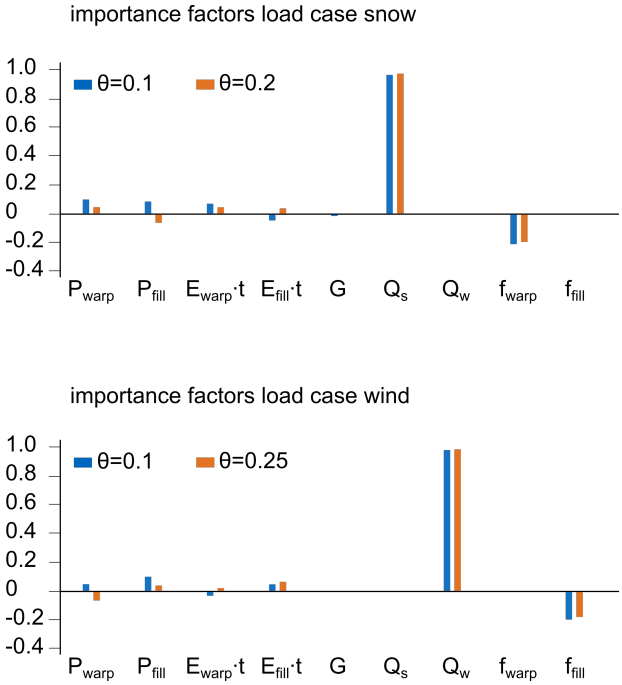

Figure 5.5: Importance factors: α-sensitivities for snow and wind loading.

FORM design points

When observing the FORM design points in physical space of the treated limit states (i.e. the parameter combination most likely leading to failure), the importance of the load intensity can clearly be detected, see Tables 5.7 and 5.6. It can be concluded, that the limit state g_{mod} is mainly reached by an increased load. The values of prestress and the stiffness variables at the design points are within the vicinity of their mean values (the variations are smaller than their standard deviations) and even the design value of the tensile strength is in the range of the standard deviation. Figures 5.6 to 5.9 show that when approaching the limit state for strength reduction factors θ of 0.1 to 0.25, the remaining load bearing part of the membrane resembles a strap between high resp. low points. In the remaining membrane straps,

the stresses only increased in a noticeable way through an increasing load. For the larger strength reduction factors, wrinkling occurred in both load cases. Although wrinkling is to be avoided in membrane design, the stress states were considered as they lead to the maximum tensile stresses in the mentioned straps. The results shown in Figure 5.7 and 5.9 show the stress and deformation of a highly refined model resulting a convergence study with respect to the wrinkle shape and extension.

Table 5.6: FORM design points load case wind.

For a strength reduction factor $\theta = 0.1$:							
P_{warp}	P_{fill}	$E_{\text{warp}} \cdot t$	$E_{\text{fill}} \cdot t$	G	Q_{w}	f_{warp}	f_{fill}
4.05	4.10	598.41	602.58	30.02	1.01	97.00	86.11
For a strength reduction factor $\theta = 0.25$:							
P_{warp}	P_{fill}	$E_{\text{warp}} \cdot t$	$E_{\text{fill}} \cdot t$	G	Q_{w}	f_{warp}	f_{fill}
3.78	4.13	603.82	611.94	30.09	2.88	97.00	84.16

Table 5.7: FORM design points load case snow.

For a strength reduction factor $\theta = 0.1$:							
P_{warp}	P_{fill}	$E_{\text{warp}} \cdot t$	$E_{\text{fill}} \cdot t$	G	Q_{s}	f_{warp}	f_{fill}
4.17	4.14	606.53	595.46	29.89	1.22	94.91	87.00
For a strength reduction factor $\theta = 0.2$:							
P_{warp}	P_{fill}	$E_{\text{warp}} \cdot t$	$E_{\text{fill}} \cdot t$	G	Q_{s}	f_{warp}	f_{fill}
4.17	3.76	612.39	607.54	29.98	2.64	92.88	87.00

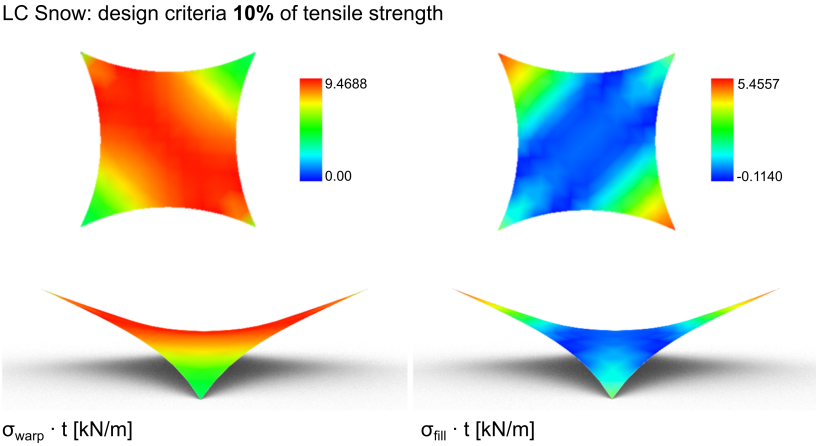

Figure 5.6: LC Snow: stress distribution at design point with a strength reduction factor $\theta = 0.1$.

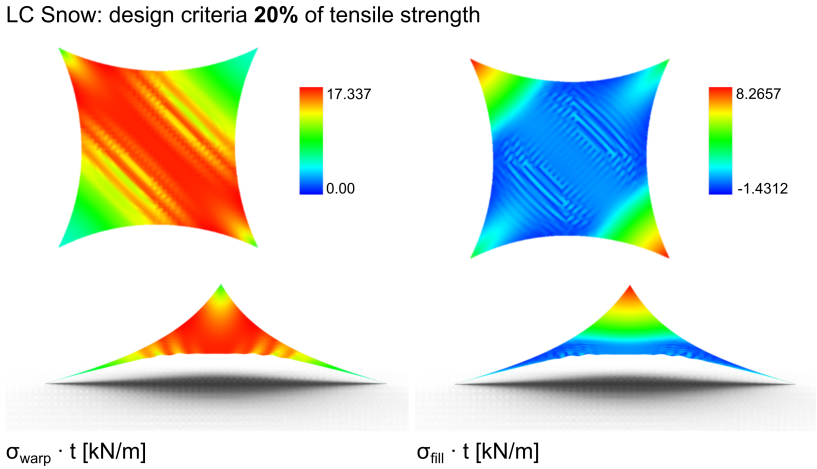

Figure 5.7: LC Snow: stress distribution at design point with a strength reduction factor $\theta = 0.2$.

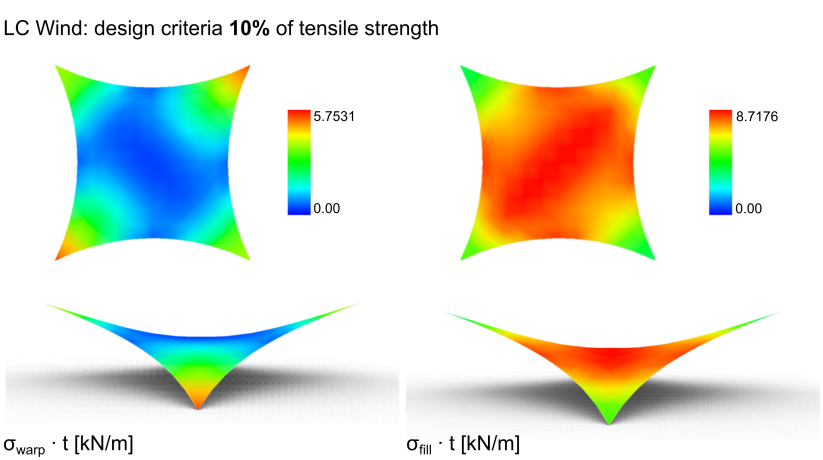

Figure 5.8: LC Wind: stress distribution at design point with a strength reduction factor $\theta = 0.1$.

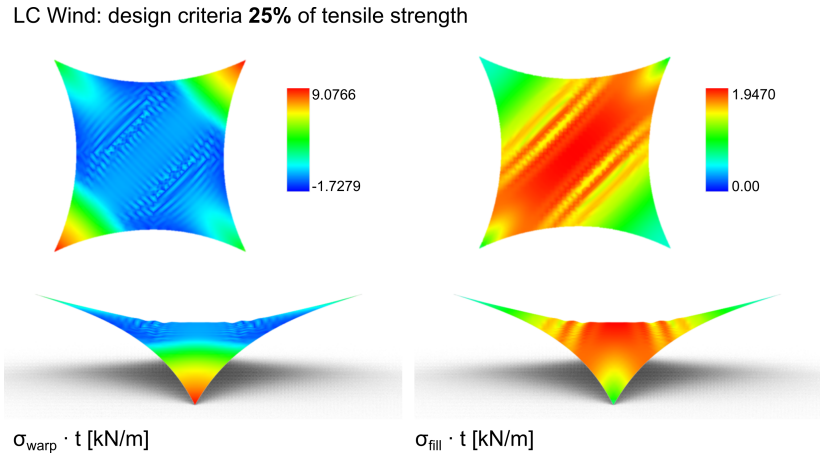

Figure 5.9: LC Wind: stress distribution at design point with a strength reduction factor $\theta = 0.25$.

For the illustration of the minor influence of the system parameters (prestress and stiffness variables), the diagrams in Figure 5.10 show the action (load $\lambda \cdot Q$) - effect of action (maximum stress) - diagram both for the system modelled with the design values for θ=0.1 and with the mean values. One can observe only a small deviation between the curves. For the same load level, the maximum stress is only slightly higher when using the system parameters of the design point.

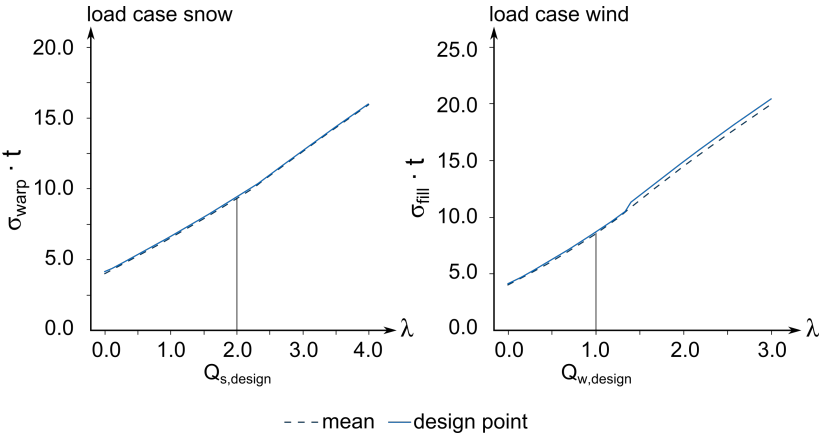

Figure 5.10: Action - effect of action diagram for the design points and mean values: left: snow load, right: wind load.

Reliability analysis with reduced dimension

Based on the parameter study and the knowledge about the low α- sensitivities of prestress and stiffness variables, the reliability analysis was repeated for the load case wind with reduced dimensions. Only the wind load and tensile strength in fill direction were considered as uncertain variables for this. A good agreement (relative deviations are smaller than 2%) can be observed between the full and the reduced reliability analysis, see Table 5.8. Without the knowledge about the α-sensitivities, the low influence of the other variables could also have been detected by a prior sensitivity analysis or parameter studies, as was shown in this section.

Table 5.8: Reliability indices reached for the load case wind under consideration of load and strength distributions only.

θ	β	rel. deviation [%] to β in Table 5.4	decisive direction
0.10	1.30	0.8	fill
0.15	2.70	0.8	fill
0.20	3.65	1.4	fill
0.25	4.52	1.3	fill

Conclusion of RR4

The conclusions that were already drawn within this section were confirmed by the comparison of our results with the ones reported at Vrije Universiteit Brussel (VUB), who hosted RR4:

- The load intensity and tensile strength are the dominant factors for the reliability analysis,
- the uncertainties of other parameters are negligible.

The reliability analysis at VUB was based on a model that was reduced to a cable net. Due to this, the model possessed some fundamentally different properties from the continuous one presented here. The additional differences in the formfound state, wind load implementation and chosen limit state functions did not allow for a direct comparison of the analysis results. However, the main conclusions listed above could be reached by both participants of the study. In Smedt et al. [106] and Smedt et al. [107], reliability analysis studies were published for the exemplary structure of the hypar.

Since load intensity and strength are the uncertain parameters which are covered with an explicit partial factor in the semi-probabilistic safety concept of the Eurocodes, it can be concluded that the hypar example's safety can be assessed with the simplified regulations for non-linearities. It should nonetheless be noted, that the semi-probabilistic safety concept was developed for linear limit state functions and thus assumes that the superposition of effects of actions is feasible, which is not the case for membrane structures.

Another remaining question is how to handle the risk that local damage like a tear is in the vicinity of the maximal stress. As Gosling et al. [53] states, a general reduction of the tensile strength is pessimistic. A stress reduction factor in combination with the discussed simulation uncertainties can lead to the situation that the target reliability index cannot be met for the given membrane. The application of a preliminary parameter study or sensitivity analysis (e.g. adjoint sensitivity analysis) can be highly recommended since it gives a first impression of system relationships and behaviour by showing which parameters are more or less important. This information can be used e.g. to verify the FORM analysis by comparing with the α-sensitivities or to reduce the dimension of the stochastic problem by a deterministic treatment of less influential parameter.
Very promising work on the subject of model and safety assessment and sensitivity analysis for lightweight and other structures is currently conducted by Martin Fußeder and his colleagues, see e.g. Fußeder et al. [41] and Fußeder et al. [42].

Wrinkle formation
When performing reliability analysis for membrane structures for stress limit states, one has to be aware that the simulation of the membrane near the limit state can become challenging. Due to wrinkle formation, the stress state becomes vague and thus an additional uncertainty is introduced. The definition of a wrinkling and thus tension-loss limit state function instead of using the tensile strength as a stress limit could prevent dealing with these uncertainties. Future research activities should focus on the role of this special simulation issue. Especially where cable nets are used to model membrane structures, the effects of both shear in the membrane and wrinkling must additionally be incorporated.

Figures 5.7 and 5.9 showed the hypar structure under snow and wind suction loading that was increased until wrinkling appeared. The loss of tension in one direction leads to wrinkles and false compressive forces unless wrinkling models are applied as suggested in e.g. Jrusjrungkiat [63]. The shape and extension of the wrinkles depends on the discretisation and thus necessitates a convergence study in order to achieve reliable results.

5.3 Verification of Stability Considering Non-Linear Structural Behaviour

The current Eurocode for structural design, prEN 1990:2020-09 [96], states that ''Non-linear analysis should be used when the behaviour of the structure or members has a significant influence on forces in and deformations of the structure'' (clause 7.2.2). Furthermore, engineers need to differentiate between the types of non-linearity, i.e. loading, material and geometry, and ensure sufficient accuracy of the representative numerical model. The reliability analysis of *Round Robin Exercise 4* showed, that the load and tensile strength are the dominant factors on the reliability. It can thus be concluded, that the semi-probabilistic safety concept of the Eurocodes, which applies partial factors to those parameters, can be employed for structural membranes under the precondition of investigating all necessary load combinations (i.e. no superposition of effects of actions). The remaining challenge lies in the non-linearity of the relation between action and effect of action. This particularity will be treated in this section and solution strategies for the verification of a sufficient safety level within the Eurocode framework will be presented.

In general, two types of non-linearity can be identified (see Figure 5.11), leading to different kinds of safety factor applications.

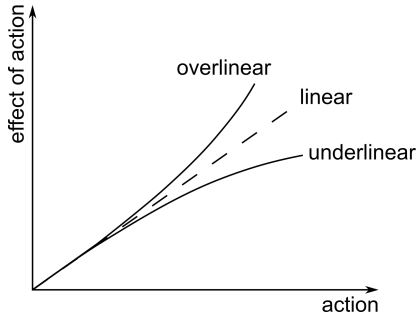

Figure 5.11: Types of non-linearity: overlinear and underlinear effect of action.

Verification of ultimate limit states

According to prEN 1990:2020-09 [96], Equation 5.6 has to hold true for the verification of the ultimate limit state (ULS), i.e. the proof of stability.

$$E_d \leq R_d \tag{5.6}$$

E_d is the design value of the effect of actions and R_d is the design value of the corresponding resistance. In general, the design value of the effect of actions, E_d, can be determined by the following equation,

$$E_d = \gamma_{Sd} E\left[\sum(\gamma_f \psi F_k); a_d; X_{Rd}\right], \tag{5.7}$$

with γ_{Sd} being the partial factor accounting for uncertainties of the actions and action effect model, the sum indicating a combination of actions, γ_f being the partial factor considering an unfavourable deviation of an action from its representative value, ψ representing a combination factor applied to a characteristic variable action, F_k the characteristic action, a_d indicating design values of geometrical properties and X_{Rd} the values of material properties used in the assessment of E_d.

The partial factors γ_f and γ_{Sd} can be multiplied, to reach simplified partial factors on actions ($\gamma_F = \gamma_f \times \gamma_{Sd}$) or on effects of actions ($\gamma_E = \gamma_f \times \gamma_{Sd}$), see Table 5.9.

Partial factors for actions γ_F are supposed to be applied for the design of linear structural systems and ''non-linear structural systems in which an increase in action causes a disproportionally larger increase in the effects of actions'', whereas γ_E applies to ''non-linear structural systems involving a single predominant action in which an increase in action causes a disproportionally smaller increase in its effect'' (prEN 1990:2020-09 [96], clause 8.3.2). Figure 5.12 depicts the principle of applying the two different factors as was discussed in detail in Philipp [91]. The precondition for the categorisation is to reach a safe-sided design. In Appendix A, the factors are applied to an exemplary membrane structure, highlighting their influence on the resulting design effects and hence the dimensioning.

Table 5.9 summarises the categories of non-linearity, as specified in prEN 1990:2020-09 [96] (clause 8.3.2).

Table 5.9: Categories of of non-linear structural behaviour according to prEN 1990:2020-09 [96].

overlinear
''an increase in action causes a disproportionally larger increase in the effect of actions''
partial factor γ_F applied to the characteristic action
$$E_d = E\left[\sum F_d; a_d; X_{Rd}\right] = E\left[\sum(\gamma_F \psi F_k); a_d; X_{Rd}\right] \quad (5.8)$$

underlinear
''an increase in action causes a disproportionally smaller increase in the effect of actions''
partial factor γ_E applied to the effect of action
$$E_d = \gamma_E E\left[\sum F_{rep}; a_d; X_{rep}\right] = \gamma_E E\left[\sum(\psi F_k); a_d; X_{rep}\right] \quad (5.9)$$

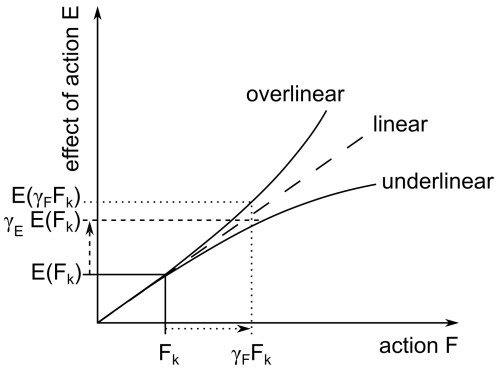

Figure 5.12: Dimensioning points resulting from applying γ_F or γ_E, adapted from Philipp [91].

Sensitivity analysis

In prEN 1990:2020-09 [96], a recommendation for sensitivity analysis is given for cases of non-linear limit state functions, in order to identify the most sensitive input parameter and in order to define the applicable usage of the partial factors.

Sensitivity analysis can help the investigations on the nature of non-linear behaviour and the consequences for the application of safety factors, as introduced in the previous section. It can also be used in order to find the importance factors of a number of varying input parameters (see Section 5.2).

In its simplest form, sensitivity analysis can be performed by evaluating a function for a small number of input parameters (e.g. load factors) and looking into the gradient or curvature between the resulting points. With respect to non-linearities in the action effects, it thus only requires the load input to be varied and the results of e.g. stresses to be documented. In Uhlemann et al. [113], it was suggested to perform a one-step sensitivity analysis to assess the category of non-linearity of EC 0. For this, the effects of actions E_k and E_{test} are evaluated for a load input values F_k and $F_k \cdot f$. The interpolation is then investigated by η/f, with η depicting the change in the structural answer: $\eta = E_{test}/E_k$ and concluding about the category of non-linearity according to Table 5.10. As this approach strongly depends on the interval that is being investigated, the conclusion is limited to this interval.

Table 5.10: Assessment of non-linear structural behaviour by Uhlemann et al. [113].

η/f	structural behaviour
>1	overlinear
1	linear
<1	underlinear

In order to overcome this limitation, Philipp [91] suggests the consideration of the curvature of the structural answer, for the categorisation of the non-linearity for structural membranes. For this, a two-step sensitivity analysis needs to performed and the radius of curvature evaluated.

For an estimation of the ''level'' of non-linearity for the structural behaviour of membranes beyond the simple hypar from RR4 and the publications mentioned above, further analyses were conducted as presented in the following section. A new approach to the categorisation is presented, in which the root of the action effect curves is shifted to the prestress level. Consequently, the formfound stress state is regarded as the starting point for the evaluation.

5.4 Investigations on the Load-Bearing Behaviour of Classical Membrane Shapes

The topic of non-linear load-response curves is highly prominent for structural membranes but yet only little investigation has been published. Due to this, typical membrane shapes as defined by Knippers et al. [67] were analysed for the loading scenarios of snow and wind suction in order to create an overview of their behaviour with the goal of identifying a pattern to the categorisation on non-linearity that was presented in the previous section. Since a membrane's shape defines the main load transfer paths (see also Section 3.2) and most built structures can be traced back to repetitions of a limited assortment of shapes, the following four basic types were considered for the analyses:

- sail-surface (hypar)
- surface defined by ridge and valley cables (tent)
- arch-supported surface (saddle)
- point-supported surface (cone)

Membrane structures draw their stiffness from the combination of prestress and curvature, as explained in Section 2. The classical shapes were thus altered in their curvature properties in order to observe the effect. Figure 5.13 shows the parametric model definitions in the formfound state, including the fibre orientation. The prestress in the membrane and edge cables was kept constant while changing the support locations to manipulate the Gaussian curvature. Isotropic prestress states were prescribed and thus, minimal surfaces were created by the formfinding analyses in order

to ensure constant prestress states throughout the surfaces as starting points for the structural analyses.

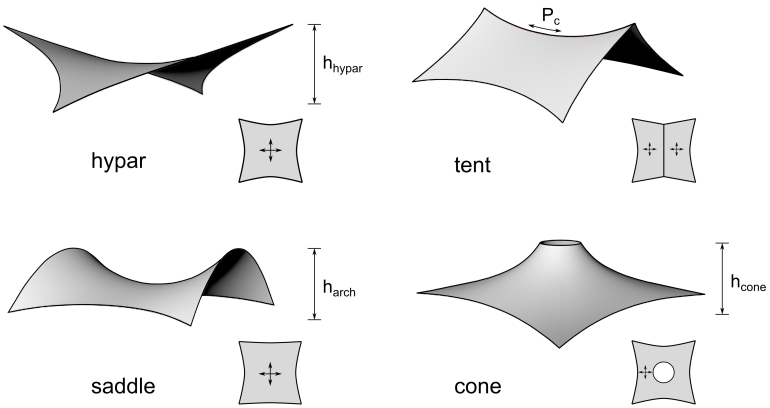

Figure 5.13: Basic shapes of membrane structures.

All basic shapes were designed on a rectangular ground space of 6 by 6 m with an initial height of 2 m, as defined in previous *Round Robin Exercises*. The prestress in the membrane P_{pre} was set to 4 kN/m at a thickness t of 0.001 m and the edge cables were prestressed with P_{cable} 30 kN. Young's moduli E_{membrane} were chosen as 1000 MN/m^2 for the membrane and E_{cable} 205 MN/m^2 for the cables.

As the *Round Robin* study (see RR4, Section 5.2) was only conducted for a hypar with quite low curvature, its geometry was investigated once more in this study, including an alteration of the curvature through varying the overall height h_{hypar}. While the saddle- and cone-shaped membranes can also be altered in curvature by changing the overall heights h_{saddle} and h_{cone}, for the tent structure the prestress of the ridge cable P_{c} was manipulated to this purpose. Figure 5.14 depicts the resulting Gaussian curvature for the investigated surfaces.

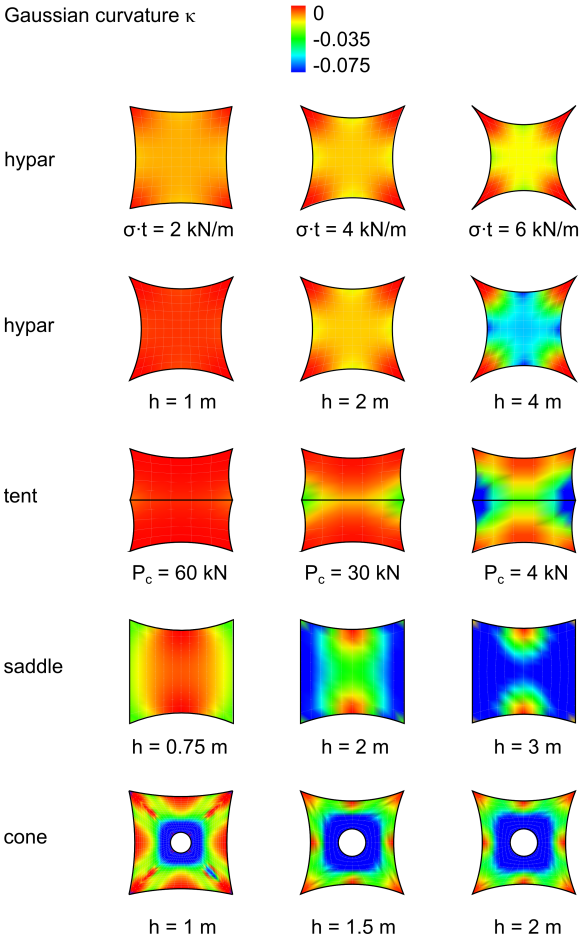

Figure 5.14: Basic shapes of membrane structures: Gaussian curvature plots ranging from 0 (red) to -0.075 (blue).

As Section 5.2 already showed for the hypar, sensitivity analysis lead to the conclusion, that the load intensity has the biggest influence on the structural answer. Consequently, this investigation of the classical membrane shapes focuses on increasing the loads by the load factor λ and portraying

non-linearities of action effects. A snow load with a characteristic value ($\lambda = 1$) of 0.6 kN/m^2 and a wind suction load with a characteristic value of 1.0 kN/m^2 are applied to the whole membrane surface in every analysis. The loads are applied in incremental steps and increased up to $\lambda = 4$. It should be noted, that these load applications are aimed at emphasizing the principal structural behaviour in simplified loading scenarios rather than portraying realistic load cases, as snow would slide off steep areas and the surface parts subjected to wind suction and compression would vary with the wind direction.

The evaluation of the stress results is conducted for the pre-integrated principal stresses ($P_{1,\max}$ and $P_{2,\min}$) and those in the defined fibre directions ($F_{\text{fibre,max}}$ and $F_{\text{fibre,min}}$), assuming linear-elastic orthotropic material properties with Poisson's ratio of 0. Furthermore, the analyses were performed regardless of the magnitude of unrealistic negative stresses and it should be noted that as soon as the taut state is lost, the stress and deformation results depend on the discretization and are only evaluable qualitatively.

In order to conclude about the type of non-linearity for each stress response, the gradient m_{lin} is determined by interpolating between the principal stresses at $\lambda = 0$ and $\lambda = 1$, i.e. between the prestress and the maximum principal stress calculated at the characteristic load level q_{k}, see Equation 5.10. The stress response curve is then categorised in comparison to the linear extrapolation with m_{lin} as over- or underlinear. In contrast to the sensitivity studies presented in Section 5.3, the formfound stress state is regarded as the starting point for the categorisation.

$$m_{\text{lin}} = \frac{P_{1,\max} - P_{\text{pre}}}{q_{\text{k}}} \tag{5.10}$$

5.4.1 Hypar

The hypar membrane spans between two low- and two highpoints that are connected by cables. The fibre directions are not defined between the supports, but with a rotation of 45°, as indicated in Figure 5.13, leading to a notable difference between the stresses in fibre direction and the principal stresses. Table 5.11 summarises the investigated geometries, their curvature properties and the gradient of the linear extrapolation m_{lin} calculated from $P_{1,\max}$ for $\lambda = 0$ to 1 (black dotted line in Figure 5.15).

Table 5.11: Parameters of the hypar membrane with varying curvature.

	h_{hypar} [m]	minimum Gaussian curvature κ_{min}	medium Gaussian curvature κ	gradient $m_{\text{lin, snow}}$ and $m_{\text{lin, wind}}$
low curvature	1.0	-0.005	-0.003	7.9 and 10.3
medium curvature	2.0	-0.020	-0.010	4.5 and 5.0
high curvature	4.0	-0.073	-0.037	2.5 and 3.3

The graphs in Figure 5.15 show the resulting stresses for the load cases of snow and wind suction. The start of wrinkling (i.e. the minimal stress value becoming negative) is marked for all curves by square and circle symbols for $P_{2,\text{min}} < 0$ and $F_{\text{fibre,min}} < 0$. The kinks appearing shortly after the start of wrinkling indicate a change in the structural behaviour that can be interpreted as the change to a one-dimensional load transfer via the respective tension cords.

A rising inclination of the stress curves can be observed with lowering curvature, that can be linked to the higher geometrical stiffness of the membrane structure with more curvature. It can also be observed, that the stresses increase in a fairly linear way until tension loss appears in one direction and hence the load bearing behaviour changes. Due to the hypar's symmetrical geometry, the structural responses are quite similar for both load cases. For the load case snow, the main tension cord is established between the highpoints and for wind suction it develops between the lowpoints.

As the point of tension loss is mainly determined by the magnitude of prestress in the membrane, the effect of varying the prestress was investigated in addition and is portrayed in Figure 5.16. It can be seen that the stresses increase with nearly the same gradient ($m_{\text{lin,snow}}$ ranging from 4.3 to 4.9 and $m_{\text{lin,wind}}$ from 4.6 to 5.0) until tension is lost in one direction.

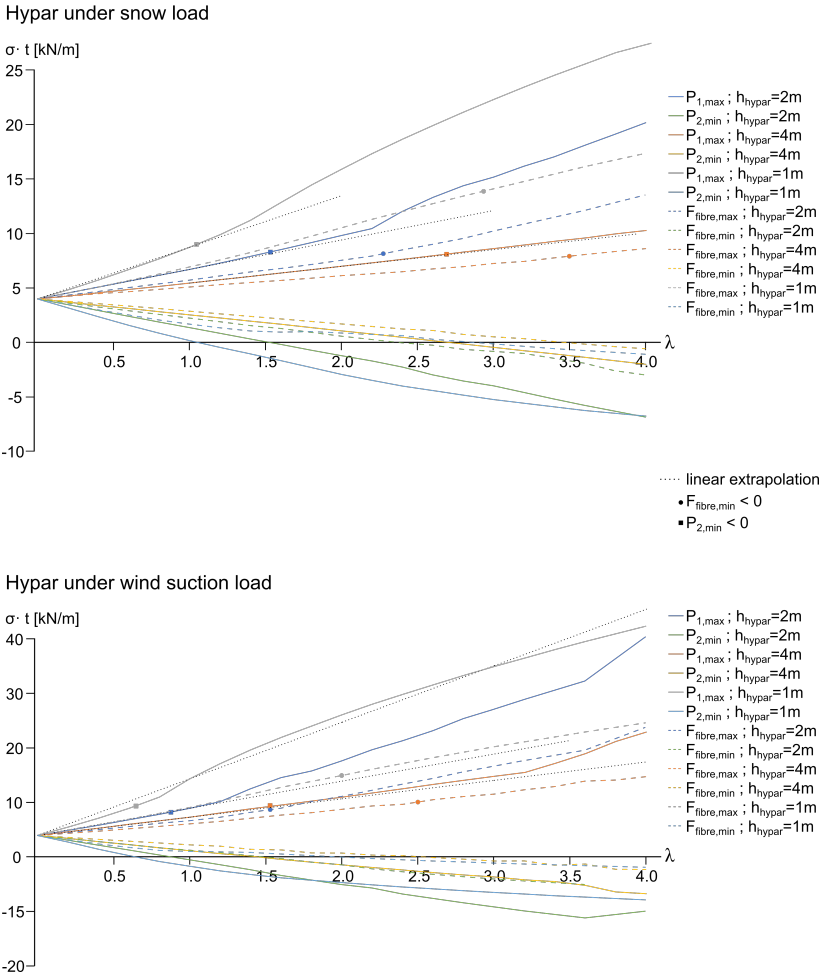

Figure 5.15: Load-stress graph for a hypar with varying curvature under snow- (top) and wind suction load (bottom).

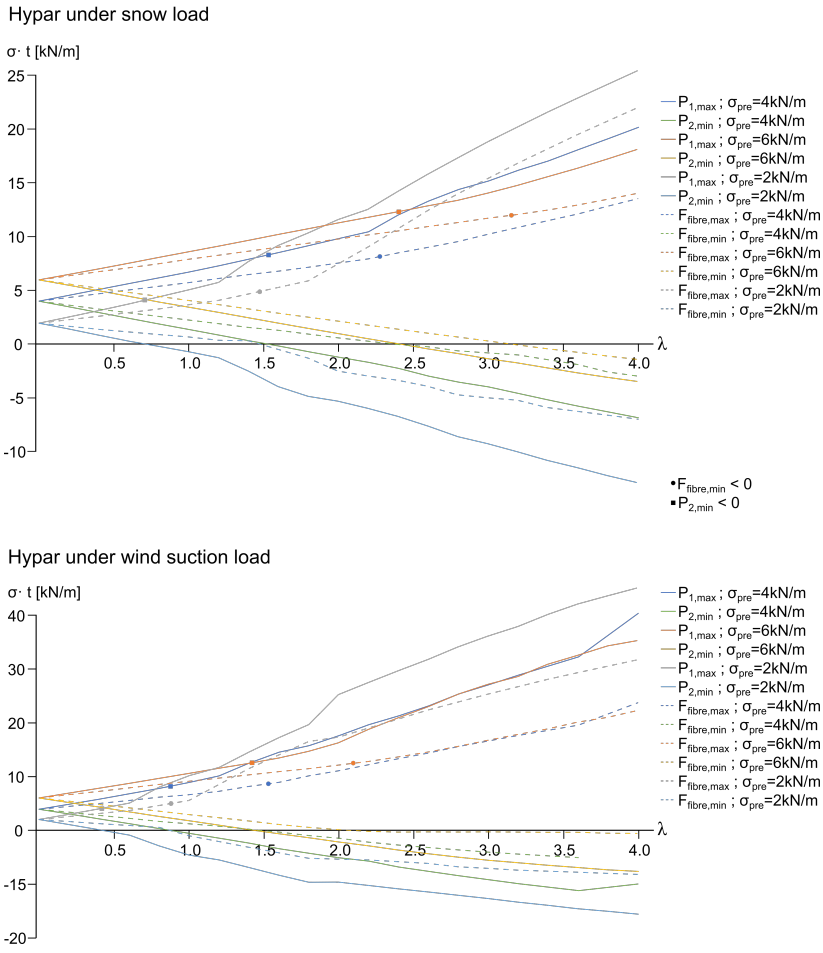

Figure 5.16: Load-stress graph for a hypar with varying prestress under snow- (top) and wind suction load (bottom).

5.4.2 Tent

The tent membrane's curvature properties are manipulated by adapting the prestress of the ridge cable P_c, resulting in different gradients m_{lin} as indicated in Table 5.12. For the tent structure with high curvature, the cable prestress was chosen such that a continuously curved surface is generated, transferring the loads to the edge cables and supports. For the other parameter combinations, the ridge cable mainly transfers the loads to the supports and the structural behaviour thus changes fundamentally. As can be seen in Figure 5.14, the surfaces between ridge and edge cables only possess little curvature once the ridge cable is prestressed with a significantly larger force.

Table 5.12: Parameters of the tent membrane with varying curvature.

	P_c [kN]	minimum Gaussian curvature κ_{min}	medium Gaussian curvature κ	gradient $m_{lin,\,snow}$ and $m_{lin,\,wind}$
low curvature	60.0	-0.008	-0.004	5.2 and 5.9
medium curvature	30.0	-0.037	-0.019	5.9 and 0.8
high curvature	4.0	-0.16	-0.08	3.9 and 7.7

The change of the load transferring mechanism of the tent structure from low to medium and high curvature can be observed in the stress plots in Figure 5.17. In contrast to the hypar case, the changing Gaussian curvature cannot directly be linked to the inclination of the stress curves due to this. A kink in the positive stress curves can be observed shortly after the loss of tension in one direction for the tent with high curvature (orange lines). Again, this can be interpreted as a change to a load-transfer in the tension cord.

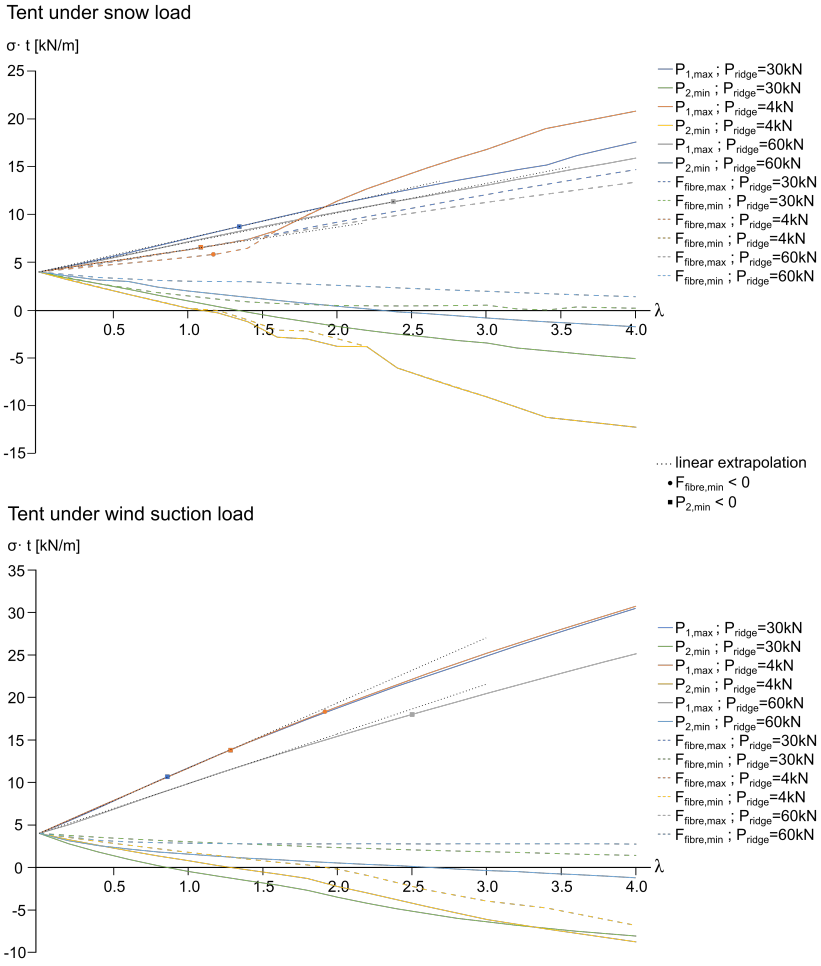

Figure 5.17: Load-stress graph for a membrane with a ridge cable with varying curvature under snow- (top) and wind suction load (bottom).

5.4.3 Saddle

The saddle-shaped membrane possesses significantly larger Gaussian curvatures in all configurations compared to the other shapes, see Table 5.13 and Figure 5.14. The arches were modelled as continuous supports for the membrane surface.

Table 5.13: Parameters of the saddle membrane with varying curvature.

	h_{arch} [m]	minimum Gaussian curvature κ_{min}	medium Gaussian curvature κ	gradient $m_{\text{lin, snow}}$ and $m_{\text{lin, wind}}$
low curvature	0.75	-0.034	-0.017	8.8 and 7.3
medium curvature	2.0	-0.086	-0.043	4.3 and 4.9
high curvature	3.0	-0.109	-0.055	2.9 and 3.7

As for the hypar case, the curvature properties can be linked to the gradient of the stress curves shown in Figure 5.18. The lower the curvature of the formfound geometry is, the higher the stress results become and vice versa. The load factor at which tension is lost in one direction (marked by the squares and circles for $P_{1,\text{max}}$ and $F_{\text{fibre,max}}$) shifts to lower values with lower curvature. Regarding the non-linearity of the stress responses, it can be noted that all curves are nearly linear, especially for the load-factor $\lambda \leq 1.5$ which is mostly relevant for the safety verification. Furthermore, the graphs show that the principal stresses $P_{1,\text{max}}$ and fibre stresses $F_{\text{fibre,max}}$ overlap in most areas due to the modelled fibre orientation along the main tension cords (i.e. between the arches for snow- and between the edge cables for wind-load).

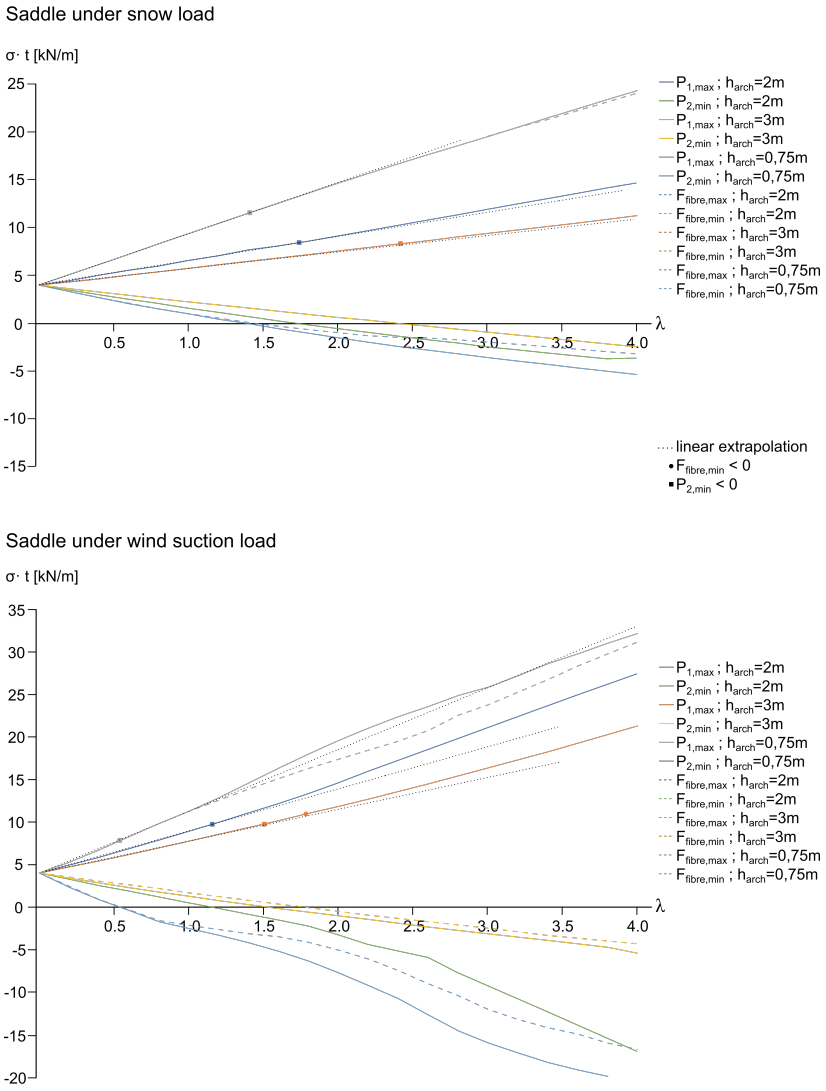

Figure 5.18: Load-stress graph for an arch-supported membrane with varying curvature under snow- (top) and wind suction load (bottom).

5.4.4 Cone

For the cone, the upper ring was modelled with a radius of 0.8 m and the height h_{cone} was chosen in order to manipulate the curvature properties. However, the minimum and medium Gaussian curvature values are mainly determined by the surface close to the upper ring (see Figure 5.14) and are summarised in Table 5.14. Due to the chosen prerequisite of generating a minimal surface in order to start structural analysis at a uniform prestress state, the cone's height could not be chosen arbitrarily, as explained in detail in e.g. Philipp et al. [90].

Table 5.14: Parameters of the cone membrane with varying curvature.

	h_{cone} [m]	minimum Gaussian curvature κ_{min}	medium Gaussian curvature κ	gradient $m_{\text{lin, snow}}$ and $m_{\text{lin, wind}}$
low curvature	1	-0.29	0	5.6 and 3.9
medium curvature	1.5	-0.70	0	4.4 and 3.4
high curvature	2.0	-0.70	0	5.3 and 3.0

The stress results of the cone subjected to snow load were very close to the linear extrapolation and the taut state was kept up to a load factor λ as high as 2.4. This can be explained by the main load transfer between the supports - i.e. in meridian direction. For the wind suction load, both the meridian and the ring direction were activated by the load acting normal to the surface. It can be observed that wrinkling starts at a much lower load intensity, but still the maximum stress curves stay rather linear until λ reaches about 2.0, as the main tension cords between the upper ring and the point supports is activated. For $\lambda > 2$, a change in curvature can be observed for these tension cords as they flap through.

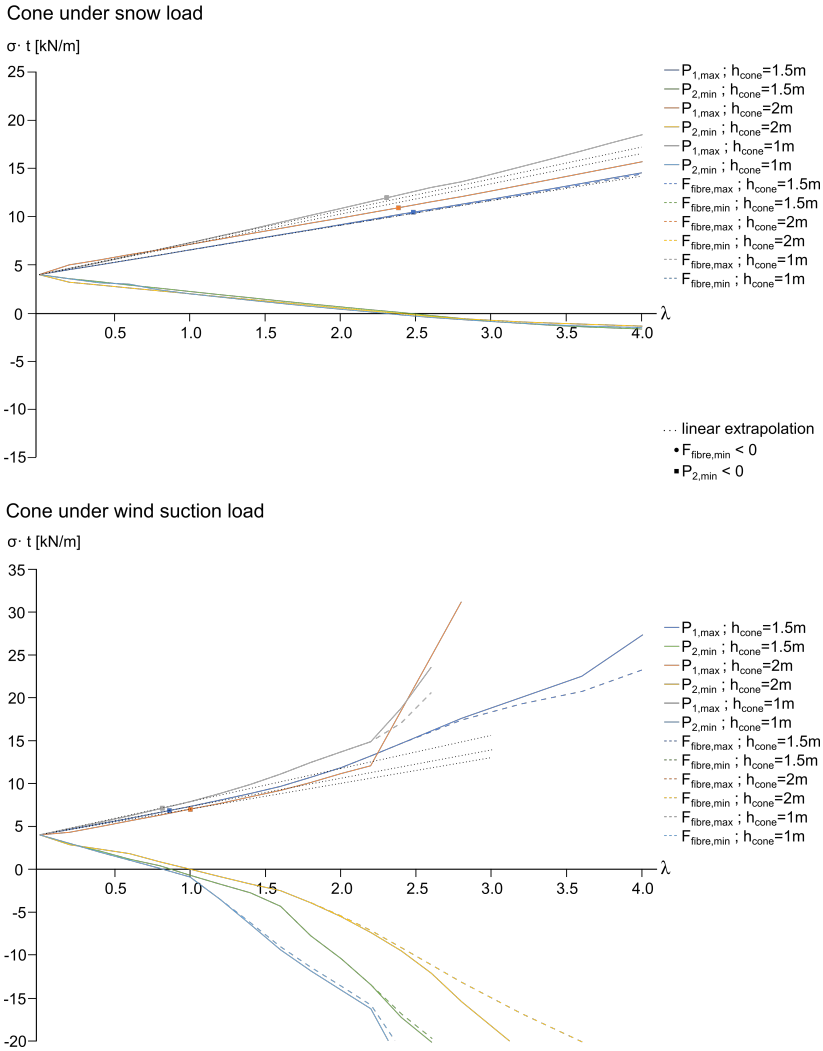

Figure 5.19: Load-stress graph for a cone with varying curvature under snow- (top) and wind suction load (bottom).

5.4.5 Comparison and Conclusion

To conclude this parameter study, the load-bearing behaviour of the introduced basic shapes with similar curvature properties is compared. Figure 5.20 indicates the maximum and minimum principal stresses resulting in the hypar, tent, saddle and cone for the previously introduced load cases. The considered geometries possess similar curvature properties in the formfound state, as summarised in Table 5.15 and visible in Figure 5.14.

Table 5.15: Parameters of compared basic shapes with similar curvature properties.

shape	minimum Gaussian curvature $\kappa_{\min}$	medium Gaussian curvature κ	gradient $m_{\text{lin, snow}}$ and $m_{\text{lin, wind}}$
hypar with $h_{\text{hypar}} = 4$ m	-0.073	-0.037	2.5 and 3.3
saddle with $h_{\text{arch}} = 2$ m	-0.086	-0.043	2.9 and 3.7
tent with $P_{\text{ridge}} = 4$ kN/m	-0.16	-0.08	3.9 and 7.7
cone with $h_{\text{cone}} = 1.5$ m	-0.70	0	4.4 and 3.4

As the graphs show and the gradients of the linear extrapolation $m_{\text{lin, snow}}$ indicate, the resulting principal stresses $P_{1,\max}$ are close up to $\lambda = 1.5$ for the snow load. For the wind-suction load, the gradients and stress results lie further apart. Especially the tent structure's maximum stress increases more, which can be explained by the rather flat area in the middle of this shape subjected to the wind suction and the flexibility of the edge cables that constitute the supports of the membrane surface.

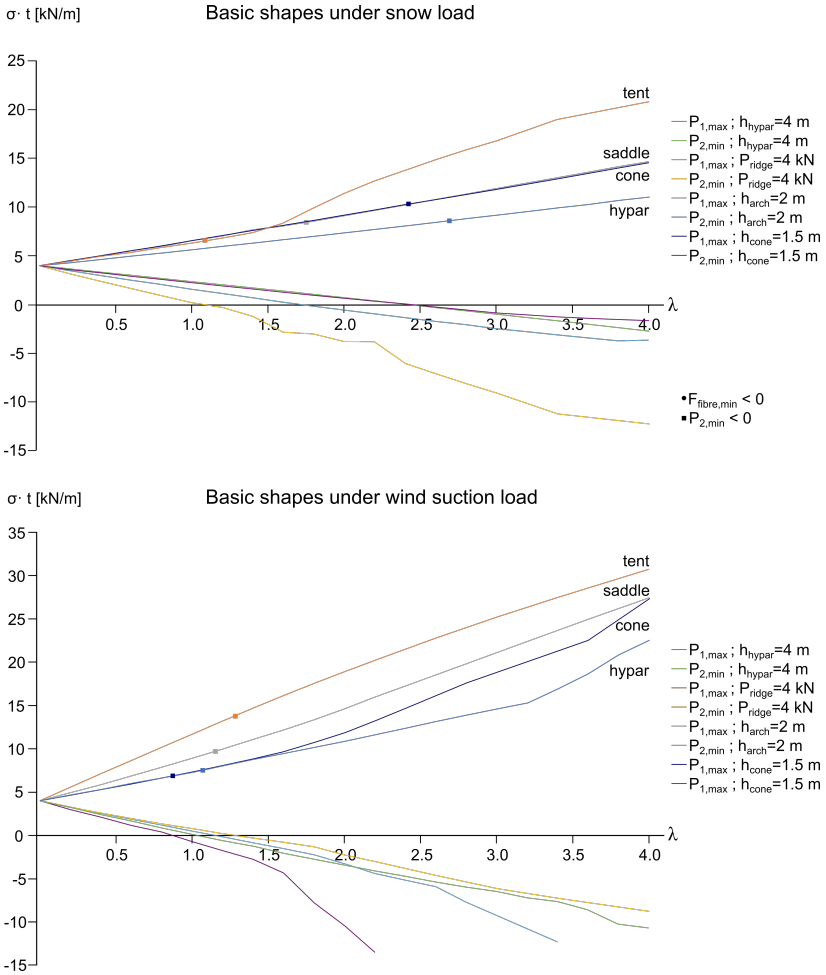

Figure 5.20: Load-stress graph for the basic shapes with similar curvature properties under snow- (top) and wind suction load (bottom).

It can be concluded that a preliminary categorisation into under- or over-linear behaviour is not possible for the classical membrane shapes with respect to geometrical properties or the applied load cases. Table 5.16 provides an overview of the detected non-linearities according to prEN 1990:2020-09 [96]. Investigations of the type of non-linearity for membrane structures should thus be conducted individually. However, a fairly linear increase in stress results was observed until tension was lost in one direction. Due to this, the parameter studies should be repeated in the future under consideration of a wrinkling model (as briefly explained in Section 3.2) to enable the quantification of the stresses developing in the wrinkled state.

Table 5.16: Categorisation of non-linear behaviour for basic membrane shapes.

shape	snow load	wind suction load
hypar	overlinear	underlinear
tent	not conclusive	underlinear
saddle	almost linear / not conclusive	almost linear / not conclusive
cone	overlinear	almost linear / not conclusive

Furthermore, the categorisation itself due to a disproportional deviation from a linear response as suggested in prEN 1990:2020-09 [96] should be discussed for future investigations. The graphs indicate nearly linearly increasing maximum stress values for all basic shapes within the typically considered load intensities. This observation raises the question of how to define the mentioned disproportional deviation and if it is at all applicable in these cases, especially if the prestress is considered as the root of the rising action effects, as explained in the beginning of this section (see Equation 5.10).

Summary

This chapter explains the challenges arising from the uncertainties of input parameters for the verification of limit states of structural membranes. It furthermore summarises the current approach to covering these uncertainties in the Eurocodes. Lightweight structures are prone to show non-linear behaviour, which is why a sensitivity analysis can be useful to reach conclusions on which influencing parameters are relevant for the verification of a sufficient safety level. This was shown with the reliability analysis performed for an exemplary hypar structure of the *Round Robin Exercise 4*. The loads' intensity proved to be the driving factor for this hypar's structural answer. As only little investigations on membranes other than the hypar have been known to this point, so-called classical membrane shapes with varying curvature properties were further investigated in a parametric study with regard to their behaviour under rising external loading. The categorisation into over- and underlinear action effects was conducted and yielded no dependable pattern, except for the observation of nearly linearly increasing stress results in the range of design actions. It can be concluded, that a categorisation of the non-linearity - as suggested for the application of the Eurocodes' safety concept that was developed for linear limit state functions - is not possible a priori and membrane structures should be evaluated individually for each project.

CHAPTER 6

CONCLUSIONS AND OUTLOOK

The CAD-integrated design cycle is presented as a highly beneficial solution for hand-in-hand design and analysis of structural membranes in this thesis. The incorporation of non-linear numerical analysis into the vast design space offered by a parametric CAD environment through Isogeometric B-Rep Analysis enables the unified workflow with one model.

Structural membranes are introduced with their main characteristics as tensile lightweight structures in Chapter 2. The fundamentals of differential geometry and continuum mechanics are conveyed, followed by a description of the most common materials used in membrane design and state-of-the art material models. Furthermore, the Finite Element Method is briefly explained with Isogeometric B-Rep Analysis as the basis for CAD-integrated design and analysis.

In Chapter 3, the design cycle for structural membranes is described and the interactions are pointed out. Well-established solutions for formfinding and structural analysis (with an outlook on the development of a harmonised verification code) are explained. The development and implementation of cutting pattern generation with IBRA lead to the completion

of the CAD-integrated design cycle and thus constitutes as a milestone of this research. Additionally, the concept of mounting analysis is briefly described.

The innovative concept of the unified workflow for the design and analysis of membranes, leading to the closed design cycle in one software environment is displayed in Chapter 4. By preserving the full B-Rep model and using embedded element formulations, the interactions of formfinding, structural analysis, cutting pattern generation and mounting are taken into account. The advantage of CAD integration is highlighted by a number of application examples and the possibility of an interactive and interdisciplinary design in a parametric environment is shown. The presented concepts were implemented in the Plugin Kiwi!3d [66] for the parametric add-on Grasshopper to Rhinoceros [101] and are freely accessible.

As reliability analysis plays a significant role for the safety evaluation of membrane structures, it is treated in Chapter 5. After introducing the essential principle and previous research endeavours towards uncertainty quantification for membrane design and analysis, the results of a *Round Robin Exercise* on the reliability of a hypar structure are shown. In addition, basic concepts for sensitivity analysis towards the categorisation of nonlinear structural behaviour in accordance with the European standards are summarised. The load-bearing behaviour of typical membrane shapes is investigated within a parametric study in this context.

In Appendix A, the current proof of safety of a simple membrane structure is laid out according to prCEN/TS, 19102:2021 [95], depicting the effect of the Eurocodes' current regulations on non-linearities.

Appendix B illustrates the application of the parametric CAD-integrated design cycle for structural membranes in teaching engagements.

This thesis thus demonstrates novel approaches that are applicable in membrane design and analysis on a large scale. Innovative design solutions are facilitated within the parametric CAD-integrated framework. As all design steps, as well as detailed geometrical aspects can be depicted by the CAD-integrated model, it can be regarded as a large step towards the creation of a digital twin.

Further research opportunities for membrane design and analysis that were beyond the scope of this thesis, are indicated in the remainder.

As pointed out in Section 2.3, the appropriate description of the mechanical behaviour of membrane materials is a challenging task. Future research should focus on an accessible material model. This implies the introduction of descriptive model parameters known in engineering, that are thus feasible for implementation and fit within the currently employed testing strategies for textiles and foils.

With respect to cutting pattern generation and mounting analysis, sophisticated material models could enhance the results and thus allow designers and engineers to perform highly accurate construction analysis on the basis of the correct reference geometry. The incorporation of manufacturing constraints into the pattern design would further improve this process.

The investigation of wrinkling models within the IGA framework is another open research topic. Their inclusion into the CAD-integrated design environment for structural membranes would advance it significantly, as wrinkling models allow for a quantitative interpretation of stress results once the taut state is lost at any point of a membrane's surface.

Finally, the recent publication of prCEN/TS, 19102:2021 [95] and the investigations on reliability analysis described in Chapter 5 showed, that further research on how to treat non-linearity in verification is necessary. First of all, the points mentioned above would help to limit model uncertainties and secondly help to quantify the effect of simplified models by direct comparisons. Therefore, detailed investigations could be conducted under the consideration of numerical models with different levels of non-linearity (e.g. material) in order to formulate requirements for predictive analysis in the field of membrane design.

The treatment of non-linear structural behaviour within the semi-probabilistic safety concept of the Eurocodes is a current research topic not only for membranes but engineering structures in general. Apart from the non-linear structural behaviour under external loading, a more detailed evaluation of the prestress state, e.g. by mounting analysis, should be investigated in the future, since the magnitude of the prestress has a significant influence on the structural answers (see Section 5.4). So far, the formfound shape and stress state build the ''starting point'' of structural analysis and hence for the stress values computed as a basis for the verification of a

sufficient safety level. Due to the double-curvature of membrane structures, it is generally not possible to achieve the exact stress state through construction. Mounting analysis can help to assess a realistic stress state, as briefly shown in Goldbach et al. [47]. The effect of the different stress states and equilibrium shapes resulting from formfinding and mounting analysis should be evaluated in a future project, by e.g. utilizing the possibilities of parametrisation and linking consecutive analyses within the CAD-integrated design cycle.

APPENDIX A

VERIFICATION EXAMPLE

In order to illustrate the effect of the current verification approach from the prCEN/TS, 19102:2021 [95], the formulae were applied to the simple example from Chapter 3 (see Figure 3.5). The considered structure is an isotropically prestressed membrane that spans between five fixed supports and uniformly prestressed edge cables. The characteristic material parameters and load intensities were chosen in accordance with common assumptions for technical textiles and the site of Munich. The application of the snow and wind-load on the whole surface presents a simplified approach, certainly not resulting in the most economical solution. The snow would only adhere to steep areas under extreme conditions and wind suction on the whole surface is also highly unlikely to occur - both loads could thus be applied to a reduced surface area. However, these load scenarios fulfil the task of possibly depicting the non-linear structural behaviour of the membrane structure and were thus chosen in the presented way. The maximum principal stress $P_{1,\max}$ was considered as the action effect for the dimensioning point. Again, this choice was made in order to illustrate the mechanical behaviour, as well as the effect of the modifying factors from

the codes, rather than aiming at an economic design. The prestress in the membrane P_{pre} was set to a pre-integrated value of 4 kN/m at a thickness t of 0.001 m and the edge cables were prestressed with P_{cable} 30 kN. Young's moduli E_{membrane} were chosen as 1000 MN/m^2 and Poisson's ratio ν to 0.4 for the membrane and E_{cable} 210 MN/m^2 for the cables. The calculated characteristic load intensities of snow and wind suction were $q_{\text{s}} = q_{\text{w}} = 0.5$ kN/m^2, following the regulations given for snow zone 1 and a simplified shed roof according to DIN EN 1991 [38].

In the first step of the verification process, the structure needs to be investigated in a geometrically non-linear analysis, in order to reach the dimensioning point from the resulting stress values. Figures A.1 and A.2 show the relation between action (load) and effect-of-action (maximum principal stress) for both load cases. Clearly, the classification of under- or overlinear behaviour cannot be made for the whole structure, but a distinction can be made with respect to the load scenario. A slightly underlinear curve emerges under snow-load, while the reaction under pure wind-suction is slightly overlinear, when regarding the maximum principal stress response $P_{1,\text{max}}$ and using the extrapolation of P_{pre} to $P_{1,\text{max}}$ at characteristic load level as the linear reference (indicated by the orange line in the figure). The figures also depict the linear extrapolation from 0 to $P_{1,\text{max}}$ at characteristic load level with dashed lines - leading to a categorisation of underlinear curves for both load cases. The dimensioning points, i.e. the resulting design effects f_{Ed} are summarised in Table A.1. Since the values resulting for a categorisation of underlinear, i.e. $f_{\text{Ed}} = 1.5 \cdot E(q_{\text{k}})$ are higher than the other ones, they clearly lie on the safe side.

However, the treatment of the prestress needs to be further discussed as it strongly influences the resulting values. As discussed in Section 5.4, structural analysis is performed on the basis of a prestressed membrane structure. Consequently, the effect of actions could also be regarded as the stress increase with respect to the given prestress. This would lead to $f_{\text{Ed}} = 1.5 \cdot E(q_{\text{k}}) - P_{\text{pre}}$ for underlinear behaviour, in this case leading to values that are very close to the (over-)linear ones, see Table A.1.

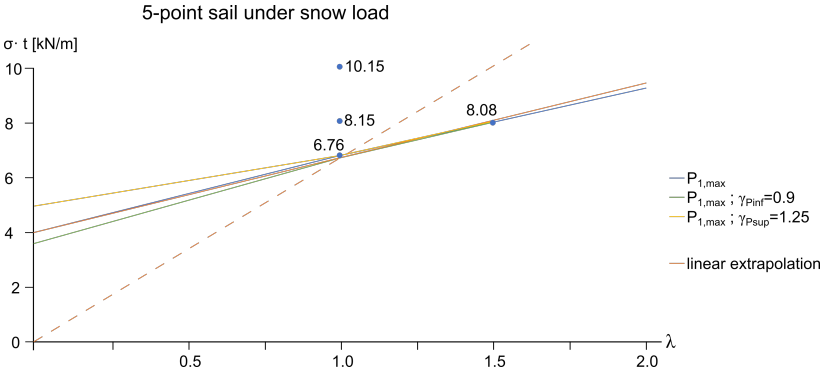

Figure A.1: Exemplary membrane structure under snow load.

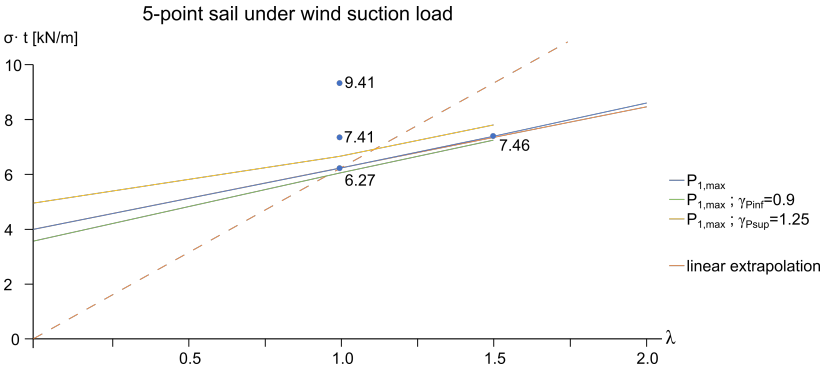

Figure A.2: Exemplary membrane structure under wind suction load.

Once the dimensioning points have been deduced from structural analysis, the modification factors from prCEN/TS, 19102:2021 [95] can be applied for the verification of ULS under consideration of the respective design situations. The two load cases in this example lead to two different design resistance values, see Equations A.1 and A.2. The provided values of modification factors are given in Table A.2.

Table A.1: Design effects f_{Ed} for snow- and windload.

design situation	underlinear dimensioning point $f_{\mathrm{Ed}} = 1.5 \cdot E(q_{\mathrm{k}})$	overlinear dimensioning point $f_{\mathrm{Ed}} = E(1.5 \cdot q_{\mathrm{k}})$	mod. underlinear dimensioning point $f_{\mathrm{Ed}} = 1.5 \cdot E(q_{\mathrm{k}}) - P_{\mathrm{pre}}$
snow	$P_{1,\max} = 10.15$ kN/m	$P_{1,\max} = 8.08$ kN/m	$P_{1,\max} = 8.15$ kN/m
wind	$P_{1,\max} = 9.41$ kN/m	$P_{1,\max} = 7.46$ kN/m	$P_{1,\max} = 7.41$ kN/m

$$f_{\mathrm{Rd,snow}} = \frac{f_{\mathrm{k,23}}}{\gamma_{\mathrm{M0}} \cdot k_{\mathrm{biax}} \cdot k_{\mathrm{age}} \cdot k_{\mathrm{dur,M}} \cdot k_{\mathrm{size}}} \tag{A.1}$$

$$f_{\mathrm{Rd,wind}} = \frac{f_{\mathrm{k,23}}}{\gamma_{\mathrm{M0}} \cdot k_{\mathrm{biax}} \cdot k_{\mathrm{age}} \cdot k_{\mathrm{size}}} \tag{A.2}$$

Table A.2: Modification factors for fabric structures, according to prCEN/TS, 19102:2021 [95].

γ_{M0}	k_{biax}	k_{age}	$k_{\mathrm{dur,M}}$	k_{size}
1.4	1.0 - 1.2	1.1 - 1.4	1.1 - 1.2	1.0

Finally, the needed characteristic tensile strength values $f_{\mathrm{k,23}}$ of a fabric for this exemplary calculation were computed with the given modification factors, such that the ULS condition of $f_{\mathrm{Ed}} \leq f_{\mathrm{Rd}}$ is satisfied. The results are summarised in Table A.3.

Table A.3: Resulting characteristic material strength $f_{\mathrm{k,23}}$ for the exemplary 5-point sail.

load case	underlinear dimensioning point $f_{\mathrm{Ed}} = 1.5 \cdot E(q_{\mathrm{k}})$	overlinear dimensioning point $f_{\mathrm{Ed}} = E(1.5 \cdot q_{\mathrm{k}})$	underlinear dimensioning point $f_{\mathrm{Ed}} = 1.5 \cdot E(q_{\mathrm{k}}) - P_{\mathrm{pre}}$
snow	$f_{\mathrm{k,23}} = 17.19$ to 28.64 kN/m	$f_{\mathrm{k,23}} = 13.69$ to 22.80 kN/m	$f_{\mathrm{k,23}} = 13.80$ to 22.99 kN/m
wind	$f_{\mathrm{k,23}} = 14.49$ to 22.13 kN/m	$f_{\mathrm{k,23}} = 11.49$ to 17.55 kN/m	$f_{\mathrm{k,23}} = 11.41$ to 17.43 kN/m

APPENDIX B

STUDENT PROJECTS

The membrane workshop at TUM as a joint teaching activity of the Chair of Structural Analysis and the former Chair of Structural Design introduces the challenges of lightweight design and analysis to students of Civil Engineering and Architecture. They learn about the different steps of membrane design and build interactive teams for a project work each year. During the last workshops, Kiwi!3d [66] was established as a design and analysis tool and the response was very positive. The application of the CAD-integrated design cycle resulted in a very large variety in the design projects and an improved atmosphere in the student teams who now worked on one project with one model. Selected projects are shown here, highlighting the applicability of the parametric CAD-integrated environment for the design and analysis of structural membranes.

The design topics of the 2019 and 2020 membrane workshop were quite different and therefore chosen as representatives of the course. In 2019, the students dealt with the permanent cover of a large leisure facility, whereas the 2020 course focused on a flexible pavilion structure. At this point I would like to express my gratitude towards Prof. Dr.-Ing. Lars Schiemann for the enriching collaboration of teaching the membrane workshop together. Guiding the students, as their design ideas evolved, was one of the highlights of my teaching activities.

Figure B.1 gives an impression of the student's take on formfinding with physical models and some final presentation models.

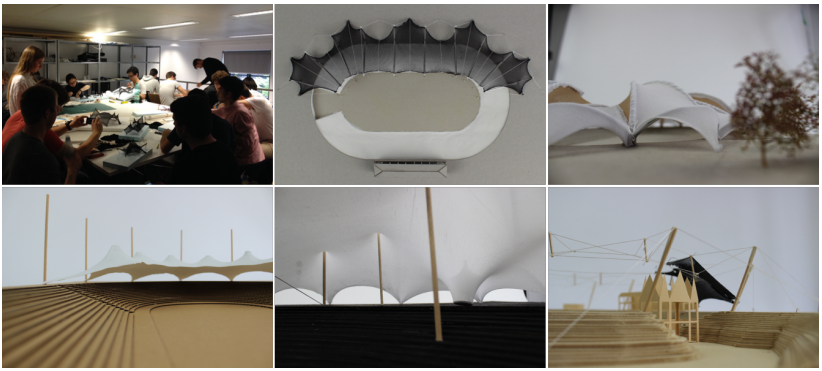

Figure B.1: Membrane workshop: physical formfinding and presentation models.

Membrane workshop 2019

Topic: Design a permanent roof for the Kaltenberg Arena, which is mainly used for a medieval knights' tournament festival.
Both of the projects teams, that are represented here, used the CAD-integrated parametric design environment in a creative way by playing with geometrical and mechanical parameters and thus finding their optimal solutions for the membrane's shape, as well as the primary structure. Figures B.2 and B.3 portray the final designs with renderings that were created from the one CAD model that all participants could work on.

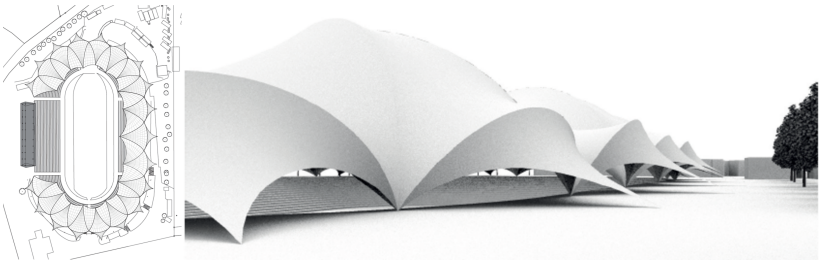

Figure B.2: Membrane workshop 2019: arena roof designed by F. De Vriendt, A. Nikolaou, A. Zanchi.

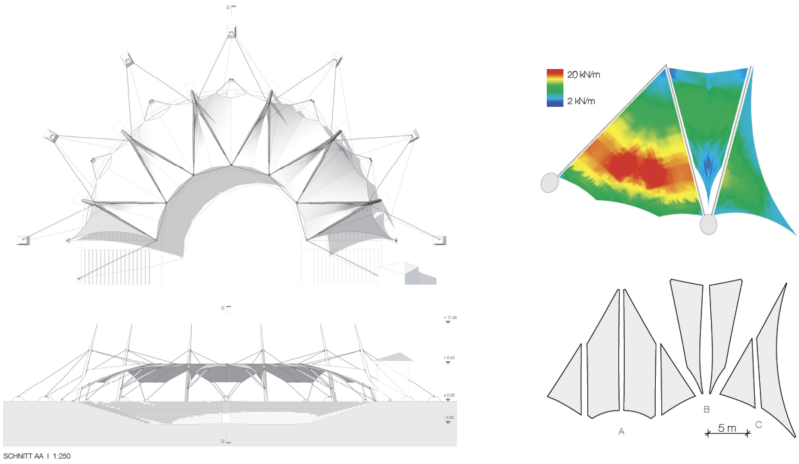

Figure B.3: Membrane workshop 2019: arena roof designed by F. Lobmüller, F. Nothdurft, F. Wahl, M. Waske.

Membrane workshop 2020

Topic: Design and conceptualise a pavilion or sculpture to be placed within the main campus of TUM.
The designs that were conducted during the 2020 membrane workshop again revealed the advantages of the unified workflow within the CAD

environment for the joint work of architects and engineers. As the course had to be held online, the project teams could clearly benefit from the possibility to perform all design steps within the CAD environment and with one model, as no data conversion was necessary. Figure B.4 shows the membrane sculpture, that was designed by one project team. In addition to extensive parameter studies that lead to the final design, they used the CAD environment to incorporate advanced design aspects such as texture and light analysis. Figure B.5 depicts a pavilion project from that year, that was built by a rather complex combination of structural elements and shapes. CAD-integrated formfinding allowed the team, to elaborate on the boundary conditions in an interactive way, in order to reach their optimal design solution.

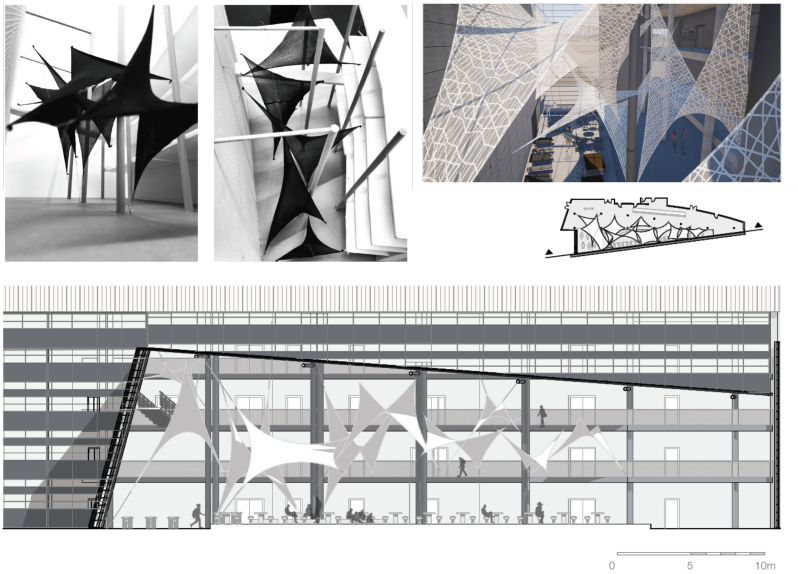

Figure B.4: Membrane workshop 2020: Membranes at StuCafé TUM, designed by D. Birk, C. De Vuono, S. Pérez Castrillo, M. Rau.

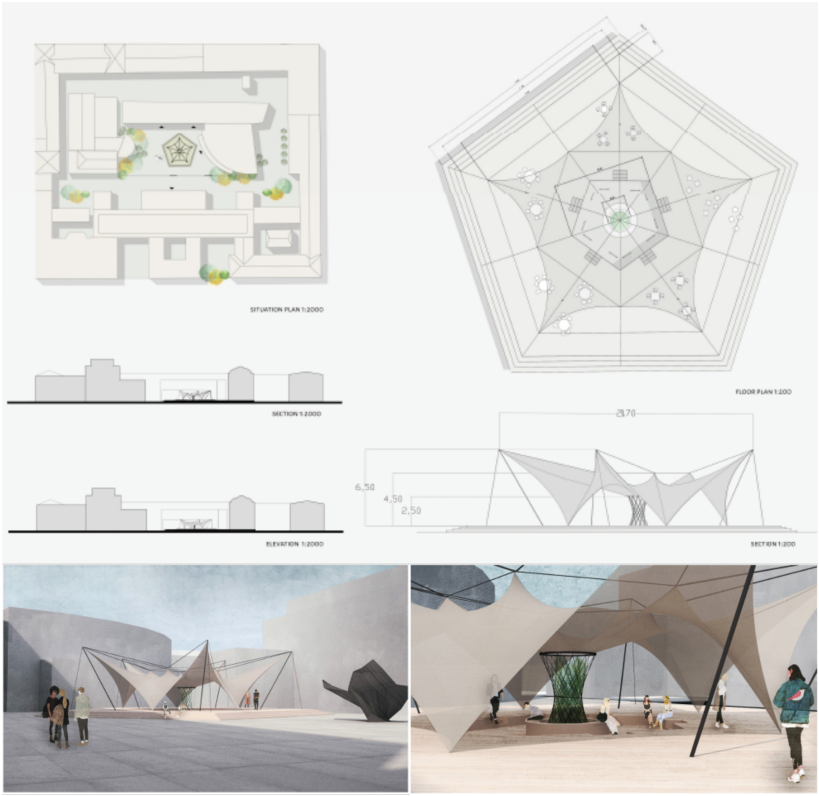

Figure B.5: Membrane workshop 2020: Pavilion at TUM, designed by V. Convence, C. Nespoli, I. Schepp, B. Stamenitis.

BIBLIOGRAPHY

[1] Y. Aimene, E. Vidal-Salle, B. Hagege, F. Sidoroff, and P. Boisse. "A hyperelastic approach for compostie reinforced large deformation analysis." In: *Journal of Composite Materials* 44 (2010), pp. 5–26.

[2] V. Alic. "Computational Methods in Conceptual Structural Design." Dissertation. Lund: Lund University, 2018.

[3] H. AlSofi, R. Wüchner, and K.-U. Bletzinger. "Evaluation of added mass modeling approaches for the design of membrane structures by fully coupled fsi simulations." In: *Textile Composites and Inflatable Structures VII*. Ed. by E. Oñate, K.-U. Bletzinger, and B. Kröplin. Barcelona: International Center for Numerical Methods in Engineering (CIMNE), 2015, pp. 318–343. ISBN: 978-84-944244-8-9.

[4] H. Altenbach, J. Altenbach, and R. Rikards. *Einführung in die Mechanik der Laminat- und Sandwichtragwerke*. Stuttgart: Deutscher Verlag für Grundstoffindustrie, 1996. ISBN: 9783527308972.

[5] A. Apostolatos, F. Péan, A. Emiroglu, R Wüchner, and K.-U. Bletzinger. "An isogeometric mortar surface coupling method for trimmmed multipatch cad geometries with application to fsi." In: *7th GACM Colloquium on Computational Mechanics*. 2017.

[6] A. Apostolatos, M. Breitenberger, R. Wüchner, and K.-U. Bletzinger. "Domain Decomposition Methods and Kirchhoff-Love Shell Multipatch Coupling in Isogeometric Analysis." In: *Isogeometric analysis and applications 2014*. Ed. by

B. Jüttler and B. Simeon. Vol. 107. Cham, Heidelberg, and New York: Springer, 2015, pp. 73–101. ISBN: 978-3-319-23314-7.

[7] D. Ballhause. "Diskrete Modellierung des Verformungs- und Versagensverhaltens von Gewebemembranen." Dissertation. Stuttgart: Universität Stuttgart, 2007.

[8] D. Balzani. "Polyconvex Anisotropic Energies and Modeling of Damage Applied to Arterial Walls." Dissertation. Darmstadt: Technische Universität Darmstadt, 2006.

[9] M. R. Barnes. "Form finding and analysis of tension space structures by dynamic relaxation." Dissertation. London: City University London, 1977.

[10] Y. Başar and W. B. Krätzig. *Mechanik der Flächentragwerke. Theorie, Berechnungsmethoden, Anwendungsbeispiele.* Braunschweig: Vieweg, 1985. ISBN: 3-528-08685-8.

[11] K.-J. Bathe. *Finite Element Procedures.* Prentice Hall, 1996. ISBN: 9780133014587.

[12] A. M. Bauer, M. Breitenberger, B. Philipp, R. Wüchner, and K.-U. Bletzinger. "Embedded structural entities in NURBS-based isogeometric analysis." In: *Computer Methods in Applied Mechanics and Engineering* 325 (2017), pp. 198–218. DOI: 10.1016/j.cma.2017.07.010.

[13] A. M. Bauer, R. Wüchner, and K.-U. Bletzinger. "Innovative CAD-integrated Isogeometric Simulation of Sliding Edge Cables in Lightweight Structures." In: *Journal of the International Association for Shell and Spatial Structures* 59.4 (2018), pp. 251–258. DOI: 10.20898/j.iass.2018.198.039.

[14] A. M. Bauer. "CAD-integrated isogeometric analysis and design of lightweight structures." Dissertation. München: Technische Universität München, 2020.

[15] P. Beccarelli. *Biaxial Testing for Fabrics and Foils.* Cham: Springer International Publishing, 2015. ISBN: 978-3-319-02227-7. DOI: 10.1007/978-3-319-02228-4.

[16] T. Belytschko, W. K. Liu, and B. Moran. *Nonlinear Finite Elements for Continua and Structures.* Wiley, 2000.

[17] W. Berger, H. Faulstich, P. Fischer, A. Heger, H.-J. Jacobasch, A. Mally, I. Mikut, and W. Bobeth. *Textile Faserstoffe*. Berlin, Heidelberg: Springer, 1993. ISBN: 978-3-642-77656-4.

[18] M. Bischoff, W. A. Wall, K.-U. Bletzinger, and E. Ramm. "Models and finite elements for thin-walled structures." In: *Encyclopedia of Computational Mechanics*. Ed. by E. Stein, R. d. Borst, and T. J. R. Hughes. Vol. 2, Solids and Structures. Chichester: John Wiley & Sons, Ltd, 2004. ISBN: 9780470846992. DOI: 10.1002/0470091355.ecm026.

[19] K.-U. Bletzinger and E. Ramm. "A General Finite Element Approach to the Form Finding of Tensile Structures by the Updated Reference Strategy." In: *International Journal of Space Structures* 14.2 (1999), pp. 131–145. DOI: 10.1260/0266351991494759.

[20] R. Blum, H. Bögner-Balz, and J. Köhnlein. "On the mechanical behaviour of ETFE-films: Elastic range, yielding conditions, break determined by different test methods and the influence of the results on the analysis of ETFE-structures." In: *Procedia Engineering* 155 (2016), pp. 496–506. DOI: doi:10.1016/j.proeng.2016.08.053.

[21] W. Boehm. "Inserting new knots into B-spline curves." In: *Computer-Aided Design* 12.4 (1980), pp. 199–201. DOI: 10.1016/0010-4485(80)90154-2.

[22] H. Bögner-Balz, R. Blum, and J. Köhnlein. "Structural behaviour of fabrics and coatings for architectural fabric structures." In: *Fabric Structures in Architecture*. 2015, pp. 123–157. ISBN: 9781782422334. DOI: 10.1016/B978-1-78242-233-4.00004-8.

[23] J. Bonet and A. J. Burton. "A simple orthotropic, transversely isotropic hyperelastic constitutive equation for large strain computations." In: *Computer Methods in Applied Mechanics and Engineering* 162 (1998), pp. 151–164. DOI: 10.1016/S0045-7825(97)00339-3.

[24] M. Breitenberger. "CAD-integrated design and analysis of shell structures." Dissertation. München: Technische Universität München, 2016.

[25] M. Breitenberger, A. Apostolatos, B. Philipp, R. Wüchner, and K.-U. Bletzinger. “Analysis in computer aided design: Nonlinear isogeometric B-Rep analysis of shell structures.” In: *Computer Methods in Applied Mechanics and Engineering* 284 (2015), pp. 401–457. DOI: 10.1016/j.cma.2014.09.033.

[26] B. Bridgens and M. Birchall. “Form and function: The significance of material properties in the design of tensile fabric structures.” In: *Engineering Structures* 44 (2012), pp. 1–12. DOI: 10.1016/j.engstruct.2012.05.044.

[27] B. N. Bridgens and P. D. Gosling. “A Predictive Fabric Model for Membrane Structure Design.” In: *Textile Composites and Inflatable Structures II*. Ed. by E. Oñate and B. Kröplin. Vol. 8. Computational Methods in Applied Sciences. Dordrecht: Springer Netherlands, 2008, pp. 35–50. ISBN: 978-1-4020-6855-3.

[28] Carat++. *https://www.bgu.tum.de/st/software/forschung/carat/*.

[29] M. Coelho, D. Roehl, and K.-U. Bletzinger. “Material model based on NURBS response surfaces.” In: *Applied Mathematical Modelling* 51 (2017), pp. 574–586. DOI: 10.1016/j.apm.2017.06.038.

[30] E. Cohen, T. Lyche, and L. L. Schumaker. “Degree raising for splines.” In: *Journal of Approximation Theory* 46.2 (1986), 170—181. DOI: 10.1016/0021-9045(86)90059-6.

[31] E. Cohen, R. F. Riesenfeld, and G. Elber. *Geometric modeling with splines: An introduction*. Natick and Mass: AK Peters, 2001. ISBN: 978-1568811376.

[32] G. Colasante. “Tensile structures: biaxial testing and constitutive modelling of coated fabrics at finite strains.” Dissertation. Milano: Politecnico di Milano, 2014.

[33] J. Colliers, M. Mollaert, J. Vierendeels, and L. de Laet. “Collating Wind Data for Doubly-curved Shapes of Tensioned Surface Structures (Round Robin Exercise 3).” In: *Procedia Engineering* 155 (2016), pp. 152–162. DOI: 10.1016/j.proeng.2016.08.016.

[34] E. Corne et al. *SaP-Report: Prospect for European guidance for the Structural Design of Tensile Membrane Structures*. Science and Policy Report. Publications Office of the European Union, 2016. ISBN: 978-92-79-54702-7.

[35] J. A. Cottrell, T. J. R. Hughes, and Y. Bazilevs. *Isogeometric Analysis: Toward Integration of CAD and FEA*. Chichester: John Wiley and Sons Ltd., 2009. ISBN: 0470748737. DOI: 10.1002/9780470749081.

[36] E. DeSmedt. *Round Robin exercise IV*. TensiNet Association. 2017.

[37] F. H. Dieringer. "Numerical methods for the design and analysis of tensile structures." Dissertation. München: Technische Universität München, 2014.

[38] DIN EN 1991. *Einwirkungen auf Tragwerke - Teil 1-1: Allgemeine Einwirkungen auf Tragwerke - Wichten, Eigengewicht und Nutzlasten im Hochbau (Deutsche Fassung EN 1991-1-1:2002 + AC:2009)*. Beuth Verlag, Berlin, 2002.

[39] O. Ditlevsen and H. Madsen. *Structural Reliability Methods*. John Wiley, 1996. ISBN: 9780471960867.

[40] M. Do Carmo. *Differential Geometry of Curves and Surfaces*. Englewood-Cliffs: Prentice-Hall, 1976. ISBN: 978-0132125895.

[41] M. Fußeder, R. Wüchner, and K.-U. Bletzinger. "Computational Sensitivity Analysis in the Design Process of Pre-Stressed Lightweight Structures." In: *Proceedings of the IASS Annual Symposium 2020/21 and the 7th International Conference on Spatial Structures*. Ed. by G. P. S.A. Behnejad and O. Samavati. submitted. 2021.

[42] M. Fußeder, R. Wüchner, and K.-U. Bletzinger. "Sensitivitätsanalyse mit verallgemeinerten Einflussfunktionen zur Tragwerksbewertung bei Modellparametervariationen." In: *Bauingenieur* 96 (2021), pp. 191–200.

[43] J. Gade, R. Kemmler, M. Drass, and J. Schneider. "Enhancement of a meso-scale material model for nonlinear elastic finite element computations of plain-woven fabric membrane structures." In: *Engineering Structures* 177 (2018), pp. 668–681. DOI: 10.1016/j.engstruct.2018.04.039.

[44] J. Gade, M. Bischoff, and R. Kemmler. “Advanced Approaches for Analysis and Form Finding of Membrane Structures with Finite Elements.” In: *Structural Membranes 2017*. Ed. by K.-U. Bletzinger, E. Oñate, and B. Kröplin. Barcelona: International Center for Numerical Methods in Engineering (CIMNE), 2017, pp. 275–293. ISBN: 978-84-946909-9-0.

[45] C. Galliot and R. H. Luchsinger. “Determination of the response of coated fabrics under biaxial stress: comparison between different test procedures.” In: *Structural Membranes 2011*. Ed. by K.-U. Bletzinger, E. Oñate, and B. Kröplin. Barcelona: International Center for Numerical Methods in Engineering (CIMNE), 2011. ISBN: 978-84-89925-58-8.

[46] A. Goldbach and K.-U. Bletzinger. “CAD-integrated Parametric Design Cycle for Structural Membranes.” In: *Journal of the International Association for Shell and Spatial Structures* 60.4 (2019), pp. 266–272. DOI: 10.20898/j.iass.2019.202.024.

[47] A.-K. Goldbach, A. M. Bauer, and K.-U. Bletzinger. “Advantages of Isogeometric B-Rep Analysis for the parametric design of lightweight structures.” In: *Proceedings of the IASS Annual Symposium 2020/21 and the 7th International Conference on Spatial Structures*. Ed. by G. P. S.A. Behnejad and O. Samavati. submitted. 2021.

[48] A.-K. Goldbach, A. M. Bauer, R. Wüchner, and K.-U. Bletzinger. “CAD-Integrated Parametric Lightweight Design With Isogeometric B-Rep Analysis.” In: *Frontiers in Built Environment* 6 (2020). DOI: 10.3389/fbuil.2020.00044.

[49] A.-K. Goldbach, A. M. Bauer, R. Wüchner, and K.-U. Bletzinger. “Der CAD-integrierte parametrische Entwurfsprozess von Membrantragwerken.” In: *Stahlbau* (2020). DOI: 10.1002/stab.202000043.

[50] A.-K. Goldbach and K.-U. Bletzinger. “CAD-integrated Cutting Pattern Generation with the Variation of Reference Strategy.” In: *Structural Membranes 2017*. Ed. by K.-U. Bletzinger, E. Oñate, and B. Kröplin. Barcelona: International Center for Numerical Methods in Engineering (CIMNE), 2017. ISBN: 978-84-946909-9-0.

[51] A.-K. Goldbach and K.-U. Bletzinger. “Isogeometric B-Rep Analysis for finding stress-optimized cutting patterns.” In: *Proceedings of the IASS Annual Symposium 2017*. Ed. by A. Bögle and M. Grohmann. 2017.

[52] A.-K. Goldbach, M. Breitenberger, A. Widhammer, and K.-U. Bletzinger. “Computational Cutting Pattern Generation Using Isogeometric B-Rep Analysis.” In: *Procedia Engineering* 155 (2016), pp. 249–255. DOI: 10.1016/j.proeng.2016.08.026.

[53] P. D. Gosling, B. N. Bridgens, and L. Zhang. “Adoption of a reliability approach for membrane structure analysis.” In: *Structural Safety* 40 (2013), pp. 39–50. DOI: 10.1016/j.strusafe.2012.09.002.

[54] P. D. Gosling et al. “Analysis and design of membrane structures: Results of a round robin exercise.” In: *Engineering Structures* 48 (2013), pp. 313–328. DOI: 10.1016/j.engstruct.2012.10.008.

[55] L. Gründig, E. Moncrieff, P. Singer, and D. Ströbel. “High-performance cutting pattern generation of architectural textile structures.” In: *IASS-IACM 2000: Fourth International Colloquium on Computation of Shell & Spatial Structures*. Ed. by Papadrakakis, M. Samartin,A. and E. Oñate. National technical University of Athens, 2000.

[56] E. Haug, P. de Kermel, B. Gawenat, and A. Michalski. “Industrial Design and Analysis of Structural Membranes.” In: *International Journal of Space Structures* 24.4 (2009), pp. 191–204. DOI: 10.1260/026635109789968227.

[57] A. J. Herrema. “A framework for isogeometric-analysis-based design and optimization of wind turbine blades.” Dissertation. Ames: Iowa State University, 2018.

[58] M. Hohenbichler and R. Rackwitz. “Sensitivity and importance measures in structural reliability.” In: *Civil Engineering Systems* 3 (1986), pp. 203–209.

[59] G. A. Holzapfel. *Nonlinear Solid Mechanics, a Continuum Approach for Engineering*. Chichester: Wiley, 2000.

[60] M.-C. Hsu, C. Wang, A. J. Herrema, D. Schillinger, A. Ghoshal, and Y. Bazilevs. “An interactive geometry modeling and parametric design platform for isogeometric analysis.” In: *Computers & Mathematics with Applications* 70.7 (2015). DOI: 10.1016/j.camwa.2015.04.002.

[61] T. J. R. Hughes, J. A. Cottrell, and Y. Bazilevs. “Isogeometric analysis: CAD, finite elements, NURBS, exact geometry and mesh refinement.” In: *Computer Methods in Applied Mechanics and Engineering* 194.39-41 (2005), pp. 4135–4195. DOI: 10.1016/j.cma.2004.10.008.

[62] ILEK. *Institut für Leichtbau Entwerfen und Konstruieren.* Universität Stuttgart, Fakultät 02.

[63] A. Jrusjrungkiat. “Nonlinear Analysis of Pneumatic Membranes: From Subgrid to Interface.” Dissertation. München: Technische Universität München, 2009.

[64] B. Kaiser. “A generalised interface for multi-level coupling of beam unit cell meso-models to macro finite elements in draping simulation.” Dissertation. München: Technische Universität München, 2020.

[65] J.-Y. Kim and J.-B. Lee. “A new technique for optimum cutting pattern generation of membrane structures.” In: *Engineering Structures* 24.6 (2002), pp. 745–756. DOI: 10.1016/S0141-0296(02)00003-2.

[66] Kiwi!3d. *https://www.kiwi3d.com.*

[67] J. Knippers, J. Cremers, M. Gabler, and J. Lienhard. *Atlas Kunststoffe + Membranen.* München: DETAIL, 2010. ISBN: 9783920034416. DOI: 10.11129/detail.9783955530037.

[68] J. Linhard. “Numerisch-mechanische Betrachtung des Entwurfsprozesses von Membrantragwerken.” Dissertation. München: Technische Universität München, 2009.

[69] K. Linkwitz and H.-J. Schek. “Einige Bemerkungen zur Berechnung von vorgespannten Seilnetzkonstruktionen.” In: *Ingenieur-archiv* 40.3 (1971), pp. 145–158. DOI: 10.1007/BF00532146.

[70] M. Mäntylä. *An introduction to solid modeling*. Vol. 13. Principles of computer science series. Rockville, University of Michigan: Computer Science Press, 1988. ISBN: 9780881751086.

[71] B. Marussig and T. J. R. Hughes. "A Review of Trimming in Isogeometric Analysis: Challenges, Data Exchange and Simulation Aspects." In: *Archives of Computational Methods in Engineering* 30.8 (2017), p. 657. DOI: 10.1007/s11831-017-9220-9.

[72] B. Maurin and R. Motro. "Cutting Pattern of Fabric Membranes with the Stress Composition Method." In: *International Journal of Space Structures* 14.2 (1999), pp. 121–129. DOI: 10.1260/0266351991494740.

[73] J. McCartney, B. K. Hinds, and K. W. Chong. "Pattern flattening for orthotropic materials." In: *Computer-Aided Design* 37.6 (2005), pp. 631–644. DOI: 10.1016/j.cad.2004.09.006.

[74] I. Meissner, E. Möller, and F. Otto. *Frei Otto: Forschen, bauen, inspirieren ; a life of research, construction and inspiration*. München: Institut für intern. Architektur-Dokumentation Ed. Detail, 2015. ISBN: 978-3-95553-252-9. DOI: 10.11129/9783955532536.

[75] Menges, G. and Meffert, B. "Mechanical behaviour of PVC coated polyester fabrics under biaxial stress." In: *Kunststoffe* (1976).

[76] N. Metropolis and S. Ulam. "The Monte Carlo Method." In: *Journal of the American Statistical Association* 44.247 (1949), pp. 335–341. DOI: 10.2307/2280232.

[77] A. Michalski, E. Haug, J. Bradatsch, and K.-U. Bletzinger. "Virtual Design Methodology for Lightweight Structures – Aerodynamic Response of Membrane Structures." In: *International Journal of Space Structures* 24 (2009), pp. 211–221. DOI: 10.1260/026635109789968245.

[78] A. Michalski, E. Haug, R. Wüchner, and K.-U. Bletzinger. "Validierung eines numerischen Simulationskonzepts zur Strukturanalyse windbelasteter Membrantragwerke." In: *Bauingenieur* 86 (2011), pp. 129–141.

[79] M. Mollaert and B. Forster. *European Design Guide for Tensile Surface Structures*. TensiNet Association, 2004. ISBN: 90 8086 871 x.

[80] E. Moncrieff and B. Topping. “Computer methods for the generation of membrane cutting patterns.” In: *Computers & Structures* 37.4 (1990), pp. 441–450. DOI: 10.1016/0045-7949(90)90034-Y.

[81] M. E. Mortenson. *Geometric modeling*. New York: Wiley, 1985. ISBN: 0471882798.

[82] M. Motevalli, D. Balzani, J. Uhlemann, and N. Stranghöner. “On the Modeling of Textile Membranes with Nonlinear Anisotropic Material Behavior.” In: *Proc. Appl. Math. Mech.* 17.1 (2017), pp. 433–434. DOI: 10.1002/pamm.201710186.

[83] M. Motevalli, J. Uhlemann, N. Stranghöner, and D. Balzani. “Geometrically nonlinear simulation of textile membrane structures based on orthotropic hyperelastic energy functions.” In: *Composite Structures* 223 (2019), p. 110908. DOI: 10.1016/j.compstruct.2019.110908.

[84] R. Münsch and H.-W. Reinhardt. “Zur Berechnung von Membrantragwerken aus beschichteten Geweben.” In: *Bauingenieur* 20 (1995), pp. 271–275.

[85] N. K. Narayanan, R. Wüchner, and J. Degroote. “Comparison of monolithic and partitioned approaches for ponding analysis on membrane structures.” In: *14th World Congress on Computational Mechanics (WCCM) ECCOMAS Congress 2020)*. Ed. by O. A. F. Chinesta R. Abgrall and M. Kaliske. 2021. DOI: 10.23967/wccm-eccomas.2020.092.

[86] T. Oberbichler, A. M. Bauer, A.-K. Goldbach, R. Wüchner, and K.-U. Bletzinger. “CAD-integrierte Analyse im Entwurfsprozess.” In: *Bautechnik* (2019). DOI: 10.1002/bate.201800105.

[87] B. Oesterle, R. Sachse, E. Ramm, and M. Bischoff. “Hierarchic isogeometric large rotation shell elements including linearized transverse shear parametrization.” In: *Computer Methods in Applied Mechanics and Engineering* 321 (2017), pp. 383–405. DOI: 10.1016/j.cma.2017.03.031.

[88] R. W. Ogden. *Non-linear Elastic Deformation*. Mineola: Dover Publications Inc., 1984.

[89] F. Otto, W. Nerdinger, and R. Barthel, eds. *Frei Otto - das Gesamtwerk: Leicht bauen, natürlich gestalten*. Basel: Birkhäuser, 2005. ISBN: 9783764372330.

[90] B. Philipp, M. Breitenberger, I. D'Auria, R. Wüchner, and K.-U. Bletzinger. "Integrated design and analysis of structural membranes using the Isogeometric B-Rep Analysis." In: *Computer Methods in Applied Mechanics and Engineering* 303 (2016), pp. 312–340. DOI: 10.1016/j.cma.2016.02.003.

[91] B. F. Philipp. "Methodological treatment of non-linear structural behavior in the design, analysis and verification of lightweight structures." Dissertation. Technische Universität München, 2017.

[92] L. Piegl and W. Tiller. *The NURBS Book*. Second Edition. Monographs in Visual Communication. Berlin and Heidelberg: Springer, 1997. ISBN: 978-3-642-59223-2. DOI: 10.1007/978-3-642-59223-2.

[93] M. A. Popescu. "KnitCrete: Stay-in-place knitted formworks for complex concrete structures." Dissertation. Zürich: ETH Zürich, 2019. DOI: 10.3929/ethz-b-000408640.

[94] H. Pottmann. *Architectural geometry*. 1st ed. Exton, PA: Bentley Institute Press, 2007. ISBN: 9781934493045.

[95] prCEN/TS, 19102:2021. *Design of tensioned membrane structures (prCEN/TS 19102:2021-04)*. CEN - European Committee for Standardization, Brussels, 2021.

[96] prEN 1990:2020-09. *Grundlagen der Tragwerksplanung; (Deutsche und Englische Fassung prEN 1990:2020-09)*. Beuth Verlag, Berlin, 2020.

[97] L. Pyl, X. Wang, E. de Smedt, J. Colliers, M. Mollaert, and L. de Laet. "Existing Eurocodes Applied to a Membrane Structure." In: *International Symposium on Novel Structural Skins: Improving sustainability and efficiency through new structural textile materials and designs*. Vol. 155. 2016, pp. 142–151. DOI: 10.1016/j.proeng.2016.08.015.

[98] L. Pyl, X. Wang, E. de Smedt, and M. Mollaert. “Approach to a reliability framework for membrane structure design and analysis.” In: *International Journal for Computational Methods and Experimental Measurements* 5.2 (2017), pp. 105 –115. DOI: 10.2495/CMEM-V5-N2-105-115.

[99] R. Rackwitz and B. Fiessler. “Structural Reliability under Combined Random Load Sequences.” In: *Computers and Structures* 9 (1978), pp. 484–494. DOI: 10.1016/0045-7949(78)90046-9.

[100] H.-W. Reinhardt. “Ein- und zweiachsige Verformungs- und Festigkeitsuntersuchungen an einem beschichteten Gittergewebe.” In: *Mitteilungen des SFB 64* 31.75 (1975).

[101] Rhinoceros. *http://www.rhino3d.com*.

[102] D. F. Rogers. *An introduction to NURBS: With historical perspective*. San Francisco: Morgan Kaufmann Publishers, 2001. ISBN: 1-55860-669-6.

[103] J. Schröder. *Theoretische und algorithmische Konzepte zur phänomenologischen Beschreibung anisotropen Materialverhaltens*. Ed. by J. Schröder. Vol. F 96/3. Hannover: Forschungs– und Seminarberichte aus dem Bereich der Mechanik der Universität Hannover, 1996.

[104] J. Schröder and P. Neff. “Invariant formulation of hyperelastic transverse isotropy based on polyconvex free energy functions.” In: *International Journal of Solids and Structures* 40 (2003), pp. 401–445. DOI: 10.1016/S0020-7683(02)00458-4.

[105] A. Sheffer and E. de Sturler. “Parameterization of Faceted Surfaces for Meshing using Angle-Based Flattening.” In: *Engineering with Computers* 17.3 (2001), pp. 326–337. DOI: 10.1007/PL00013391.

[106] E. de Smedt, M. Mollaert, R. Caspeele, W. Botte, and L. Pyl. “Reliability-based calibration of partial factors for the design of membrane structures.” In: *Engineering Structures* 214 (2020), p. 110632. DOI: 10.1016/j.engstruct.2020.110632.

[107] E. de Smedt, M. Mollaert, M. van Craenenbroeck, R. Caspeele, and L. Pyl. “Reliability-based analysis of a cable-net structure and membrane structure designed using partial factors.” In: *Architectural Engineering and Design Management* (2020), pp. 1–10. DOI: 10.1080/17452007.2020.1738997.

[108] M. Tamke, Y. Sinke Baranovskaya, F. Monteiro, J. Lienhard, R. La Magna, and M. Ramsgaard Thomsen. “Computational knit - design and fabrication systems for textile structures with customised and graded CNC knitted fabrics.” In: *Architectural Engineering and Design Management* (2020), pp. 1–21. DOI: 10.1080/17452007.2020.1747386.

[109] TensiNet Association. *TensiNet https://www.tensinet.com/*.

[110] B. H. V. Topping. *Finite element mesh generation*. Stirling and Scotland: Saxe-Coburg Publications, 2004. ISBN: 1-874672-10-5.

[111] B. H. V. Topping and P. Iványi. *Computer aided design of cable membrane structures*. Kippen: Saxe-Coburg Publications, 2007. ISBN: 978-1874672111.

[112] J. Uhlemann. “Elastic constants of architectural fabrics for design purposes.” Dissertation. Duisburg-Essen: Universität Duisburg-Essen, 2015.

[113] J. Uhlemann, B. Stimpfle, and N. Stranghöner. “Application of the semiprobabilistic safety concept of EN 1990 in the design of prestressed membrane structures.” In: *Proceedings of Eurosteel 2014* (2014).

[114] D. Veenendaal and P. Block. “An overview and comparison of structural form finding methods for general networks.” In: *International Journal of Solids and Structures* 49.26 (2012), pp. 3741–3753. DOI: 10.1016/j.ijsolstr.2012.08.008.

[115] R. Wagner. *Bauen mit Seilen und Membranen*. Berlin: Beuth Verlag GmbH, 2016.

[116] A. M. Widhammer. “Variation of Reference Strategy: Generation of Optimized Cutting Patterns for Textile Fabrics.” Dissertation. München: Technische Universität München, 2015.

[117] R. Wüchner. “Mechanik und Numerik der Formfindung und Fluid-Struktur-Interaktion von Membrantragwerken.” Dissertation. München: Technische Universität München, 2007.

[118] Y. Zhang, Y. Lu, Y. Zhou, and Q. Zhang. “Resistance uncertainty and structural reliability of hypar tensioned membrane structures with PVC coated polyesters.” In: *Thin-Walled Structures* 124 (2018), pp. 392–401. DOI: 10.1016/j.tws.2017.12.026.

[119] O. C. Zienkiewicz. *The finite element method*. 5th ed. Oxford and Boston: Butterworth-Heinemann, 2000. ISBN: 0750650494.

[120] R. Zorrilla Martinez. “Towards the Virtual Wind Tunnel for Civil Engineering Applications.” Dissertation. Barcelona: Universitat Politecnica de Catalunya, 2020.

Bisherige Titel der Schriftenreihe

Band	Titel
1	Frank Koschnick, *Geometrische Lockingeffekte bei Finiten Elementen und ein allgemeines Konzept zu ihrer Vermeidung*, 2004.
2	Natalia Camprubi, *Design and Analysis in Shape Optimization of Shells*, 2004.
3	Bernhard Thomée, *Physikalisch nichtlineare Berechnung von Stahlfaserbetonkonstruktionen*, 2005.
4	Fernaß Daoud, *Formoptimierung von Freiformschalen - Mathematische Algorithmen und Filtertechniken*, 2005.
5	Manfred Bischoff, *Models and Finite Elements for Thin-walled Structures*, 2005.
6	Alexander Hörmann, *Ermittlung optimierter Stabwerkmodelle auf Basis des Kraftflusses als Anwendung plattformunabhängiger Prozesskopplung*, 2006.
7	Roland Wüchner, *Mechanik und Numerik der Formfindung und Fluid-Struktur-Interaktion von Membrantragwerken*, 2006.
8	Florian Jurecka, *Robust Design Optimization Based on Metamodeling Techniques*, 2007.
9	Johannes Linhard, *Numerisch-mechanische Betrachtung des Entwurfsprozesses von Membrantragwerken*, 2009.
10	Alexander Kupzok, *Modeling the Interaction of Wind and Membrane Structures by Numerical Simulation*, 2009.
11	Bin Yang, *Modified Particle Swarm Optimizers and their Application to Robust Design and Structural Optimization*, 2009.

Band	Titel
12	Michael Fleischer, *Absicherung der virtuellen Prozesskette für Folgeoperationen in der Umformtechnik*, 2009.
13	Amphon Jrusjrungkiat, *Nonlinear Analysis of Pneumatic Membranes - From Subgrid to Interface*, 2009.
14	Alexander Michalski, *Simulation leichter Flächentragwerke in einer numerisch generierten atmosphärischen Grenzschicht*, 2010.
15	Matthias Firl, *Optimal Shape Design of Shell Structures*, 2010.
16	Thomas Gallinger, *Effiziente Algorithmen zur partitionierten Lösung stark gekoppelter Probleme der Fluid-Struktur-Wechselwirkung*, 2011.
17	Josef Kiendl, *Isogeometric Analysis and Shape Optimal Design of Shell Structures*, 2011.
18	Joseph Jordan, *Effiziente Simulation großer Mauerwerksstrukturen mit diskreten Rissmodellen*, 2011.
19	Albrecht von Boetticher, *Flexible Hangmurenbarrieren: Eine numerische Modellierung des Tragwerks, der Hangmure und der Fluid-Struktur-Interaktion*, 2012.
20	Robert Schmidt, *Trimming, Mapping, and Optimization in Isogeometric Analysis of Shell Structures*, 2013.
21	Michael Fischer, *Finite Element Based Simulation, Design and Control of Piezoelectric and Lightweight Smart Structures*, 2013.
22	Falko Hartmut Dieringer, *Numerical Methods for the Design and Analysis for Tensile Structures*, 2014.
23	Rupert Fisch, *Code Verification of Partitioned FSI Environments for Lightweight Structures*, 2014.
24	Stefan Sicklinger, *Stabilized Co-Simulation of Coupled Problems Including Fields and Signals*, 2014.

Band Titel

25 Majid Hojjat, *Node-based parametrization for shape optimal design*, 2015.

26 Ute Israel, *Optimierung in der Fluid-Struktur-Interaktion - Sensitivitätsanalyse für die Formoptimierung auf Grundlage des partitionierten Verfahrens*, 2015.

27 Electra Stavropoulou, *Sensitivity analysis and regularization for shape optimization of coupled problems*, 2015.

28 Daniel Markus, *Numerical and Experimental Modeling for Shape Optimization of Offshore Structures*, 2015.

29 Pablo Suárez, *Design Process for the Shape Optimization of Pressurized Bulkheads as Components of Aircraft Structures*, 2015.

30 Armin Widhammer, *Variation of Reference Strategy - Generation of Optimized Cutting Patterns for Textile Fabrics*, 2015.

31 Helmut Masching, *Parameter Free Optimization of Shape Adaptive Shell Structures*, 2016.

32 Hao Zhang, *A General Approach for Solving Inverse Problems in Geophysical Systems by Applying Finite Element Method and Metamodel Techniques*, 2016.

33 Tianyang Wang, *Development of Co-Simulation Environment and Mapping Algorithms*, 2016.

34 Michael Breitenberger, *CAD-integrated Design and Analysis of Shell Structures*, 2016.

35 Önay Can, *Functional Adaptation with Hyperkinematics using Natural Element Method: Application for Articular Cartilage*, 2016.

36 Benedikt Philipp, *Methodological Treatment of Non-linear Structural Behavior in the Design, Analysis and Verification of Lightweight Structures*, 2017.

37 Michael Andre, *Aeroelastic Modeling and Simulation for the Assessment of Wind Effects on a Parabolic Trough Solar Collector*, 2018.

Band Titel

38 Andreas Apostolatos, *Isogeometric Analysis of Thin-Walled Structures on Multipatch Surfaces in Fluid-Structure Interaction*, 2018.

39 Altuğ Emiroğlu, *Multiphysics Simulation and CAD-Integrated Shape Optimization in Fluid-Structure Interaction*, 2019.

40 Mehran Saeedi, *Multi-Fidelity Aeroelastic Analysis of Flexible Membrane Wind Turbine Blades*, 2017.

41 Reza Najian Asl, *Shape Optimization and Sensitivity Analysis of Fluids, Structures, and their Interaction using Vertex Morphing Parametrization*, 2019.

42 Ahmed Abodonya, *Verification Methodology for Computational Wind Engineering Prediction of Wind Loads on Structures*, 2020.

43 Anna Maria Bauer, *CAD-integrated Isogeometric Analysis and Design of Lightweight Structures*, 2020.

44 Andreas Winterstein, *Modeling and Simulation of Wind-Structure Interaction of Slender Civil Engineering Structures Including Vibration Systems*, 2020.

45 Franz-Josef Ertl, *Vertex Morphing for Constrained Shape Optimization of Three-dimensional Solid Structures*, 2020.

46 Daniel Baumgärtner, *On the Grid-based Shape Optimization of Structures with Internal Flow and the Feedback of Shape Changes into a CAD Model*, 2020.

47 Mohamed Khalil, *Combining Physics-based models and machine learning for an Enhanced Structural Health Monitoring*, 2021.

48 Long Chen, *Gradient Descent Akin Method*, 2021.

49 Aditya Ghantasala, *Coupling Procedures for Fluid-Fluid and Fluid-Structure Interaction Problems Based on Domain Decomposition Methods*, 2021.